RECENT DEVELOPMENTS IN HIGH p_T PHYSICS*

By R. Møller

Niels Bohr Institute, Blegdamsvej 17, DK-2100 Copenhagen Ø, Denmark

(*Received April 2, 1984*)

Recent developments in high p_T hadron physics are reviewed. After a brief historical overview, the theoretical framework is sketched. The main emphasis of the paper is on new experimental results. These concern events with single hadrons and symmetric pairs of hadrons at large p_T, direct photons, and other highly inelastic events, defined as events with a large transverse energy in an extended solid angle. Measurements of the inclusive cross section for jet production are treated in some detail.

PACS numbers: 13.85.-t, 13.85.Hd

Content

* Presented at the XXIII Cracow School of Theoretical Physics, Zakopane, Poland, May 29-June 12, 1983.

1. Introduction

High p_T physics refers to the study of hadron-hadron collisions at high energy which give rise to particles at large transverse momentum, p_T, with respect to the collision axis. By large p_T one typically means $p_T \gtrsim 1$–2 GeV/c, i.e. the p_T region where the inclusive cross section rises significantly above the thermal spectrum

$$(Ed\sigma/d^3p \propto e^{-bp_T}, \quad b \simeq 6\ \text{GeV}^{-1})$$

which is characteristic of the bulk of the particle production. It is the hope, and the current belief, that high p_T physics provides a window to see in a rather direct way interactions of hadron constituents, the quarks and gluons, and this is what gives it its important status in the study of strong interactions. Indeed, the power laws observed already 10 years ago for the shape of the inclusive particle spectra at large p_T, already indicated that the high p_T particles originate in collisions of point like subparticles of the colliding hadrons.

When collisions giving rise to a particle at large p_T were studied more fully, it was soon confirmed that the basic event configuration had a four jet structure, with two jets at large p_T emerging from the "background" of the two "beam jets". By a jet, one means a collimated set of hadrons with exponentially damped momentum components transverse to a common direction. Over a period of several years, this picture was more firmly established, and more and more details of the event structures were studied.

Following the early developments of the field, which will be briefly reviewed below, it was also thought interesting to study in a general way hadron-hadron collisions in the limit of large inelasticity, as measured by the radiation of a large transverse energy, $\sum E_T$, inside a restricted rapidity interval (usually around $y = 0$).

Such an azimuthally symmetric selection criterion for the events obviously does not in itself impose any structure on the azimuthal distribution of particles, and in particular does not require that the particles be concentrated in some limited regions of azimuth and rapidity smaller than the region used in the defining requirement. It was, however, expected that hard collisions of constituents, giving rise to high p_T jets of hadrons, would become the dominating processes at large values of $\sum E_T$. With the aid of hindsight one may add that also the collision energy, $\sqrt{s}$, must be large for this to occur.

After a period of rather slow progress (see e.g. [1]) the last couple of years has brought a wealth of new information largely due to new calorimeter experiments at the ISR and the start of the SPS $\bar{p}p$ collider, but also due to experiments following the classical lines of development in the field. At the same time significant theoretical advances have taken place. The aim of these lectures is to review these recent developments. The main emphasis will be put on the experimental results that have become available since the Paris conference [2].

Several other excellent reviews from recent years are available ([3–6]). In addition the interested reader is referred to the forthcoming proceedings of the recent study conference on jet properties [7].

The paper is organized as follows: After a brief historical review (Section 2), the theoretical framework is sketched in Section 3. Section 4 deals with new results based on single

hadron and symmetric pair triggers and contains a short discussion of some recent results on direct photons at large p_T. Section 5 deals with high transverse energy triggers and the inclusive cross section for jet production.

Evidently the presentation deals with high p_T physics from the personal vantage point of the author, who is a member of the Axial Field Spectrometer Collaboration at the ISR.

2. *A short historical survey*

In this section some key points in the development of the field of high p_T physics will be listed, and briefly commented upon. A fuller historical survey of the progress achieved during the last decade can be found in [4].

After the development of the parton model in the late sixties [8, 9], originally in the context of lepton-hadron scattering at high momentum transfer (so-called deep inelastic scattering), it was soon realized that incoherent collisions of individual partons in hadron--hadron collisions at high energy would give rise to hadrons at large transverse momentum [10]. By this one means that beyond a certain p_T the production rate becomes large compared to the sharply cut off "thermal" spectrum (e^{-6p_T}) characteristic of the majority of the produced particles. From electromagnetic interactions of partons alone this transition was estimated to occur around $p_T = 4$ GeV/c, but it was conjectured that strong interactions might give rise to a significant departure from the exponential spectra already at much lower p_T. The application of the parton model to high p_T scattering will be described in more detail in the next section, as it is still at the basis of much of the understanding that has been gained.

In 1972 three groups [11–13] working at the newly started ISR discovered that the particle yields in the p_T region above 1–2 GeV/c were much larger than expected from a direct extrapolation of the exponentially damped cross sections at low p_T. Furthermore, it was soon found that, whereas the inclusive spectra at low p_T vary only slowly with the collision energy ($\sqrt{s}$), the spectra at large p_T show a strong energy dependence. Also the particle composition was found to vary with p_T, showing a transition-like behaviour at 1.5–2 GeV/c [11b, 14].

From the parton model one could expect that the inclusive cross section for the production of a hadron c at large p_T in collisions of hadrons h_1, h_2, scales like

$$E\frac{d\sigma}{d^3p}(h_1+h_2 \to c+X) = \frac{A}{p_T^N} f(x_T, \theta), \tag{1}$$

where $x_T = 2p_T/\sqrt{s}$ and θ is the emission angle, when the masses of the involved hadrons can be neglected. As the partons are assumed to be point-like, the only momentum scales in the problem are p_T and $\sqrt{s}$, and for dimensional reasons one expects to find $N = 4$ (as in Rutherford scattering).

The ISR data do indeed fit the form (1) well, but instead of the power of 4 one found $N \approx 8$ [1], which showed that the production mechanism is not as simple as one had first expected.

[1] This holds for pions and kaons. For protons and antiprotons one found $N \simeq 12$.

Data on π^0 production at the ISR reaching p_T values of $\sim$ 16 GeV/c [15, 16], and also recent data on charged pion production [17], indicate that the power N may decrease towards values of 6–7 at large x_T. When the direct production of high p_T photons is taken into account in the analysis of the π^0 data (where one could not at first distinguish between π^0's and γ's) the evidence for a change in N is, however, not strong.

A more recent comparison of data from the SPS $\bar{p}p$ collider with data from the ISR is shown in Fig. 1. The p_T range covered at the collider is still too small to allow an overlap in x_T with the high p_T region at the ISR, and hence to get a reliable estimate of N for this energy range. It is gratifying, however, to see the good agreement with a calculation representing the present state of the art understanding of QCD [18].

The large value of the power N, and in general the systematics of the single particle spectra, brought into attention the so-called constituent interchange model (CIM) [19], in which it is assumed that the scattering of quarks on mesonic partons is the dominant subprocess at moderate p_T. The p_T dependence of the meson form factor now gives rise

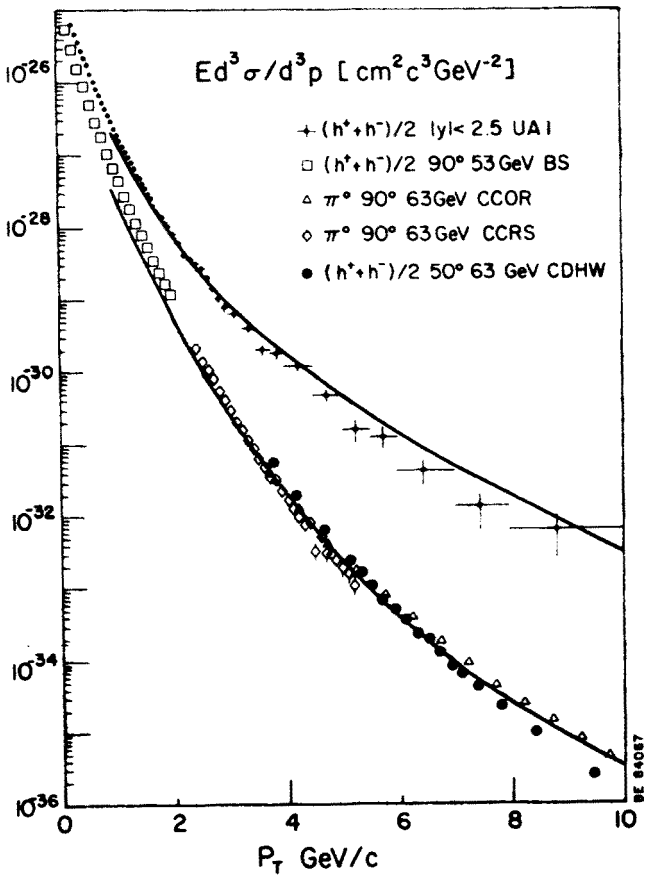

Fig. 1. Inclusive spectrum for charged hadrons at $\sqrt{s}$ = 540 GeV compared with data on charged hadron and π^0 production at the ISR. The lines show the results of a recent QCD calculation, which includes soft gluon bremsstrahlung effects [18]

to an extra power of 2 in the matrix element, so that the scaling law (1) follows with $N = 8$ ($N = 12$ for baryon production). Combined with the so-called dimensional counting rules [20, 21] the CIM lead to a large number of successful phenomenological predictions [19, 22]. It ran into serious problems, however, in confronting data on charge ratios in $\pi^- p \to \pi^{\pm} + X$ reactions [23], and is also not able to describe the recent data from the ISR on high p_T production in $\bar{p}p$ collisions (see Section 4.1).

In the parton model, the scattered partons do not appear directly in the final state (except for directly produced mesons and photons), but are transformed into narrowly collimated bunches of hadrons, so-called jets. The first experimental observation of correlations of the type expected from jets, among the high p_T particles emitted in pp collisions in association with a high p_T "trigger" particle, came in 1975 [24]. It was followed in the years after by quite extensive investigations of the structure of the events giving rise to single high p_T particles [25–27]. By the time of the 1978 Copenhagen meeting on Jets in High Energy Collisions [28] the major features of the event structures were known and the jet picture firmly established [25c, 29–31].

During the same period, also the theoretical understanding of the phenomena advanced significantly, and there was a strong interplay between theory and experiment. Bjorken [32], and Jacob and Landshoff [33] discussed the so-called "trigger bias" effect, for experiments triggered by a single particle at high p_T. In this situation the competition between the fragmentation process and the steeply falling p_T-spectrum leads to a balance, where the high p_T particle required by the trigger condition often takes a large fraction of the momentum of the jet it belongs to. The effect will be discussed more generally in Section 3.4. In consequence of this a trigger designed to collect a whole jet should have a rate 2–3 orders of magnitude larger than the corresponding rate for single particles at the same p_T. This large factor was indeed observed in calorimeter experiments at Fermilab [34]. Furthermore it was found that the trigger bias effect could in general fully account for the dissimilarity between the jet accompanying the trigger particle, and the recoil jet, thus reducing the need for the direct production of mesons at high p_T expected from the CIM.

At this time Feynman, Field and Fox [35–37] and independently the Bielefeld group [38] started a phenomenological analysis of large amounts of data from deep inelastic lepton hadron scattering, e^+e^- annihilation and large p_T hadron physics, in order to determine the form of the parton parton scattering cross section. One found that a form $d\sigma/dt \propto 1/st^3$ could adequately describe the data, provided one introduced internal transverse momenta k_T of the incoming partons in the model. The values of $\langle k_T \rangle$ needed were, however, quite large, around 800–900 MeV/c.

A major step was taken with the realization [39–41] that most high p_T results, both regarding inclusive spectra and correlations, were not inconsistent with lowest order QCD expectations, once one took into proper account the various effects due to scale breaking of the structure functions and fragmentation functions, and admitted the large values of k_T mentioned above.

Terms involving more than the minimum number of fields, similar to the CIM, (so-called higher twist terms) are also expected in QCD [42], and may be emphasized by

certain triggering conditions, e.g. single particle triggers at moderately large p_T. Their relative importance is not clear at the moment, neither theoretically nor experimentally.

It was also realized [43] that directly produced photons at high p_T could be very discriminating between models. In particular, in lowest order QCD one expected substantial photon yields at high p_T (e.g. $\gamma/\pi^0 \sim 1$ at $p_T \simeq 14$ GeV/c at the ISR). The experimental finding [44] of a direct photon yield in the p_T range of 3 to 8 GeV/c of the expected magnitude was a major breakthrough in the field.

The trigger bias effect discussed above, and the realization that also experiments triggering on jets with small solid angle calorimeters might pick a rather special class of events, lead to the consideration of large solid angle calorimeters to investigate highly inelastic hadron-hadron collision in a supposedly bias-free way [45]. The results of the first experiment, NA5 at the SPS [46], using a calorimeter covering the full azimuth to trigger on high transverse energy, were discouraging, however. In the experiment π^-p collisions at 150 and 300 GeV/c, and pp collisions at 300 GeV/c were investigated. The cross section for emission of a large transverse energy E_T in the rapidity range $-0.88 < y < 0.67$ (corresponding to scattering angles from 54°–135°) was found to be ~ 10 times larger than the cross section predicted from a first order QCD model, and the events did not show a predominant two jet structure, even for events with an E_T of more than 2/3 of $\sqrt{s}$.

In Section 5 we shall return to the topic of total transverse energy triggers and see how the dilemma has been resolved as data from higher energies have become available.

3. Theoretical framework

Before discussing the data, we shall in this section describe the major theoretical models of high p_T reactions in current use, emphasizing the underlying physical ideas. All models are hard scattering models, supposedly based on QCD. It is in general not possible in this field to escape from the difficulties associated with the unsolved problems of confinement in QCD. Therefore all the models contain essential elements of phenomenological nature, in order to deal with the structure of the colliding hadrons, and with the formation of the final state hadrons.

3.1. The parton model

In the parton model [9] the wave functions of the colliding hadrons are described in terms of weakly interacting subfields, partons. A high p_T reaction is thought to proceed via a hard binary collision of partons, followed by the formation of hadrons from the struck partons and from the left-over spectator partons. A central assumption is the separation of the time scale associated with the hard collision and the much slower time scales associated with the initial state interactions of partons, and with the final state hadronization, whereby quantum numbers (colour, non-integer charges) are redistributed and hadrons are formed.

The essential ingredients in the model are shown symbolically in Fig. 2. The structure functions $G_{B\to j}(x)$ determine the probability that a parton of type j is found in the hadron

B with a fraction x of its momentum. They are generally obtained from the analysis of deep inelastic hadron scattering.

The fragmentation functions $F_l^C(z, q_T)$ similarly determine the probability that a hadron C is emitted from a scattered parton l with a longitudinal momentum fraction z, and a transverse momentum q_T relative to the parton direction. These functions are generally obtained from the analysis of e^+e^- annihilation into hadrons.

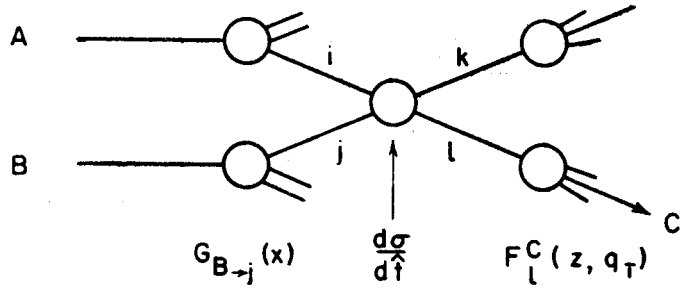

Fig. 2. Basic ingredients of the parton model for high p_T reactions

Finally $d\sigma/d\hat{t}$ (ij → kl) is the differential cross section for scattering of partons i, j to k, l. This is in most cases obtained from perturbative QCD taken to lowest or second order (i.e. including hard gluon bremsstrahlung). It is, however, also possible to describe the CIM and/or other higher twist subprocesses in this scheme, by admitting also mesonic partons in the initial and/or final state, and introducing the appropriate differential cross sections, although in this case a special difficulty arises in establishing the correct relative normalization of the mesonic part of the structure functions.

Notice that this approach, as well as the two following, is essentially classical, in that the structure functions and fragmentation functions are just probability distributions, and all interference effects are neglected.

As already stated in the previous section, several refinements were found necessary to achieve good agreement with experiments, and/or consistency with theoretical prejudices based on QCD. They involve:

1) scale breaking of the structure functions and fragmentation functions, i.e. $G_{B\to j}(x)$ and $F_l^C(z, q_T)$ are allowed to depend also on the squared momentum transfer, Q^2, in the hard process;

2) allowing the partons to have a transverse momentum k_T in the initial state;

3) going to higher order in the hard scattering, viz. allowing hard gluon bremsstrahlung. The higher twist terms are other examples of this kind. When scale breaking is introduced, it is not inherently clear how to choose the scale Q^2. A popular choice is to take [41]

$$Q^2 = \frac{2\hat{s}\hat{t}\hat{u}}{(\hat{s}^2+\hat{t}^2+\hat{u}^2)}, \tag{2}$$

where $\hat{s}$, $\hat{t}$ and $\hat{u}$ are the Mandelstam variables in the hard subprocess.

The so-called primordial transverse momentum, k_T, needed if the parton model, with $d\sigma/d\hat{t}$ taken from lowest order QCD processes, is to fit the data, is quite large, $\langle k_T \rangle$ = 800–900 MeV. This value is constrained in particular by the softness of the away side transverse momentum distributions, and the substantial imbalance in the transverse momenta of the two high p_T jets. The value needed seems uncomfortably large. A similar value is, however, needed to understand the p_T distribution of heavy lepton pairs in hadron-hadron collisions.

The effects of hard gluon bremsstrahlung have not been convincingly demonstrated in high p_T data yet, although tantalizing glimpses have been seen both at the SPS collider [47, 48] and at the ISR [49].

Possible "K-factors"[2] different from one have so far been neglected in most calculations. As an exception, it is shown that reasonable agreement of the spectra shown in Fig. 1 with lowest order QCD without gluon bremsstrahlung effects can be achieved using K factors of 2–3.

3.2. The Lund model

The Lund model [51] is basically a model for hadron formation, based on the concept of relativistic strings. In its present implementation for high p_T physics [52] standard parametrizations of the structure functions [53, 54] are used, and the hard cross section is calculated to second order in α_s. The hadron formation is assumed to take place in the force field spanned between the scattered constituents. This field is modelled by the massless relativistic string, and only colour triplet strings are recognized. Colour octet objects (e.g. gluons) are treated as kinklike excitations of the string. The various topologically different string configurations are treated separately and are added incoherently. It has been speculated that different string topologies may actually correspond to different values of an underlying topological quantum number in QCD [55], with the implication that interferences between different string configurations would vanish.

In the model the string is allowed to break up not only into quark-antiquark pairs, but also in diquark-antidiquark pairs, thus leading to a possible description of baryon pair production.

A conceptual difficulty in the model is the need for very long colour strings in some reactions. This may be viewed, however, as an effective parametrization of the higher order effects neglected in the calculation of the parton process.

In the Lund model the emphasis is most naturally put on the structure of complete events, whereas the jets are fuzzy objects, with no sharp separation from the background event.

3.3. The parton shower approach

The non-observation of a dominant jet structure in events with a large transverse energy in the NA5 experiment led to the realization that gluon bremsstrahlung might play a much more important role than had previously been recognized.

[2] Normalization constants applied to a low order calculation to take into account the effective contribution of the higher order terms.

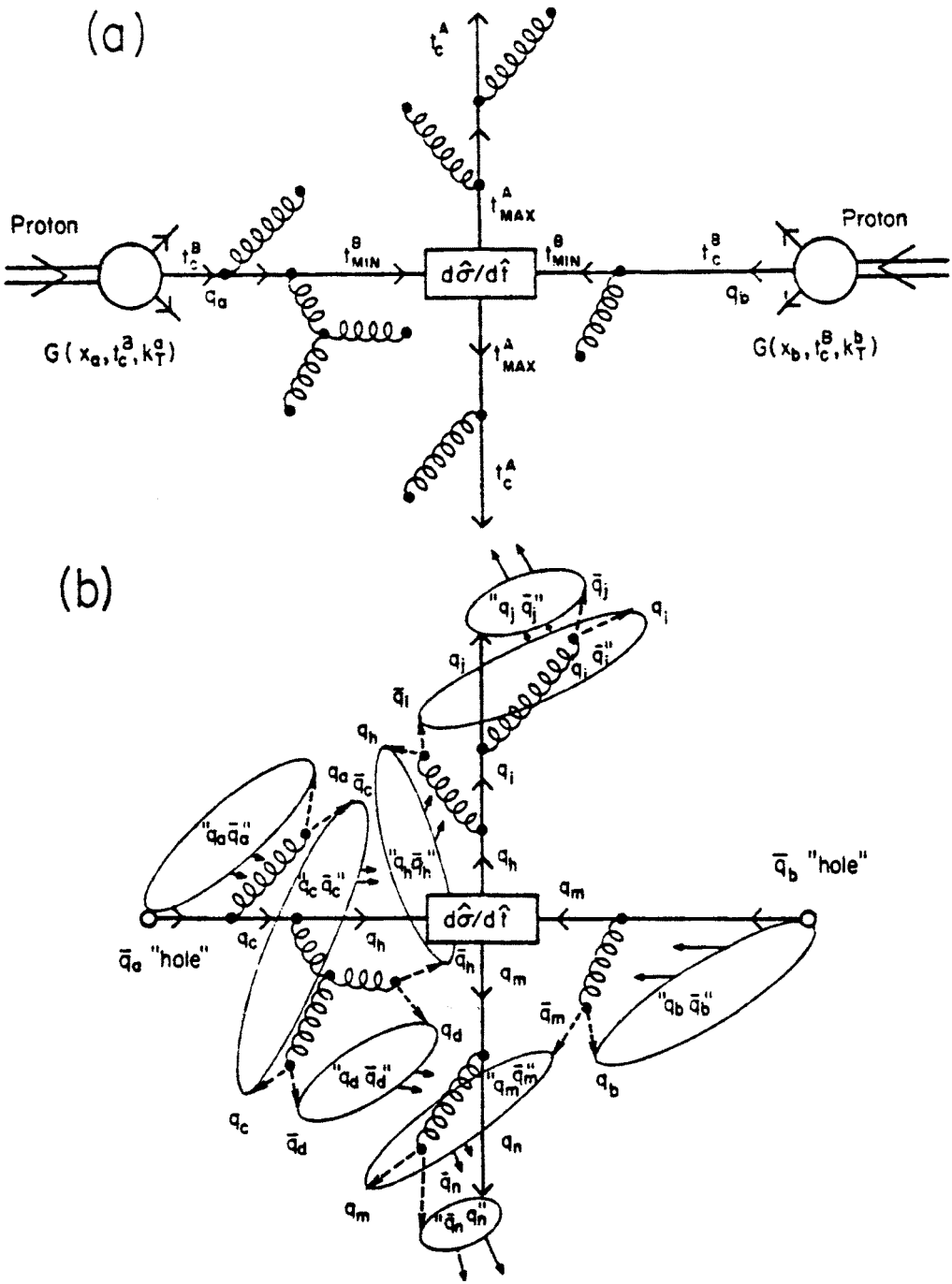

Fig. 3. a) The QCD parton shower approach applied to high p_T hadron-hadron collisions. b) Illustration of the procedure used to form colour neutral clusters

Models were developed [56, 57] in which both the initial state and final state partons are allowed to emit gluons, according to perturbative QCD in the leading log aporoximation, until mass scale of typically $\sqrt{t} = 1$–2 GeV are reached (see Fig. 3a). At this point the coupling α_s becomes so large that confinement effects must set in, and a perturbative treatment can certainly no longer be trusted. In the branching, full off shell kinematics is used. The radiated gluons may themselves emit more gluons, producing a shower of partons in both the initial and final states. In [57] the Feynman Field fragmentation model is used to convert the final state quarks and gluons into hadrons. In [56] it is argued, however, that a new hadronization scheme is needed for the not very energetic quanta that typically emerge from this approach. As illustrated in Fig. 3b, one keeps track of the flow of colour indices, and forms colour neutral clusters by forcibly splitting all gluons in the parton level final state into $q\bar{q}$ pairs. The masses of these clusters are typically in the range 0–2 GeV, with a strongly damped mass spectrum. They are allowed to decay according to a simple phase space model. Baryon pairs can be produced by heavy clusters, but because of the damping of the cluster mass spectrum, they are strongly suppressed.

As in the Lund model, there is no longer a simple, direct connection between a scattered parton and a hadron jet, and one is naturally lead to consider more global event characteristics, such as the spectrum of transverse energy, energy flow distributions vs E_T, etc.

In a first step beyond the classical approximation, it has recently been pointed out that interference effects are important in the treatment of soft gluon radiation [58], implying the use of a form factor of the Sudakhov type for the partons. This leads to a depletion of particles near $z = 0$ in the jet, and may be an important effect in the structure of very high energy jets, e.g. at the SPS $\bar{p}p$ collider, and in e^+e^- annihilations at LEP.

As we shall see in Section 5, the parton shower approach is quite successful in describing the recent calorimeter results at high E_T. In view of the sophistication now reached in the analysis, it seems surprising, however, that the possible role of multiple (hard) scattering of partons has so far received only little attention [59].

3.4. Trigger types and "trigger bias"

Whereas the first generations of high p_T experiments were based on the selection of events which contained a single particle of large transverse momentum (single particle trigger), current experiments exploit a variety of additional triggers, mostly using calorimeters. Because the structure of the events selected are governed by several conflicting effects, it is important to be aware of the various types of selection bias imposed by the different triggering conditions. The discussion of the various effects can be based on the trivial observation that when you impose certain requirements on the events, they are fulfilled in the cheapest way, i.e. the way that is most easily accessible to nature, and which therefore occurs most frequently.

The first example of such an effect is the trigger bias effect for the structure of events triggered on a single particle [33], briefly discussed above. Since the inclusive parton (jet) cross section is a steeply falling function of p_T, the requirement of a certain p_T on a single particle is most easily fulfilled by jets having only little more transverse momentum than the trigger particle itself. The distribution of the fractional jet momentum, z_{trig}, taken by the

trigger particle is determined by the competition between the cross section and the fragmentation function, $F(z)$, which is a falling function of z. Whereas $\langle z \rangle$ of the fastest particle in the jet in general is around 0.3 for e^+e^- jets in the current momentum range, $\langle z_{trig} \rangle$ is typically around 0.8–0.9. As an example Fig. 4 shows a recent measurement by the CCOR collaboration [60] of $\langle z_{trig} \rangle$ for inclusive π^0 production as a function of x_T in pp collisions at three ISR energies. One finds that $\langle z_{trig} \rangle$ is to a good approximation a function of x_T, rather than p_T (trig).

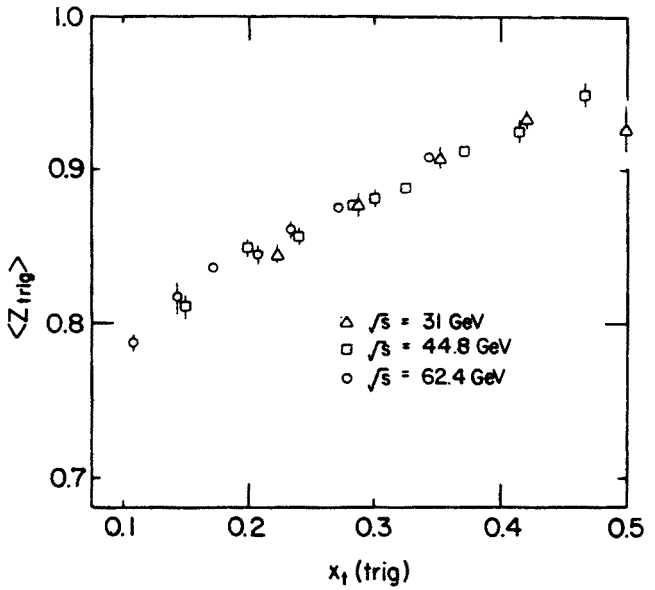

Fig. 4. $\langle z_{trig} \rangle$ vs. x_T for inclusive π^0 production in pp collisions at $\sqrt{s}$ = 31, 45 and 63 GeV. Data from CCOR [60]

When one studies the away side particle distributions in high p_T events one finds that the trigger side jet is only partially balanced in momentum by the away side jet. In the framework of the parton model this is interpreted as a result of another bias, in which the trigger condition selects predominantly events where the intrinsic transverse momentum of the partons undergoing the hard scattering, are already pointed in the direction of the trigger particle.

As pointed out several years ago [38], this type of trigger bias can be avoided by triggering on two particles balancing each other in transverse momentum (symmetric pair trigger).

The first bias can be avoided by triggering on complete jets by means of a calorimeter covering a suitable solid angle ($\sim$ 1 sr). This procedure gains a factor 10^2–10^3 in rate at a given p_T[3]. In view of results of the investigations of the parton shower model (Section

[3] There is an inherent uncertainty by a factor $\sim$ 10 in this prediction, depending on whether one chooses to compare at fixed p_T or E_T.

3.3), distortions still arise from gluon bremsstrahlung effects, and evidently the effects of the intrinsic transverse momentum of the partons discussed above will influence any asymmetric trigger condition.

Azimuthally symmetric triggers on total transverse energy, E_T, in a given range of scattering angle, were introduced mainly to avoid any bias as to the jet structure of the final state. The expectation was that events with a large value of E_T would nevertheless be dominated by hard scattering giving rise to jets.

In the NA5 experiment at the SPS this was found not to be the case, and from the discussion of the parton shower model it appears that this trigger predominantly picks events where a large amount of gluon bremsstrahlung helped to build up E_T. The events have large multiplicities, a somewhat elevated $\langle p_T \rangle$, but the jet structure from the hard subprocess is efficiently masked. Recently it has been found that at larger collision energy and larger E_T the jet structure does emerge. This will be discussed in detail in Section 5.

If one uses an azimuthally symmetric trigger that picks only charged particles [61] or mainly neutral particles [62], this again imposes a bias on the event structure selecting events that have few neutral or charged particles respectively.

It appears that a comparative study of various event characteristics (such as energy flow vs. azimuth in bins of E_T etc.) for widely different trigger conditions may be a powerful tool in distinguishing between models.

4. New results based on single and symmetric pair triggers

The use of single particle triggers and symmetric pair triggers at large p_T has reached a high level of sophistication. In this section some of the newest results, all coming from the ISR, will be discussed. They concern the comparison of inclusive particle spectra in $\bar{p}p$ and pp collisions, new measurements of particle ratios at high p_T, mesurements of the parton cross section exploiting a symmetric pair trigger, and investigations of the charge structure of the trigger side and away side jets. Also the beautiful analysis of the CDHW collaboration concerning the relative importance of various parton subprocesses will be briefly discussed. The recent measurements of inclusive hadron production at large p_T at the SPS $\bar{p}p$ collider have already been discussed above.

4.1. Comparison of $\bar{p}p$ and pp collisions

Whereas the bulk of particle production in $\bar{p}p$ and pp collisions is supposed to differ only at the few per cent level at ISR energies, the particle yield at large p_T may show substantial differences. For example, whereas direct γ production at high p_T in pp collisions (discussed in Section 4.6) is dominated by the gluon-Compton process, $qg \to q\gamma$, the annihilation process, $\bar{q}q \to g\gamma$, may become dominant in $p\bar{p}$ collisions, resulting in much larger rates for direct γ's. The QCD Born diagrams lead to a substantial increase in the yield of hadrons only at very large p_T, where qq ($q\bar{q}$) scattering is expected to dominate, but if higher order processes like $q\bar{q} \to M\bar{M}$ are important, as in the CIM, the difference between $\bar{p}p$ and pp collisions might be substantial also at moderate values of p_T.

So far — and indeed for quite some years into the future — the highest energy for which a direct comparison of $\bar{p}p$ and pp collisions is possible, has been obtained at the ISR.

Although the luminosity achieved in $\bar{p}p$ collisions in this machine has so far limited most investigations to a study of "$\ln s$ physics", recently two experiments have succeeded in reaching p_T values of 6–8 GeV/c triggering on single hadrons [63, 64], and with the coming, last $\bar{p}p$ run with the machine, one may foresee jet physics extending to $p_T \simeq 12$–14 GeV/c.

The Axial Field Spectrometer is shown in Fig. 5. For the study reported on here only three of the four calorimeter walls were installed. The calorimeter was used to trigger on single hadrons. Electromagnetic showers were strongly suppressed by requiring that

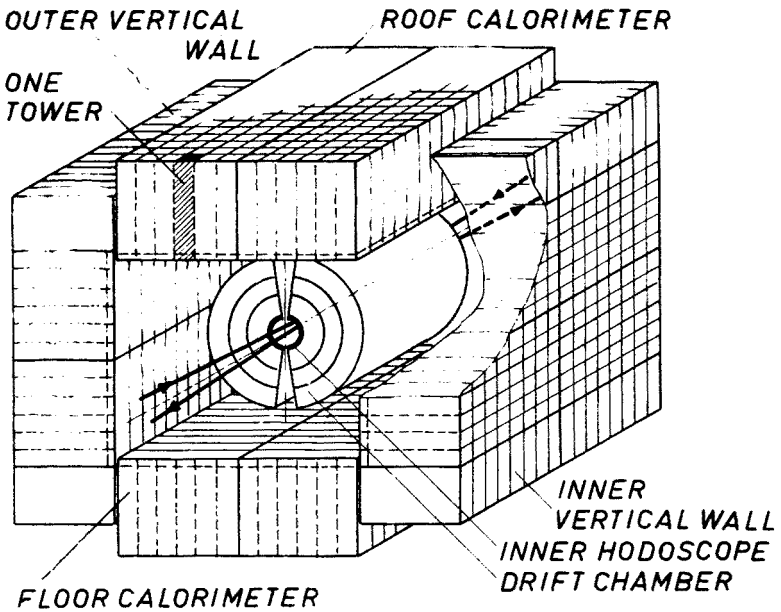

Fig. 5. The Axial Field Spectrometer at the CERN ISR, used by experiments R807 and R808. The vertex detector for charged particles covers the full azimuth except for two wedges of $\Delta\Phi = 16°$. The calorimeter consists of Uranium, Copper and scintillator plates, and is read out by two wavelength shifter bars per stack for the front end (electromagnetic part) and two for the back end (hadronic part). The Axial Field Magnet is not shown

the energy deposit in the front part of the triggering elements was less than 30% of the total energy deposit in the cluster of calorimeter cells. This was done in order to avoid difficulties in the interpretation of the results due to a possible direct γ component. Using in addition the drift chamber information available for charged tracks, it was found that $\sim 90\%$ of the reconstructed energy clusters in the calorimeter which satisfy the trigger threshold and additional cuts contain only one hadron.

The ratio between the inclusive spectra in $\bar{p}p$ and pp collisions is relatively free from systematic errors, and is shown as a function of p_T in Fig. 6 for two ISR energies. It is consistent with 1.0 for both energies.

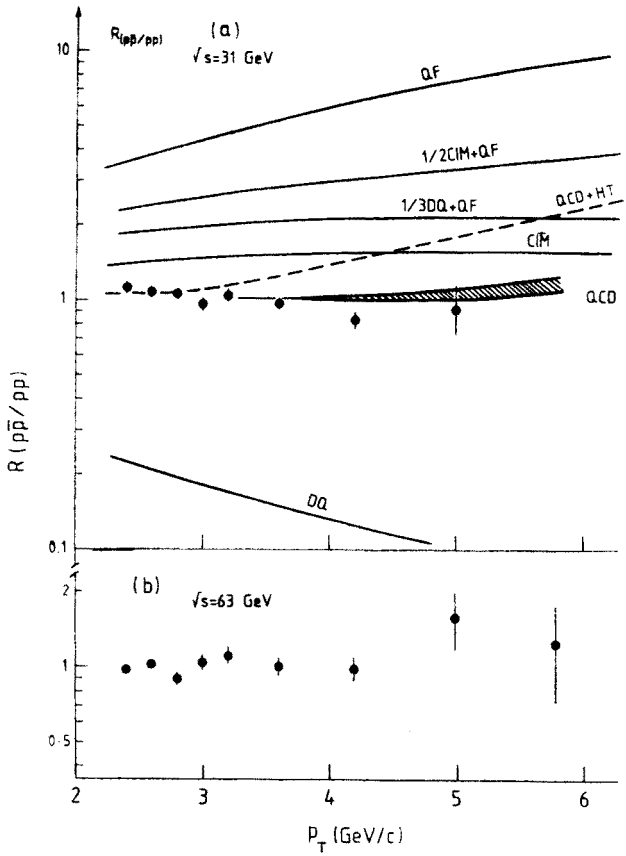

Fig. 6. Ratios of the single particle inclusive cross section in $\bar{p}p$ and pp collisions at $\sqrt{s}$ = 31 GeV and 63 GeV. Data from the AFS [63]. The curves shown are from the Chase and Stirling parametrization of possible higher order subprocesses [65], and perturbative QCD calculations [66]

The ratio is sensitive to the presence of CIM terms, in particular the $q\bar{q}$ fusion mentioned above. The solid lines show calculations by Chase and Stirling [65] of various higher order processes that could be dominant contributions to π production. (Neither the diquark curve, DQ, nor the quark fusion, QF, would be expected to apply separately, but rather some mixture of them, as in the curve labelled 1/3 DQ+QF.) None of the proposed mixtures of terms are in agreement with the data, showing that these higher order processes are not very important even at the rather moderate values of p_T investigated.

A similar conclusion was reached from comparison of π^- and π^+ production in π^-p collisions at Fermilab [23]. In this case the measured ratio π^-/π^+ is close to one, whereas the CIM prediction is an order of magnitude higher.

The data also do not agree with a perturbative QCD calculation including higher twist terms (QCD+HT) [66], whereas a lowest order QCD calculation by the same authors is in good agreement with the measured ratio.

The CMOR collaboration was able to do a similar study on neutral particles (π^0, η, γ) [67]. They also see no significant deviation in the ratio $\bar{p}p/pp$ in the p_T range from 1–8 GeV/c.

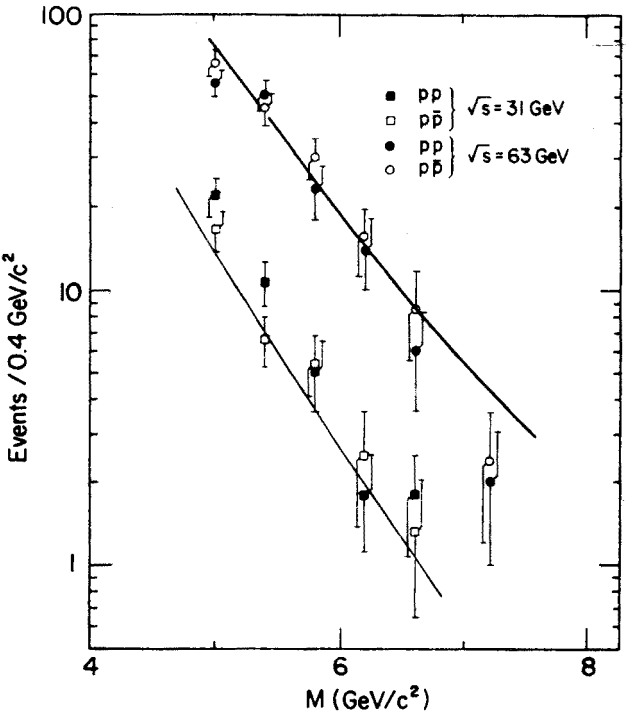

Fig. 7. Invariant mass spectrum at high p_T pairs in $\bar{p}p$ and pp collisions (assuming a π mass for the particles) normalized to the same luminosity, at $\sqrt{s}$ = 31 GeV and 63 GeV. The lines show results of a calculation of $\pi^0\pi^0$ invariant mass [68c], with an overall arbitrary normalization factor applied

A further test of the presence of higher order differences between $\bar{p}p$ and pp collisions was possible in the AFS experiment [63], selecting symmetric pairs of hadrons with $p_T > 2$ GeV/c (statistics extended to ~ 4 GeV/c). The mass spectrum of the high-p_T pairs (assuming a π mass for the particles) is shown in Fig. 7 at the two energies. No significant differences are seen between $\bar{p}p$ and pp collisions, indicating in particular that the quark fusion process $q\bar{q} \to M\bar{M}$ cannot contribute strongly in this p_T region. The increase by a factor ~ 5, going from $\sqrt{s}$ = 31 to 63 GeV is predicted by QCD [68].

In summary, the ratios of π^-/π^+ in π^-p scattering and of single particle inclusive cross sections in $\bar{p}p/pp$ scattering are in agreement with lowest order perturbative QCD calculations, and do not allow large contributions from higher order subprocesses like CIM, quark fusion or diquark scattering.

4.2. Particle ratios at large p_T

Whereas the inclusive spectrum of π^0's[4] was measured quite early at the ISR to substantial values of p_T, the inclusive spectra of (identified) charged hadrons have been much

[4] "π^0"'s in this context has generally been taken to mean the sum of all neutral particles giving rise to electromagnetic showers in a calorimeter, i.e. π^0, η, γ. Resolved signals for π^0 and γ's at large p_T have only been obtained in recent years (See Section 4.6).

harder to obtain. This is basically due to the fact that the resolution, $\Delta E/E$, for electromagnetic calorimeters (e.g. lead glass) goes down as $E^{-1/2}$, whereas $\Delta p/p$ for a magnetic spectrometer is proportional to p. Furthermore several of the early experiments on charged particles were limited by the solid angle available for triggering, and hence in the statistics that could be obtained.

Recently new data have become available on the spectra of charged pions [17, 69], and on particle ratios at ISR energies [70, 71]. The charged pion spectra now extend to $p_T \sim 12$ GeV/c at $\sqrt{s} = 63$ GeV at a production angle of $\theta \simeq 50°$.

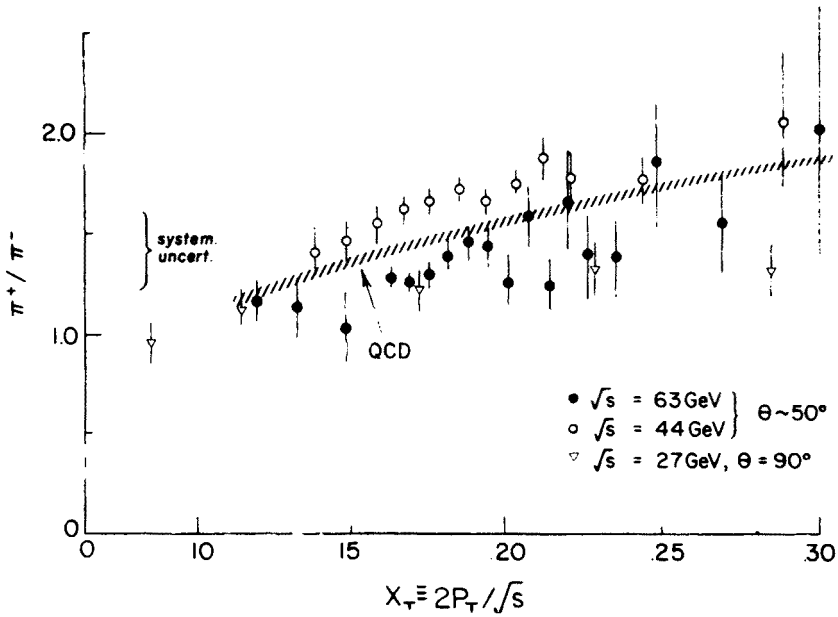

Fig. 8. Ratio of the production rates of π^+ and π^- in pp collisions at $\sqrt{s} = 27$ GeV [72] and at $\sqrt{s} = 44$ and 63 GeV [17]. Also shown is the result of a first order QCD Monte Carlo calculation [17]

Fig. 8 shows the ratio of π^+ and π^- spectra as a function of x_T. Also shown are results from the classical measurements of the Chicago/Princeton Collaboration [72] at Fermilab. Due to the rather large overall systematic errors the seeming deviation between the results at the different energies and directions should not be taken seriously.

The ratio approaches the value 2 at large x_T, which is in qualitative agreement with the expectations from the quark composition of the proton. Naively, for large p_T the π^+ mesons are expected to be produced mostly from scattered valence u quarks and π^- mesons from scattered d quarks. A first order QCD Monte Carlo calculation [17], also shown on the figure, agrees well with the data. It is close in spirit and phenomenological input to the Feynman, Field and Fox analysis [42] of the application of QCD to high p_T physics.

Fig. 9a, b show a break-down of the yields of positively and negatively charged particles respectively, in fractions of π, K and p's [70, 71].

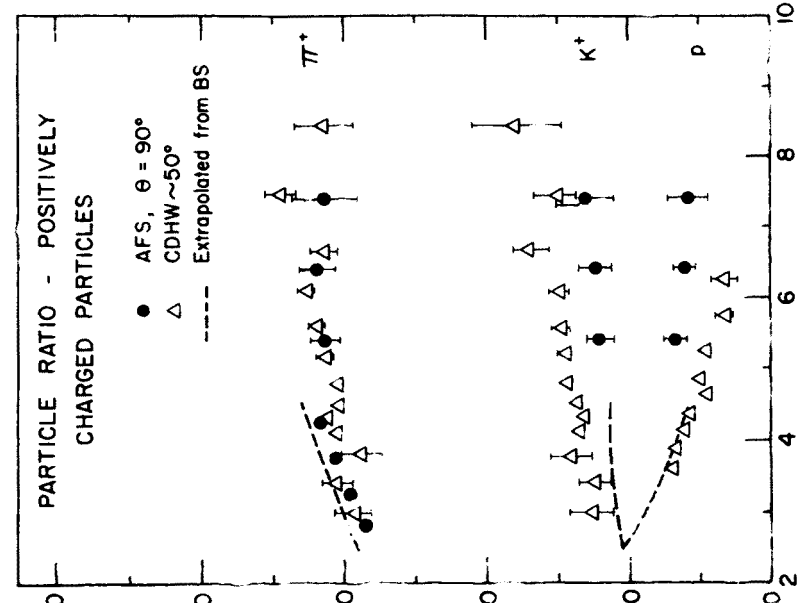

Fig. 9a

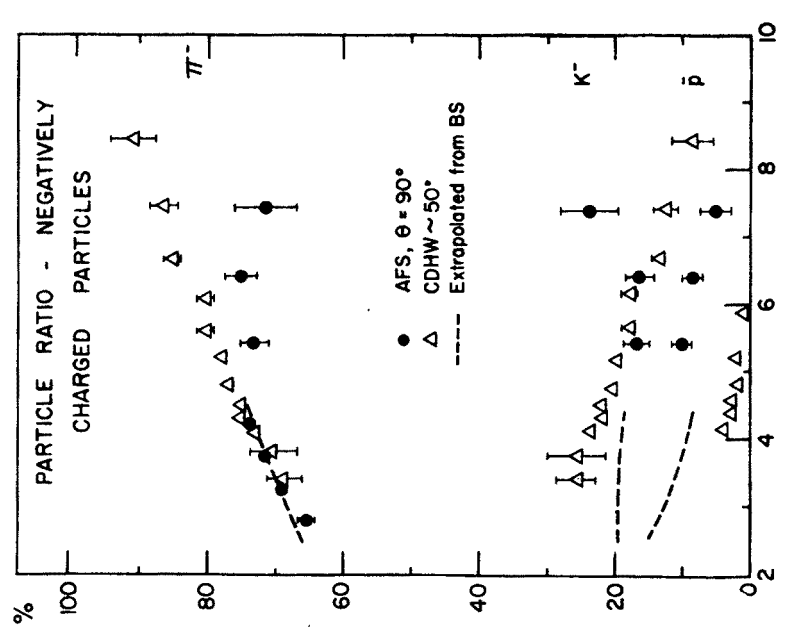

Fig. 9b

Fig. 9. Fractional composition of the charged particle yield in pp collisions at $\sqrt{s} = 63$ GeV, into π's, K's and p's, for a) positively charged particles and b) negatively charged particles [70, 71]. The CDHW data for π^+ and π^- are at $\theta = 49°$ and 53°, respectively, and their K and p data are at $\theta = 45°$

In contrast to the situation at low p_T, where pions account for $\sim 90\%$ of the long-lived particles, the π^+ fraction at large p_T (4–9 GeV/c) is rather constant at $\sim 62\%$. K^+'s show a slight increase, and p's a decrease with p_T.

The π^- fraction increases from $\sim 70\%$ to $\sim 90\%$ in the same p_T range, reflecting falling fractions of K^-'s and $\bar{p}$'s. In this context it is worth remembering that K^- and $\bar{p}$ have no valence quarks in common with protons, and cannot therefore be produced as first rank particles in the fragmentation chain of a scattered valence quark, whereas this is quite possibly a dominant source of high-p_T π's.

The increase in both the fractional p and $\bar{p}$ yield when going from $\theta \sim 50°$ to $\theta = 90°$ may reflect a stronger baryon pair production near 90°. From the variation of the proton fraction with angle [71], this implies that there is a minimum in the inclusive proton cross section somewhere in the interval $50° < \theta < 90°$.

4.3. Symmetric pairs at large p_T

In a beautiful analysis [60], following the lines suggested by Baier et al. [68], the CCOR collaboration has exploited pairs of π^0's at high p_T produced in pp collisions at 45 and 63 GeV to determine the angular dependence of hard constituent scattering.

The π^0's have transverse momenta in the range 2.5–8 GeV/c and are required to be roughly back-to-back, and have a total $p_T < 1$ GeV/c.

Because of the trigger bias effect (see Section 3.4) the π^0's each carry most of the momentum of their parent jets, and their momenta are used to estimate the parton momenta. Furthermore, because of the approximate symmetry of the trigger condition, the pair cross section should be relatively insensitive to effects of the primordial transverse momentum of the partons. Hence, in this approximation, the (average) scattering angle, θ^*, in the longitudinal rest frame of the two pion system, measures directly the scattering angle in the hard parton collision.

In a scaling model, the $\pi^0\pi^0$ spectrum must have the form

$$\frac{d\sigma}{dm d\cos\theta^*} = \frac{A}{m^n} G\left(\frac{m}{\sqrt{s}}\right) f(\cos\theta^*), \tag{3}$$

where m is the mass of the $\pi^0\pi^0$ system, and $n = 3$ for dimensional reasons. A fit to this form gives $n = 6.5 \pm 0.5$.

The distribution in $\cos\theta^*$ is shown in Fig. 10 in bins of m at $\sqrt{s} = 63$ GeV. It appears that the angular distribution is independent of m to a good approximation. This is borne out by fits to the form

$$\frac{d\sigma}{dm d\cos\theta^*} = \frac{A}{m^n} G(m/\sqrt{s}) \left[\frac{1}{(1+\cos\theta^*)^a} + \frac{1}{(1-\cos\theta^*)^a}\right] \tag{4}$$

resulting in values of a which do not depend significantly on m. A global fit gives $a = 2.97 \pm 0.05$.

It is difficult to compare this result directly with predictions from QCD, because several subprocesses with different angular dependence are expected to contribute to the reaction studied. The group therefore used a Monte Carlo simulation, based on the

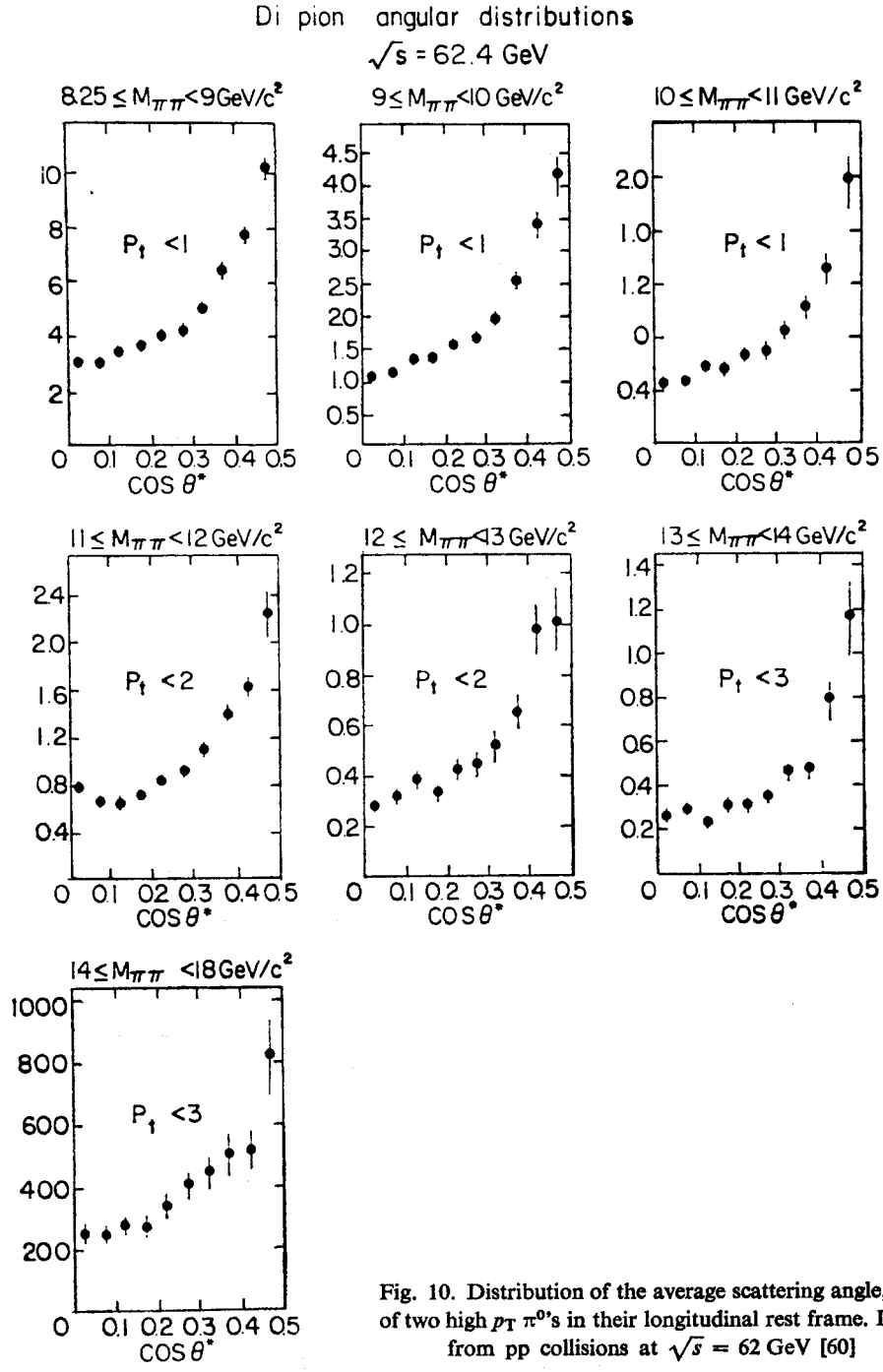

Fig. 10. Distribution of the average scattering angle, θ^*, of two high p_T π^0's in their longitudinal rest frame. Data from pp collisions at $\sqrt{s} = 62$ GeV [60]

first order QCD subprocesses in a standard way. Whereas the description of the mass dependence obtained is only tolerable, the angular dependence observed is reproduced very well.

A somewhat similar analysis was used by the CDHW collaboration [73] in an attempt to determine the spin of the gluon. Their analysis is based on a sample of pp collisions at $\sqrt{s} = 63$ GeV triggered by a π^+ with $p_T > 4$ GeV/c at $\theta = 40°$ (corresponding to $y = 0.8$), obtained at the Split Field Magnet. They study the rapidity distribution of particles on the away side ($140° < \varphi < 220°$) with $x_E = p_T/p_{T\text{trig}} > 0.5$ (see Fig. 11).

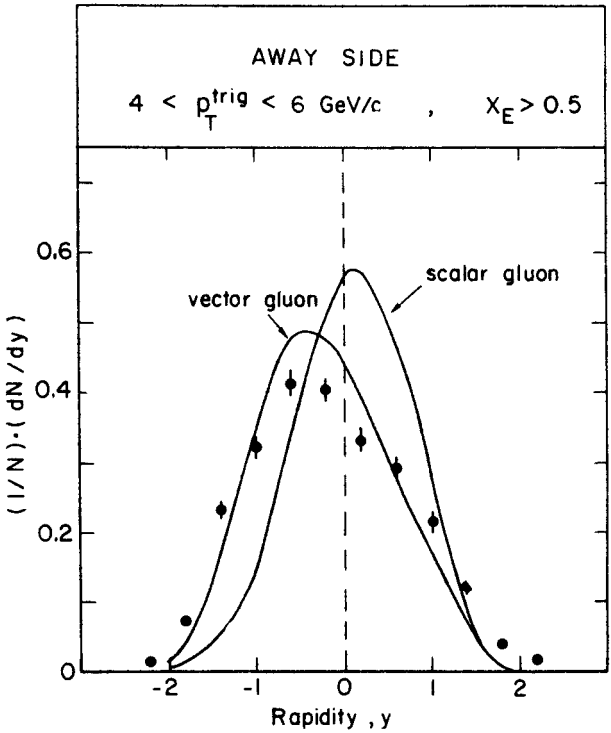

Fig. 11. Rapidity distribution of away side particles with $x_E > 0.5$. The data are from pp collisions at $\sqrt{s} = 63$ GeV with a π^+ with $4 < p_T < 6$ GeV/c at $\theta = 49°$ [73]. The lines show model calculations by the authors

The distribution is clearly shifted away from $y = 0$, towards negative y. This is taken as a reflection of the spin of the exchanged quantum in the contributing hard subprocesses. Indeed, a standard lowest order QCD model by the group (referred to above, Section 4.2), which of course has vector gluons, gives a fairly good description of the data, whereas a mutilated version of the model in which the gluon spin is assumed to be zero is in definite disagreement with the data.

Thus the angular distributions of hadron pairs at large p_T support the conclusion that gluons have spin 1, and give a first experimental determination of the angular dependence of the hard subprocesses.

4.4. Charge structure of the trigger side jet

The motivation to study in more detail the structure of the jets high p_T hadron reactions is at present two-fold. Firstly, it evidently provides a testing ground for jet formation physics comparable to e^+e^- annihilations and deep inelastic lepton scattering experiments, but with the special feature that gluon jets are expected to be abundantly present. Secondly, a detailed investigation of the structure of jets may allow one to disentangle to some degree the various contributions to high p_T scattering at the parton level, and thereby perform more stringent tests of theoretical predictions (in particular perturbative QCD).

Whereas the momentum distributions in high-p_T jets have been studied in some detail, information has been more meager on the distribution of charges and other quantum numbers (see e.g. [25b, 74, 75]). New information has recently become available from two ISR experiments.

The AFS Collaboration has analysed events with an identified charged particle at high p_T near 90°, and studied charge correlations between this particle and other identified, charged particles in the event [70]. The trigger particle had $p_T > 3.0$ GeV/c ($\langle p_T \rangle = 4.1$ GeV/c), and could be identified by means of a set of threshold Cerenkov counters covering the polar angle from 45° to 135°, and with an azimuthal coverage of $\Delta\varphi = 45°$. It could be identified as a $\pi^\pm$, or heavy ($h^\pm = K^\pm$ or $p/\bar{p}$) for p_T up to 5.3 GeV/c and as a $\pi^\pm$, $K^\pm$, p or $\bar{p}$ above this value. In addition some K's could be identified in the p_{lab} interval 2.0–3.5 GeV/c. Secondary particles could be identified by means of the Cerenkov counters in three momentum intervals inside the angular regions specified above, and at low p_T by the measurement of dE/dx in the central drift chamber.

In the analysis the trigger side jet axis was found by a jet algorithm [76], using the charged tracks with $p_T > 0.3$ GeV/c. Due to the trigger bias effect, this axis is in most cases given by the direction of the trigger particle to within a few degrees.

Measuring rapidities along the jet axis, the charge compensation $\tilde{A}(y)$ is now defined by

$$\tilde{A}(y) = \int_{y_0}^{y_{max}} (\varrho_{opp}(y, y') - \varrho_{same}(y, y'))dy' \Big/ \int_{y_0}^{y_{max}} \varrho(y, y')dy', \tag{5}$$

where $\varrho_{opp}(y, y')$ and $\varrho_{same}(y, y')$ are the two particle densities for pairs of particles with opposite and like charges at rapidities y and y', and $\varrho(y, y')$ is their sum. In the AFS analysis, integration limits are chosen as $y_0 = 2$, and $y_{max} = 5$.

An equivalent expression for $\tilde{A}(y)$ can be obtained if one introduces the charge asymmetry $A(y, y') = 2P(y, y') - 1$, where $P(y, y')$ is the differential probability that two particles at y and y' have opposite charges. Then

$$\tilde{A}(y) = \int_{y_0}^{y_{max}} A(y, y') \cdot \varrho(y, y')dy' \int_{y_0}^{y_{max}} \varrho(y, y')dy'. \tag{6}$$

$\tilde{A}(y)$ ranges from -1 to $+1$, and measures the strength of the compensation of the charge of a test particle in the rapidity interval $y_0 - y_{max}$, per secondary particle at rapidity y.

Fig. 12a shows $\tilde{A}(y)$ as a function of y for positive and negative trigger particles.

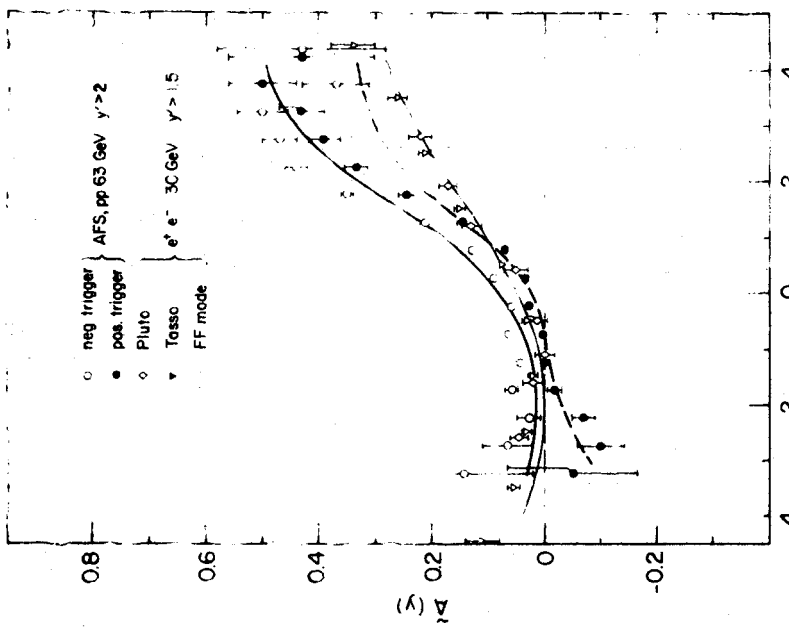

Fig. 12a

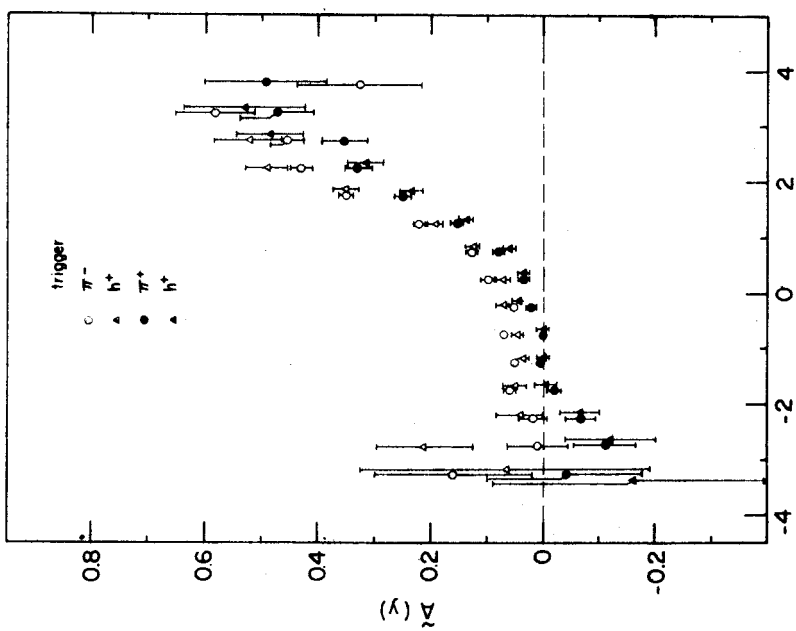

Fig. 12b

Fig. 12. a) Charge compensation $\tilde{A}(y)$ for positive and negative trigger particles in high p_T jets with $y' > 2$ in pp collisions at 63 GeV [70]. The lines show the prediction of the Lund model [52]. Also shown are data from e^+e^- collisions at ~ 30 GeV, with $y' > 1.5$ (measured along the jet axis) [77, 78], and the results of a corresponding calculation of $\tilde{A}(y)$ [78] in the Feyman Field model. b) $\tilde{A}(y)$ as a function of y for π^+, π^-, heavy positive (h^+) and heavy negative (h^-) trigger particles with $y' > 2$

The charge compensation on the trigger side is clearly larger for negative trigger particles than for positive trigger particles. The effect also extends to the away side, but here $\tilde{A}(y)$ is roughly symmetric around zero for positive and negative trigger particles, indicating that the effect is mainly a consequence of the overall larger density of positively charged particles. The following figures demonstrate that this is not the major contribution to the difference in $\tilde{A}(y)$ on the trigger side.

Fig. 12a also shows $\tilde{A}(y)$ for jets in e^+e^- collisions [77, 78]. Here the "trigger particle" has $y' > 1.5$, and the two charges are averaged. The e^+e^- data are well described by a calculation [78] using the Feynman-Field model for the mixture of quark types expected.

The average strength of $\tilde{A}(y)$ for positive and negative triggers in pp collisions is almost two times larger than the e^+e^- results for $y > 2$, however. From Monte Carlo studies it seems, that the most important source of this difference is due to the trigger bias effect, which means that jets of low multiplicity are primarily selected. Another contribution to the difference could be due to the different mixture of parton types available in pp collisions. In particular one expects the charge compensation to be large in gluon jets.

The result of a Monte Carlo simulation using the Lund model [52], is also shown on Fig. 12a. The general trend of the data is well reproduced, but the strength of $\tilde{A}(y)$ achieved in the trigger side jet is somewhat lower than in the data. This may in part be related to the fact that the model, with the choice of parameters given in [52], does not reproduce the particle ratios discussed in Section 4.2 (Figs. 9a, b) very well, especially for the heavy particles. It predicts constant ratios ($\pi^+/K^+/p = 0.65/0.175/0.175$ and $\pi^-/K^-/p^- = 0.70/0.15/0.15$) over the p_T range studied. As we shall see, different trigger particles have different strengths of $\tilde{A}(y)$, so that a wrong mixture of particle types will lead to an error in $\tilde{A}(y)$ for the general case.

Fig. 12b shows $\tilde{A}(y)$ as a function of y when the trigger particle is identified as $\pi^\pm$ or heavy$^\pm$ ($h \equiv \text{non}-\pi$). It shows that the charges of h^+ and h^- triggers are compensated with the same strength as the charges of π^+ and π^- triggers.

A similar observation is due to the CDHW collaboration [80]. They compare the fractional momentum distributions in jets with a π^+ and a h^- (called a K^-) leading particle, and conclude that the h^- jets are more neutral than the π^+ jets. From the AFS investigation we see that this is mainly due to the different charges of the two trigger particles.

Figs 13a, b, c and d show $\tilde{A}(y)$ as a function of y for the four cases when the trigger particle is identified as π or heavy particle, and the secondary particle, at rapidity y with respect to the jet axis, is also identified as a π or a heavy particle. In this case the away side is only covered to $y = -2.5$ for π's and $y = -1.5$ for heavy particles, due to the limited range of momenta where dE/dx identification can be applied.

Figs. 13a, b show that the charge compensation from secondary π's is about equal for positive and negative triggers. This is expected from isospin invariance. The slightly larger values of $\tilde{A}(y)$ for negative than for positive triggers, which may be noticed at close scrutiny, is probably a reflection of the overall excess of positive charge in the events.

A comparison of Fig. 13b and 13c, showing the compensation of the charge of heavy trigger particles by π's and of the charge of π triggers by heavy particles, indicates that the

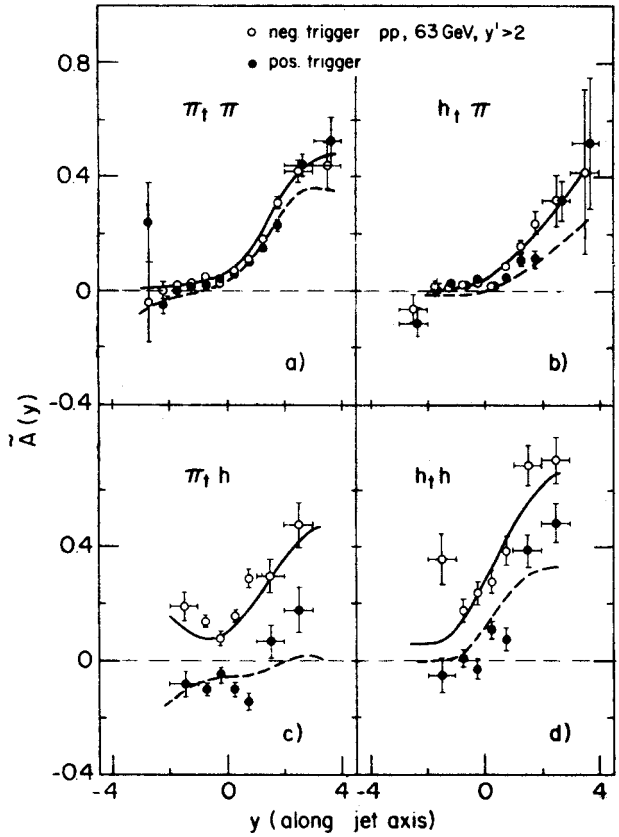

Fig. 13. Charge compensation $\tilde{A}(y)$ for a) π triggers, π secondaries, b) heavy ($\equiv$ non π) triggers, π secondaries, c) π triggers, heavy secondaries, d) heavy triggers, heavy secondaries. The trigger particle has $y' > 2$. Data from the AFS [70]. The lines show the prediction of the Lund model [52]

ordering of the particles in rapidity is decisive for the charge compensation. For π^+ triggers the charge compensation by heavy particles is close to zero, whereas it is strong for π^- triggers.

The charge compensation of heavy particle triggers by other heavy particles is strong for both signs, but substantially larger for negative than for positive triggers (Fig. 13d).

These features can be understood at a qualitative level from simple considerations of the "fragmentation" chains of scattered valence quarks or gluons, neglecting at first baryons and antibaryons.

Consider, as an example, the case of π triggers compensated by K's. A π^+ ($u\bar{d}$), containing a scattered u quark, can only be followed by a K^0 ($d\bar{s}$) in the chain, whereas a $\pi^-(d\bar{u})$ is most likely to be followed by $K^+(u\bar{s})$, leading to the qualitative difference in the strength of $\tilde{A}(y)$ seen in Fig. 13c.

In the case of K triggers compensated by K's, one would expect roughly equally strong charge compensation for K^+ and K^- triggers originating from scattered valence quarks.

A $K^+(u\bar{s})$ trigger can contain a scattered valence quark, and can be followed in the chain by a $\bar{K}^0$ or a K^-. A $K^-(\bar{u}s)$ trigger has no valence quark in common with the protons, but can be a promoted second rank meson following a $K^+(u\bar{s})$ or a $K^0(d\bar{s})$ in the chain (in agreement with the fact that the K^-/K^+ ratio is a falling function of p_T at large p_T).

Also for K's originating in gluon jets, one would expect about equally strong compensation of the charge of a leading K^+ or K^-. Because the gluon jets are neutral, one expects a stronger charge compensation than in the case of quark jets. If, as has been suggested [80], K^- triggers preferentially originate from scattered gluons, this could lead to a larger value of $\tilde{A}(y)$ for K^- triggers than for K^+ triggers.

All of the features seen in Fig. 13a–d are reproduced rather well by the Lund model, as shown by the lines on the figures. The only noticeable difference from the data is a systematically too low value of $\tilde{A}(y)$ for positive trigger particles and $y > 2$.

The points discussed can be elaborated further on the basis of the data shown in Fig. 14. With some loss of statistics, heavy particles can be further identified as K or $p/\bar{p}$. Figs. 14a–h show $\tilde{A}(y)$ vs. y for π triggers with associated K's and $p/\bar{p}$'s, and for K and $p/\bar{p}$ triggers with associated π's, K's and $p/\bar{p}$'s.

Figs. 14a and 14c are in agreement with the interpretation of Figs. 13c and 13d given above, but with less statistical significance.

The compensation of the charge of π and K triggers by $p/\bar{p}$'s (Fig. 14b and d), show at first sight strong effects. $\tilde{A}(y)$ seems to be independent of y, however, and the values can be understood simply from the observation that in these events the $p/\bar{p}$ ratio at low p_T in the central region is close to the value 1.6 observed in minimum bias events [79]. This in itself gives rise to constant contributions to $\tilde{A}(y)$ at -0.24 for π^+ and K^+ triggers, and at $+0.24$ for π^- and K^- triggers, and these values are roughly consistent with the data.

Associated production of K's with hyperons will in general give negative contributions to $A(y)$ for Kp and pK (Fig. 14d and h). Since this production mechanism is more important for K^+ than for K^- in pp collisions, the effect should be most noticeable for positive triggers (whether K^+ or p). Although no evidence is visible for this effect in the data of Fig. 14, it could still give a contribution to the difference in the strength of the charge compensation of h^+ and h^- by h seen in Fig. 13d.

The Lund model predicts very strong K^+K^- and $p\bar{p}$ correlations. Although the data may follow this trend (Figs. 14c and h), the effect does not seem so strong. For the $\bar{p}p$ case this is brought out clearly when one considers the $p/\bar{p}$ ratio at low p_T with p or $\bar{p}$ triggers. This is found to be $1.13 \pm 0.25/1.30 \pm 0.30$ with a high p_T $p/\bar{p}$ trigger whereas the model predicts values of $0.40 \pm 0.04/5.7 \pm 0.7$.

The qualitative features observed in the charge structure of the trigger side jet cannot be understood simply in terms of correlations stemming from resonance production at hight p_T. This is in particular the case for the compensation of the charge of π triggers by K's, which from resonance effects would be equally strong for positively and negatively charged triggers.

Another example of the strong local compensation of quantum numbers in the trigger side jet is shown in Fig. 15 [80]. It shows the ratio of K_s^0's to charged particles as a function of the fractional momentum component z_F along the trigger particle direction

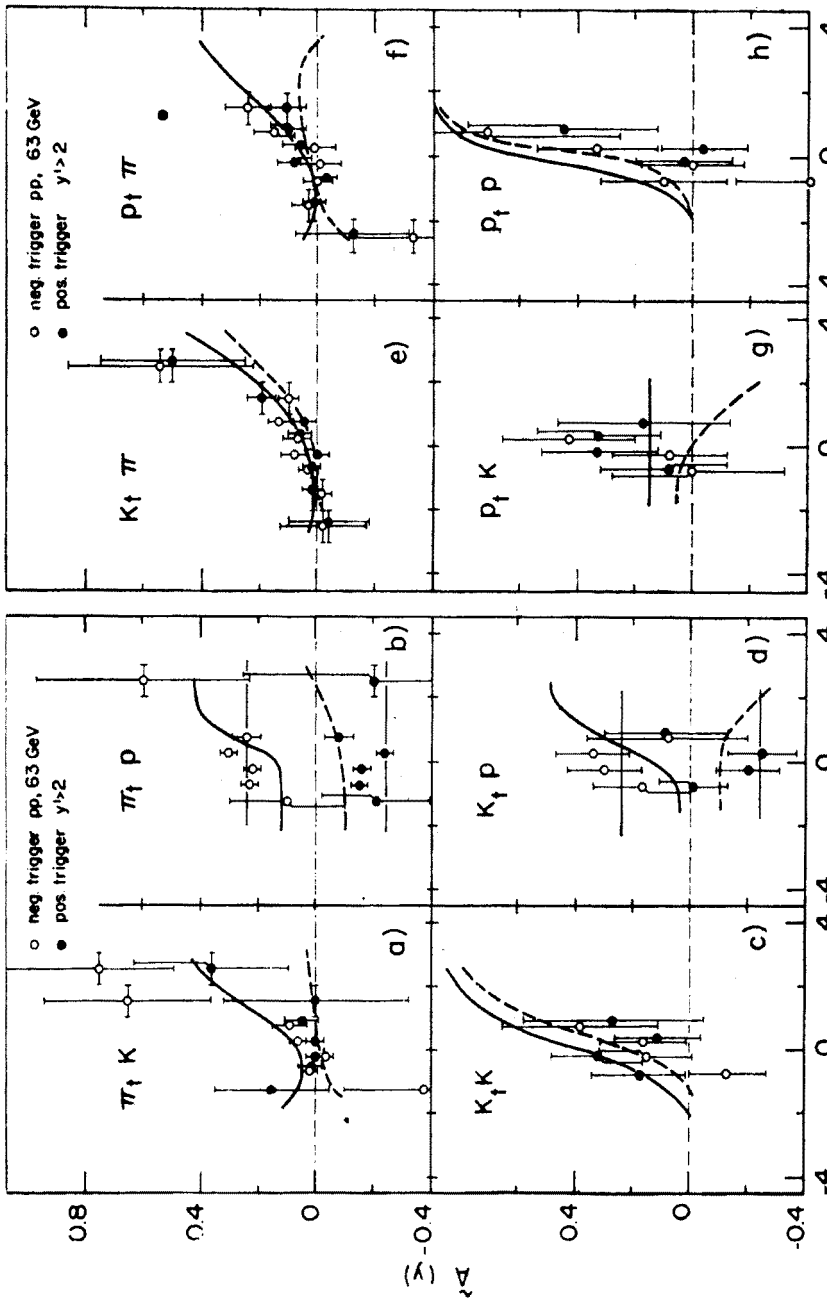

Fig. 14. Charge compensation $\tilde{A}(y)$ for a) π triggers, K secondaries, b) π triggers, $p/\bar{p}$ secondaries, c) K triggers, K secondaries, d) K triggers, $p/\bar{p}$ secondaries, e) K triggers, π secondaries, f) $p/\bar{p}$ triggers, π secondaries, g) $p/\bar{p}$ triggers, K secondaries, h) $p/\bar{p}$ triggers, $p/\bar{p}$ secondaries. The trigger particle has $y' > 2$. Data from the AFS [70]. The lines show the prediction of the Lund model [52]

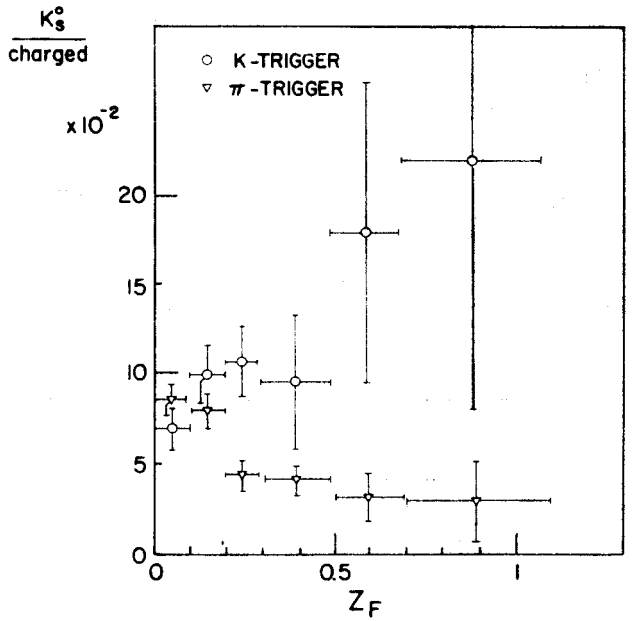

Fig. 15. Ratio of K_s^0 and charged particles as a function of z_F for events with a high p_T K and π. Data from CDHW [80b]

$tz_F = \vec{p} \cdot \vec{p}_{trig}/p_{trig}^2$), for K and π triggers near $\theta = 50°$. The larger K_s^0/charged ratio in K (riggered events indicates a local conservation of strangeness in the event.

These observations constitute evidence for the cascade picture of jet formation, or for a similar mechanism leading to a rank ordering of the produced particles. This is exemplified in the good overall agreement with the predictions of the Lund model, which in this context may be taken as a representative cascade model for the jet formation.

The Lund model, with the set of parameters used, seems to have some difficulties with the baryon production, both at low and high p_T.

4.5. The away side jet

In an interesting analysis [80], the CDHW collaboration uses data obtained at the Split Field Magnet to discuss the general structure of events with a high p_T particle. They focus in particular on the possibility of using an identified high p_T particle (π^+, K^-, etc.) as a tag to disentangle contributions from various hard parton subprocesses. Only a few points from the analysis will be mentioned here.

Fig. 16a shows the rapidity distributions of same side ($|\varphi| < 25°$) and away side ($|\varphi - 180°| < 25°$) particles with $p_T > 1$ GeV/c in pp events at $\sqrt{s} = 62$ GeV, with a trigger particle (unidentified) of $p_T = 2{,}4$ and 6 GeV/c. As p_T of the trigger particle is increased, the broad away side enhancement, averaging the away side jets which fluctuate in direction, becomes larger, and a pronounced asymmetry around $y = 0$ develops. This is not just a consequence of kinematics, as shown by Fig. 16b, which demonstrates that the

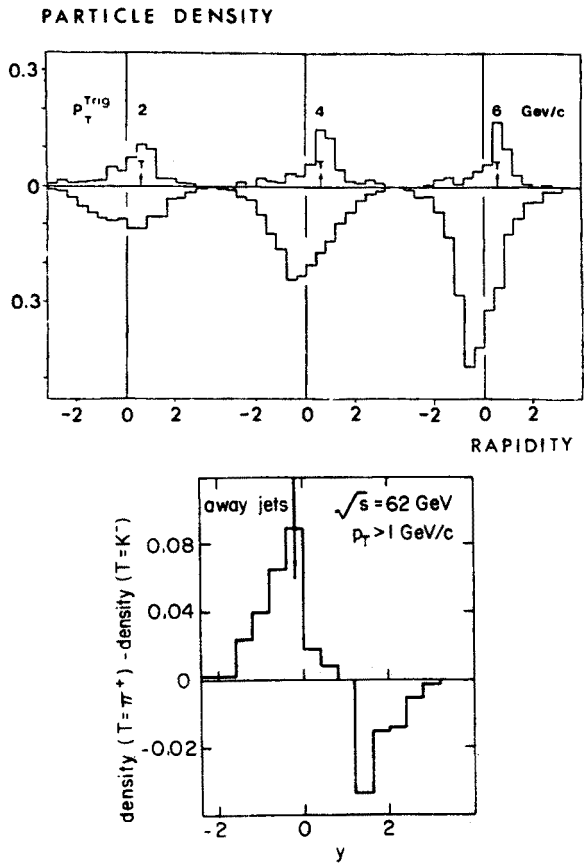

Fig. 16. a) Rapidity distribution on the toward ($|\varphi| < 25°$) and away ($|\varphi - 180°| < 25°$) side of particles with $p_T > 1$ GeV/c, in bins of p_T^{Trig}. b) Difference between the away side rapidity distributions for a π^+ and a K^- trigger with $p_T^{Trig} > 4$ GeV/c. Data for pp collisions at $\sqrt{s} = 62$ GeV, from [80]

away side rapidity distribution is different for a π^+ and a h^- (called K^-) trigger with $p_T^{trig} > 4$ GeV/c.

From a comparison of the z_F distributions of positive and negative particles in the trigger side jet with the Feynman-Field fragmentation model [36] the group concludes that their π^+ triggers originate from scattered u quarks.

If their K^- triggers similarly originate predominantly from scattered gluons, the different away side rapidity distributions for π^+ and K^- triggers can then be understood rather simply. Because the gluon x-distribution is more narrow than the valence quark distributions, and because quark-gluon scattering is expected to be an important part of the cross section at the x_T values obtained, selecting a gluon jet will more often select events of the "back-to-antiback" configuration (i.e. with the same sign for the rapidity of the trigger side jet and the away side jet), than selecting a quark jet.

Thus the asymmetry seen in Fig. 16b is taken as evidence, together with several other arguments, that K^- triggers at 50° select gluon jets with high efficiency.

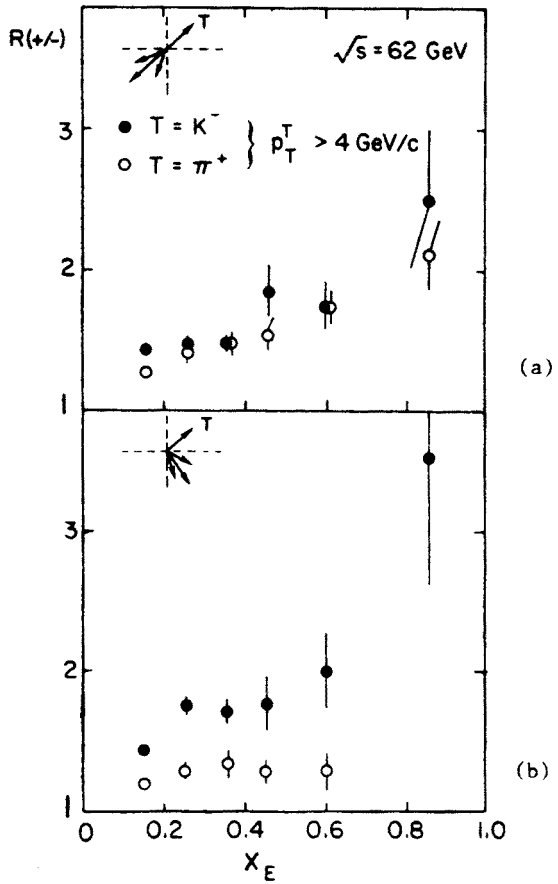

Fig. 17. Charge ratio, $R(+/-)$ of away side particles with a) $y < 0$, b) $y > 0$ as a function of $x_E = p_T/p_T^{Trig}$ for π^+ and K^- triggers at $\theta = 50°$ with $p_T^{Trig} > 4$ GeV/c. Data for pp collisions at $\sqrt{s} = 62$ GeV, from [80]

The charge ratio, $R(+/-)$, in away side jets is shown in Fig. 17 as a function of x_E (here defined as p_T/p_T^{trig}), for secondaries with $y < 0$ ("back-to-back") and $y > 0$ ("back--to-antiback") [80]. In the back-to-back configuration, $R(+/-)$ is about equal for π^+ and K^- triggers, and increases towards $R(+/-) = 2$ for $x \to 1$, consistent with the expectation for scattered valence quarks.

In the back-to-antiback configuration, $R(+/-)$ for π^+ triggers is significantly smaller, although still larger than unity. This could be due to a larger admixture of gluon jets, which would be more favoured kinematically.

For K^- triggers, $R(+/-)$ in the back-to-antiback configuration is significantly larger than for π^+ triggers showing that processes other than quark-quark scattering via gluon exchange must contribute. Furthermore the value of $R(+/-)$ suggests that scattered valence quarks are a major source of the away side jets. This indicates, on a kinematical basis, that the parton yielding the trigger particle has a softer structure function than quarks, pointing again to gluons as a major source of K^- triggers.

The CDHW analysis shows that the interplay between kinematics and different structure functions for the different constituents can generate quite subtle effects, when coupled with different trigger requirements.

In order to be able to appreciate more fully this nice analysis of the origin of the trigger side and away side jets under different conditions, one would, however, like to have a more systematic comparison of the various types of trigger particle, i.e. including also π^-, K^+ and possibly p, $\bar{p}$.

4.6. Direct photons

In lowest order QCD, the basic mechanisms giving rise to direct photons at high p_T are the so-called gluon Compton scattering (Fig. 18a) and quark-antiquark annihilation into γg (Fig. 18b) [43]. In addition, electromagnetic bremsstrahlung of a photon from a quark may of course contribute (as e.g. Fig. 18c).

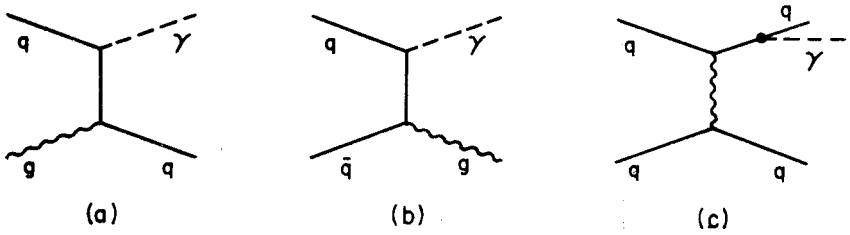

Fig. 18. Some diagrams contributing to direct photon production at high p_T

The importance of direct photon production in hadronic interactions stems from the fact that the photon comes directly from a (calculable) subprocess at the parton level, thus bypassing the need for phenomenological models of hadronization to treat the process. Furthermore it enters into the process with a known coupling.

The predicted cross section for gluon Compton scattering — which is expected to be the dominant source of direct photons at large angles in pp collisions — is much smaller than the cross section for parton-parton scattering giving rise to jets. Nevertheless, the γ/π^0 ratio is predicted to be large, of order 0.1–1 in the p_T range 4–12 GeV/c. This is because π^0 is normally the fragmentation product of a parton which therefore has to be produced at a higher momentum, whereas the photon momentum does not undergo this degradation.

The first measurements [44] of single photon production suffered fromi nstrumental biases, which permitted only the ratio γ/π^0 to be extracted.

For the ABC collaboration at the ISR [44a] this included a cut on unassigned energy in their calorimeter, and a requirement that no additional shower was detected in the calorimeter. Last year, the collaboration used information from the AFS central drift chamber, which was installed at the same ISR intersection for the last part of their data taking, to evaluate the effect of these biases and extract the inclusive cross section for single γ production in pp collisions at $\sqrt{s} = 63$ GeV [81]. This is shown in Fig. 19, which

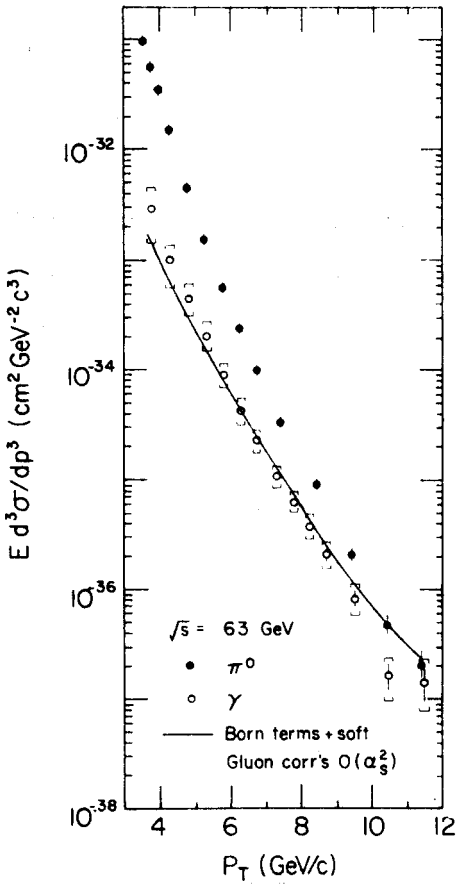

Fig. 19. The inclusive cross section for single γ and π^0 production in pp collisions at $\sqrt{s} = 63$ GeV and $\theta \simeq 90°$, as functions of p_T [81]. The line represents a calculation of the single γ cross section in lowest order QCD, including various corrections [82]

also shows the inclusive π^0 cross section in the same p_T range (3–12 GeV/c), now obtained for π^0's where the two photons are fully resolved.

Calculations based on the CIM model [43f] are in disagreement with these data, predicting a higher γ/π^0 ratio at low p_T than observed. Also the first QCD calculations [e.g. 43e] were only in qualitative agreement with the data. In a more recent calculation [82], which includes effects of soft gluon radiation, the authors find that a normalization factor of $K' = 1.7$ has to be applied to the lowest order calculation. The result is shown in Fig. 19, and describes the data well.

The correction procedure used to obtain the single inclusive cross section from the γ/π^0 ratio could not be applied at ISR energies different from 63 GeV because the drift chamber had not been installed during the data taking at these energies. If one assumes however, that the correction at $\sqrt{s} = 45$ GeV is similar to that at 63 GeV, it is possible to extract the inclusive cross section at this energy from the measured γ/π^0 ratio and the π^0

cross section [83]. Assuming a form as Eq. (1), one finds that scaling is well satisfied with $N \simeq 6$. This is demonstrated in Fig. 20, which shows the cross sections at the two energies, multiplied by p_T^6, as functions of x_T. A recent experiment at Fermilab [84] also finds clear evidence for direct photons in pC and π^+C collisions, and finds that the energy dependence when compared with ISR results can be parametrized as Eq. (1), with $N = 6.6 \pm 0.3$.

These results suggest that the deviation of the power $N = 8$, found for π production at large p_T, from the naively expected $N = 4$, is not only caused by scale breaking of the

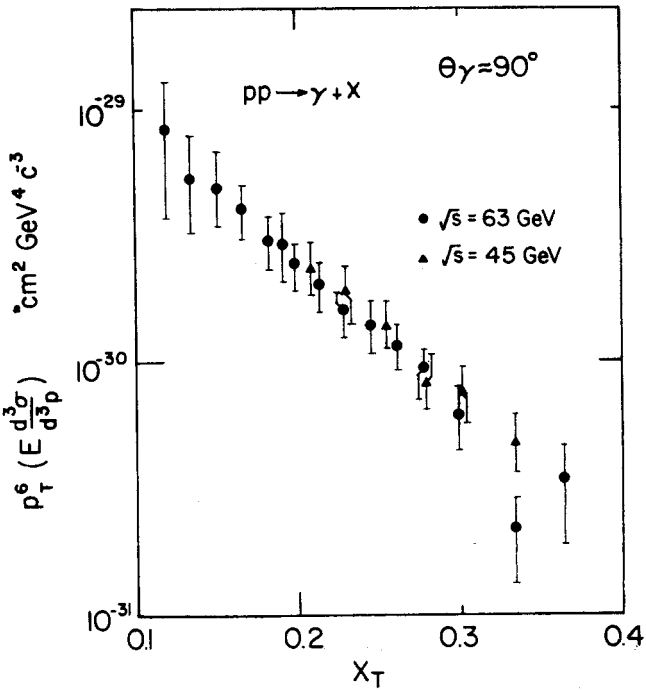

Fig. 20. Inclusive cross sections for single γ production at $\sqrt{s} = 45$ and 63 GeV multiplied by p_T^6, as functions of x_T [83]

structure functions, and the smearing due to the parton transverse momentum, k_T, but also by scale breaking in the fragmentation process.

Notice also, that $N = 6$ is the expectation from the simplest CIM type process giving rise to direct γ's, $Mq \to q\gamma$, even though the CIM does not predict the γ/π^0 ratio correctly.

Earlier measurements of direct γ production have all been at $\theta \simeq 90°$. Recently the γ/π^0 ratio has been measured at $\theta = 11°$ in pp collisions at 63 GeV [85], at a value consistent with measurements at 90° up to $p_T = 4$–5 GeV/c.

New data on the structure of events with a single proton have come from the AFS collaboration [86]. In such events, several distinct signatures are expected [87]. 1) As contributions from bremsstrahlung (Fig. 18c) are expected to be small, the photon will most often not have an accompanying jet. 2) In pp collisions the dominant subprocess is expected to be gluon Compton scattering (Fig. 18a). Because the photon couples more strongly

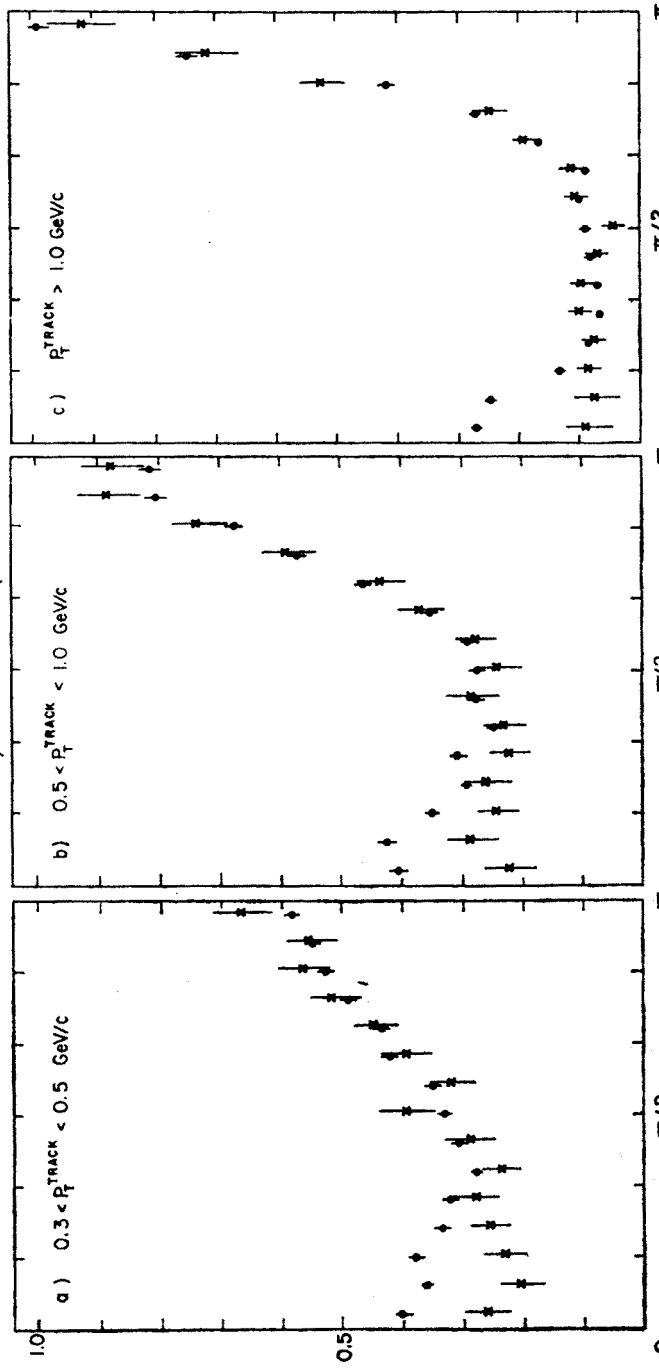

Fig. 21. Distribution of the difference in azimuth ($\Delta\varphi$) between a γ or π^0 trigger in pp collisions at 63 GeV and a charged track, for $p_T^{Trig} > 4.5$ GeV/c. The trigger particle is at $y = 0$, and the charged tracks are restricted to $|y| < 0.8$. Data from the AFS [86]

to a u quark than to a d quark, the away side jet is expected to be mostly initiated by u quarks, and hence have a larger $+/-$ ratio than in events with a π^0 trigger.

The charged particle density as a function of $\Delta\varphi$ from the trigger particle (γ or π^0) is shown in Fig. 21. On the away side ($\Delta\varphi > \pi/2$) the densities are about equal for π^0 and γ triggers, whereas the density on the trigger side ($\Delta\varphi < \pi/2$) is significantly lower for events with a γ than for events with a π^0. In the γ events, the particle density is consistent with being independent of $\Delta\varphi$ up to $\Delta\varphi = \pi/2$. This is in agreement with the expectation

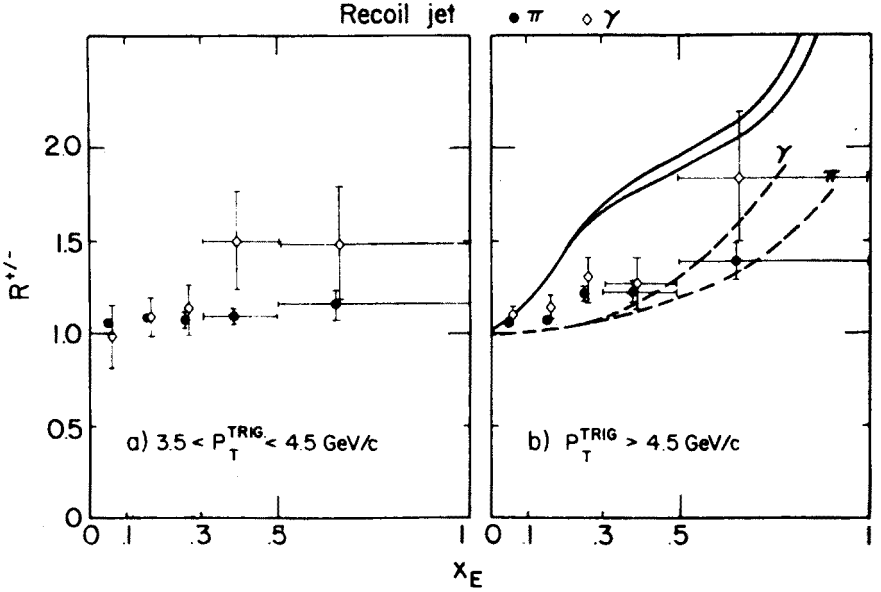

Fig. 22. $R^{+/-}$ for away side particles within $|y| < 0.8$ as a function of x_E in events triggered by a γ or a π^0 [86]. The full lines represent a calculation by Halzen et al. [87] for γ triggers with $p_T = 6$ GeV/c, and the broken lines represent a calculation by Benary et al. [88]

from gluon Compton scattering, and has been used by the group to extract an upper limit [116] of 30% (2σ) for the relative importance of bremsstrahlung from a scattered quark as a source of the direct γ's.

The positive to negative ratio, $R^{+/-}$, on the away side in events with a high p_T γ or π^0 is shown in Fig. 22 as a function of x_E. The data do show systematically larger values of $R^{+/-}$ for γ triggered events than for π^0 triggered events, but with marginal statistical significance. This is an example of an important measurement which will unfortunately not be improved in the foreseeable future due to lack of running time before the ISR is closed down by the end of this year.

The lines show lowest order QCD calculations by Halzen et al. [87] and a more recent calculation by Benary et al. [88]. While the latter agrees reasonably well with the data, the large difference between the calculations shows that the result is quite sensitive to the details of the fragmentation model used.

As stated earlier, a comparison of direct γ production in pp and $\bar{p}p$ collisions would be very interesting.

5. *Large transverse energy and jets*

In this section we shall address the question of the shape of highly inelastic events, and review the recent measurements of the inclusive cross section for high p_T jet production at the ISR and SPS $\bar{p}p$ colliders.

Highly inelastic hadron collisions, defined as collisions where a large transverse energy, $\sum E_T = \sum \sqrt{p_T^2+m^2}$, is emitted, are of interest in the systematic investigation of hadronic many body reactions. Their topical interest at present comes from the expectation that they might provide a particularly unbiassed way of studying hard constituent interactions.

In experiments based on large solid angle calorimeters, $\sum E_T$ is often denoted E_T (for no good reason).

5.1. The shape of highly inelastic events

Let us start by briefly reviewing the NA5 results [46] alluded to in Section 2. The cross section for emission of a transverse energy E_T into the rapidity range $-0.88 < y < 0.67$ in pp collisions at 300 GeV/c ($\sqrt{s}$ = 24 GeV) is shown in Fig. 23 as a function of E_T. Three different ranges of azimuth are selected: $\Delta\varphi = \pi/2$ ("jet trigger"), two back-to-back regions of each $\Delta\varphi = \pi/2$, and $\Delta\varphi = 2\pi$. In the analysis of NA5 it was found that a simple two-constituent scattering model (see Section 3.1), although it agreed within a factor 2 with the cross section observed for the first two triggers, failed by an order of magnitude to explain the $\Delta\varphi = 2\pi$ cross section. A low p_T cluster model agreed quite well with the data to substantial values of E_T, however, as shown by the dashed lines on the figure.

Also the event shape did not agree with expectations from the jet model (nor with the low p_T cluster model). The event shape can be studied e.g. in terms of a quantity P, called planarity, which is defined as

$$P = \frac{a-b}{a+b}, \tag{7}$$

where a and b are the sums of the squares of the components of the transverse momenta along the major and minor principal p_T-axes (see Appendix A). The planarity measures the shape of the distribution of the momentum vectors in the transverse plane, and is ~ 0 for an isotropic distribution, and ~ 1 for narrow, back-to-back jets. Fig. 24 shows the planarity distribution for $E_T > 10$ GeV, together with predictions from the low p_T cluster model and the two-constituent scattering model by NA5. Both models disagree with the data.

Also the shape of the events selected by the $\Delta\varphi = \pi/2$ trigger differs from the predictions of the hard scattering model, although the cross section is well reproduced. In particular, the particle density at 90° to the trigger direction in azimuth is larger than expected.

Both the cross section and the planarity distributions are quite well described by the QCD shower model of Ref. [56], when hadronization is taken into account. This is shown in Figs. 23 and 24. Fig. 23 also shows that the cross section in the model without hadronization (but still including gluon bremsstrahlung) is a factor ~ 10 below the data for $\Delta\varphi = 2\pi$. This illustrates the fact that in the model, transverse energy is built up in all

phases of the interaction, when a large solid angle trigger is employed. Within the framework of this and similar [57] models, the large solid angle trigger at this collision energy and E_T essentially selects events which have had a lot of gluon bremsstrahlung, leading to a large multiplicity of hadrons, with a fairly isotropic distribution in the transverse plane.

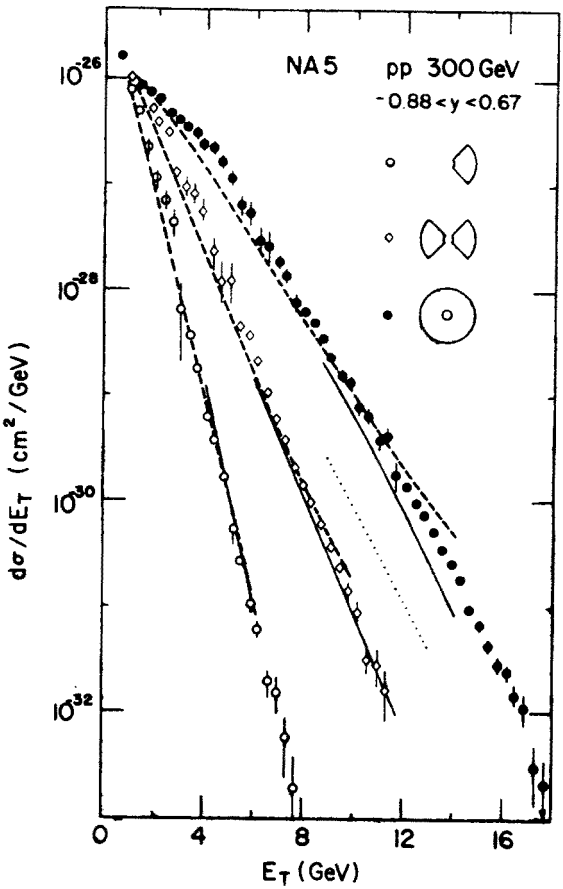

Fig. 23. Cross sections $d\sigma/dE_T$ vs. transverse energy E_T in the interval $-0.88 < y < 0.67$ for three regions of azimuthal acceptance in 300 GeV pp reactions [46]. The dashed lines show the results of a low p_T cluster model calculation by NA5. The full lines show the result of a QCD shower model [56] with hadronization. The dotted line shows the result of the same model at the parton level for the $\Delta\varphi = 2\pi$ case

Over the last year or so, it has, however, become clear that the expected dominance of jet production in highly inelastic collisions is indeed seen, when the required transverse energy and the collision energy are sufficiently large. Jets have been clearly observed as dominant structures at both ISR and $\bar{p}p$ collider energies.

As an illustration, Fig. 25 shows an event from the 1981 collider run. This was the highest transverse energy event in the UA2 experiment at the time of the Paris conference [89]. The total E_T in a $(\Delta\eta, \Delta\varphi)$ range of (2,300°) is 127 GeV, out of the CMS energy

$\sqrt{s}$ = 540 GeV, and the two jet structure is evident from the display of the event[5]. We shall return to the collider results below.

At the ISR, the first calorimeter based investigation of events at large E_T used the top quarter of the AFS Uranium/scintillator calorimeter (see Fig. 5), covering a (y, φ) range of $|y| < 0.93$, $\Delta\varphi = 69°$ [90]. The raw (i.e. uncorrected for resolution etc.) E_T spectrum observed in ~ 7 hrs of running covers almost 8 orders of magnitude at $\sqrt{s}$ = 63 GeV, and is shown in Fig. 26 in cross section units.

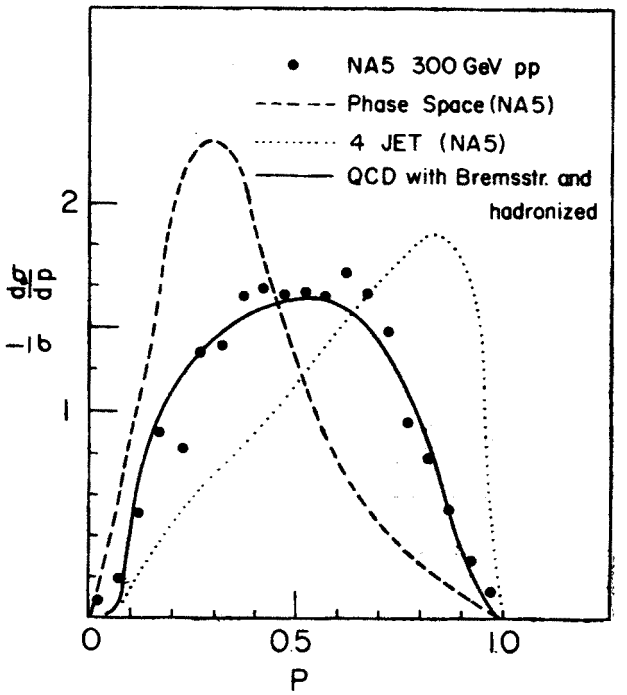

Fig. 24. Distribution of planarity, P, for particles with a total transverse energy $E_T > 10$ GeV in the rapidity interval $-0.88 < y < 0.67$. Data from NA5 [46]. Also shown are the predictions of the NA5 low p_T cluster model, of their simple two-constituent hard scattering model ("4-jet"), and of the QCD shower model of R. Field et al. [56]

After timing cuts to reduce overlapping events and other background, and the requirement that a primary vertex could be formed by the charged tracks recorded in the central drift chamber, the remaining events (~ 70%) were analysed in the following way: Clusters of energy deposition in the calorimeter (each typically corresponding to $O(1)$ incident particle) were ordered in E_T, and clusters with $E_T < 0.025$ GeV were rejected. The vector sum, $\vec{E}'$, was formed of the ordered clusters making up 80% of the total E_T in the calorimeter wall. $\vec{E}'$ was required to point inside a fiducial region $(|\varphi - \varphi(\text{centre})| < 25°$,

[5] At the time of writing, the highest E_T event recorded by UA2 has E_T = 250 GeV (CERN Courier Oct. 1983).

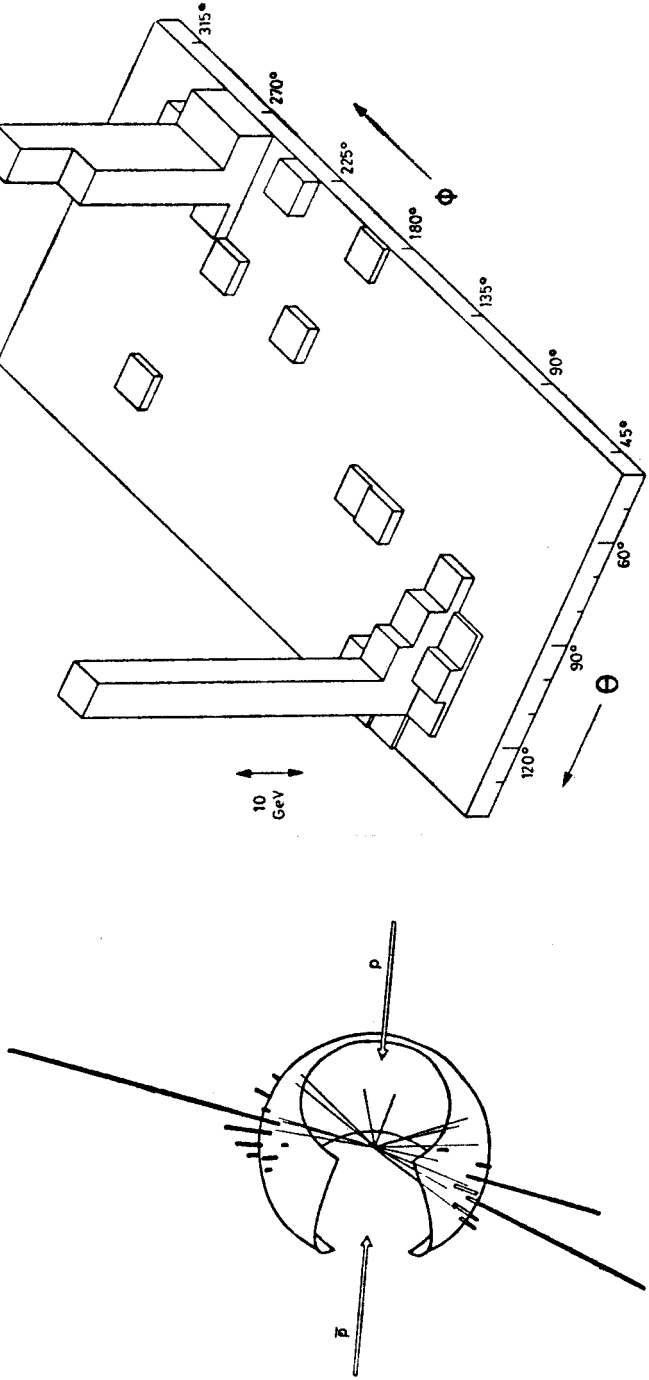

Fig. 25. Display of the highest transverse energy event registered by the UA2 experiment in the 1981 $\bar{p}p$ collider run. E_T = 127 GeV and the mass of the two-jet system is 140 GeV/c^2 [89]

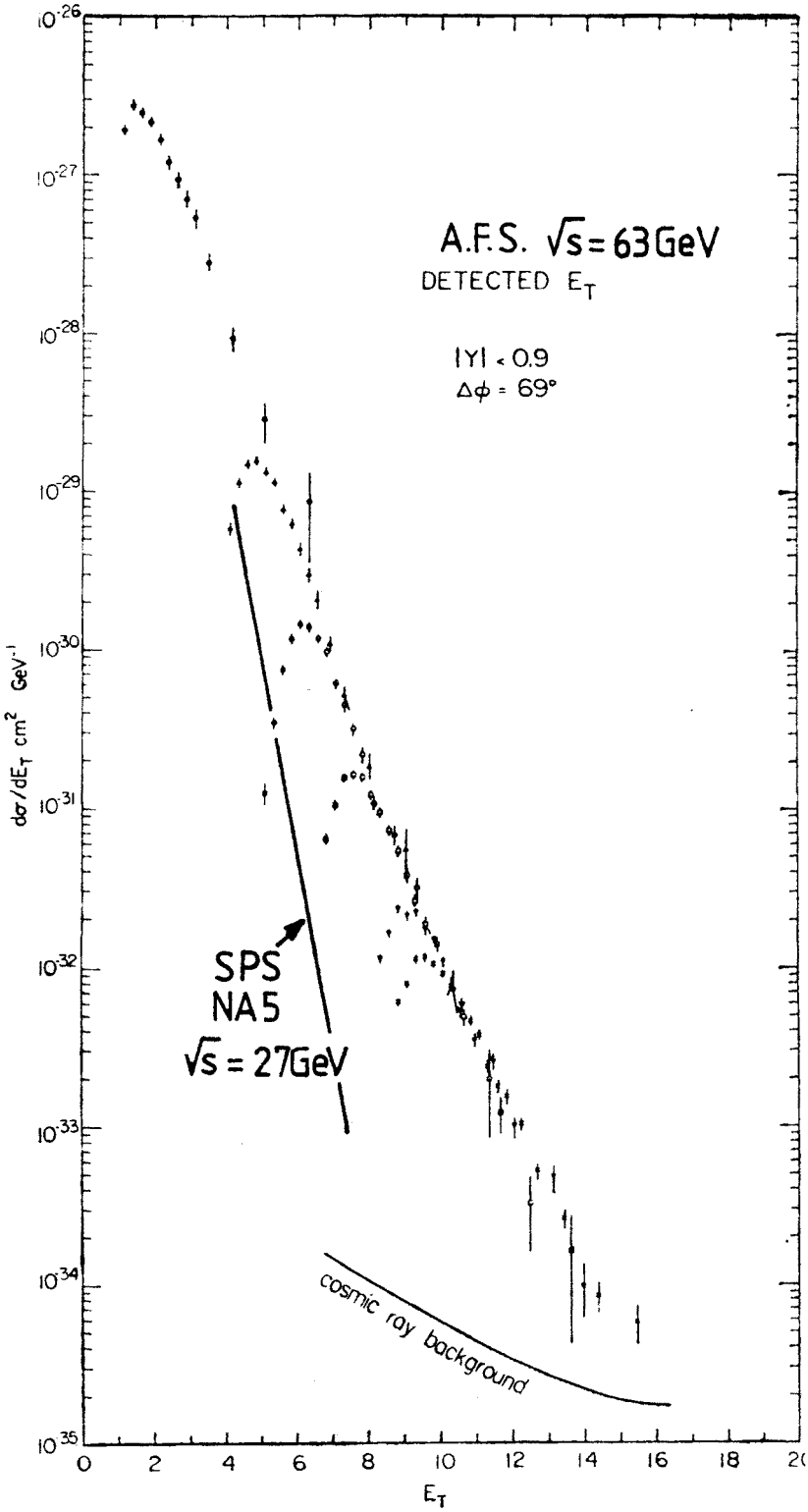

Fig. 26. $d\sigma/dE_T$ into a 1.7 sr calorimeter, uncorrected for resolution, in pp collisions at $\sqrt{s} = 63$ GeV. An estimated limit for background from cosmic rays is indicated. Data from [90]

$|y| < 0.5$) to avoid edge effects in the calorimeter. Finally a quantity T was calculated:

$$T = \sum_i |\vec{E}' \cdot \vec{E}_i| / \sum_i |\vec{E}'| \cdot |\vec{E}_i| \tag{8}$$

using all the clusters, with energy vectors $\vec{E}_i$ defined by their energy deposition and direction. T is closely similar to the thrust variable (see Appendix A) used in e^+e^- analysis, but

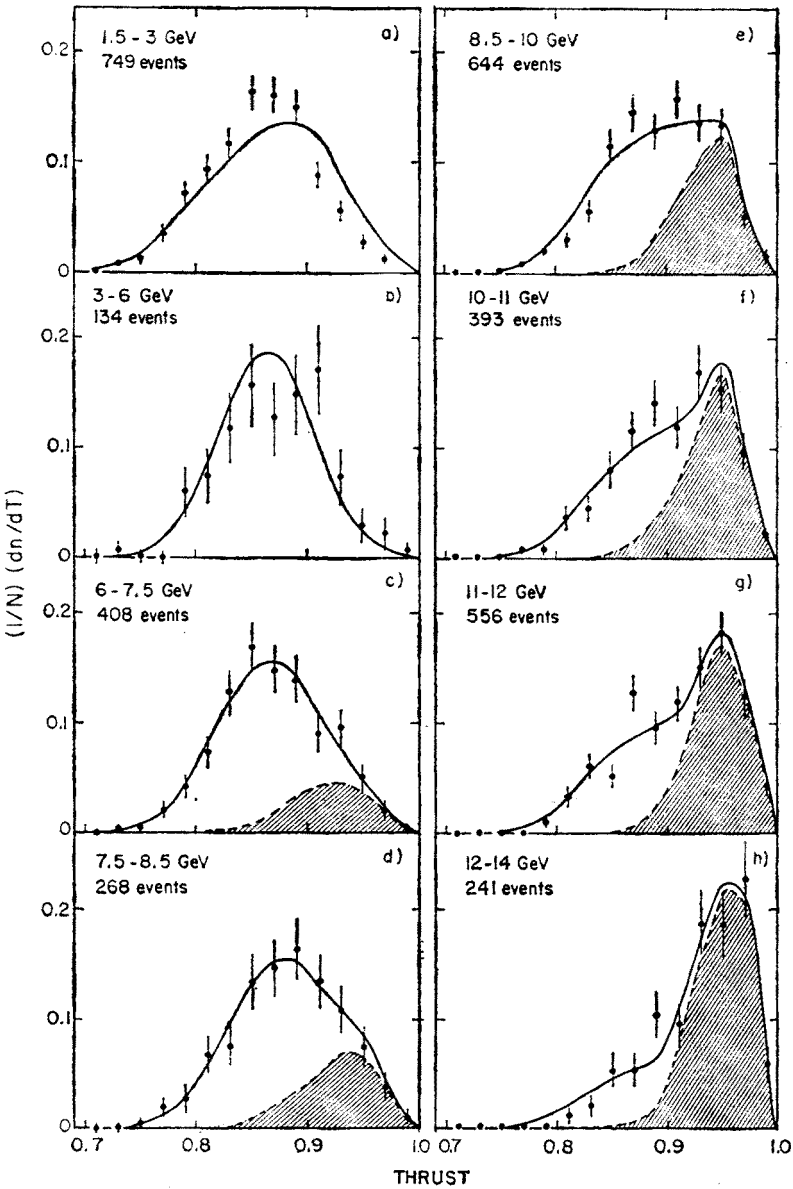

Fig. 27. Thrust distribution in 8 bins of transverse energy, E_T, into a 1.7 sr calorimeter. Data from pp collisions at $\sqrt{s} = 63$ GeV [90]. The curves and shaded areas refer to a fit described in the text

is not maximized explicitly by variation of the $\vec{E}'$ direction. For the solid angle covered by the calorimeter, T can take values between 0.7 and 1.0, being close to 1.0 for a narrow jet.

The distribution of T is shown in Fig. 27 in bins of the total E_T. For low E_T the distribution is wide, peaking around $T = 0.85$, which corresponds to a wide, unstructured particle distribution. For $E_T \gtrsim 8$ GeV a clear change in the distribution occurs, and at the highest E_T, it is dominated by a narrow peak between 0.9 and 1.0. This change in the T distribution is interpreted as evidence for the emergence of jets at high E_T. Indeed, a "typical" event with an E_T in the calorimeter wall of 14 GeV, shown in two projections in Fig. 28, illustrates nicely the quality of the jets now seen at the ISR.

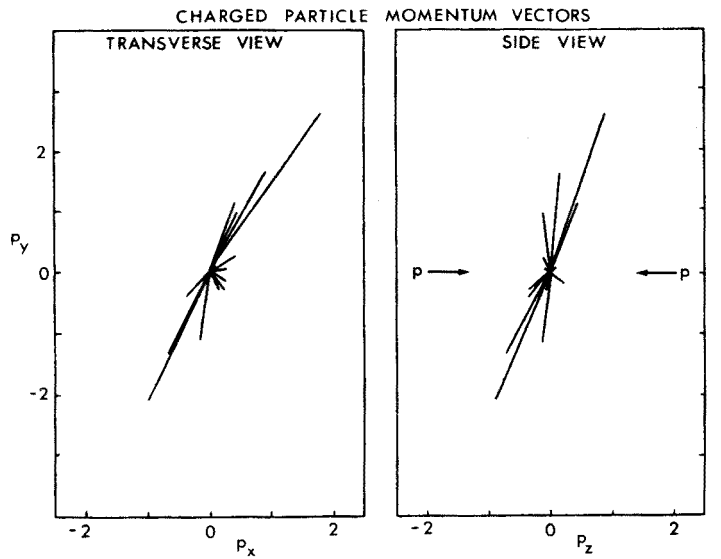

Fig. 28. Charged particle momentum vectors of an event with $E_T = 14$ GeV into a wall of the AFS calorimeter covering $55° < \varphi < 125°$ and $|y| < 0.93$ [90]. It has T(roof) = 0.97. Tracks with $|y| \gtrsim 1$ are not recorded

The conformity of this interpretation with the knowledge about jet structures gained earlier at the ISR has been checked by a study of the distribution of the charged tracks registered in the central drift chamber in the events with large E_T [90b]. As an example, Fig. 29 shows the so-called transverse energy "flow", i.e. the azimuthal distribution (measured from the $\vec{E}_T$ axis) of the transverse energy carried by charged particles, plotted in bins of the E_T in the calorimeter wall. The narrow peak at $\Delta\varphi = 0°$ corresponds to the trigger jet. Another somewhat wider peak develops at $\Delta\varphi = 180°$, corresponding to the recoil jet, which at high E_T is often inside the acceptance of the apparatus. At $\Delta\varphi \sim 90°$ the distribution is flat, and decreases with E_T, consistent with a small, roughly constant contribution from the rest of the event.

The T distributions shown in Fig. 27 could be understood to some extent in the framework of a rather standard 4-jet model for high p_T scattering, implemented in the Monte

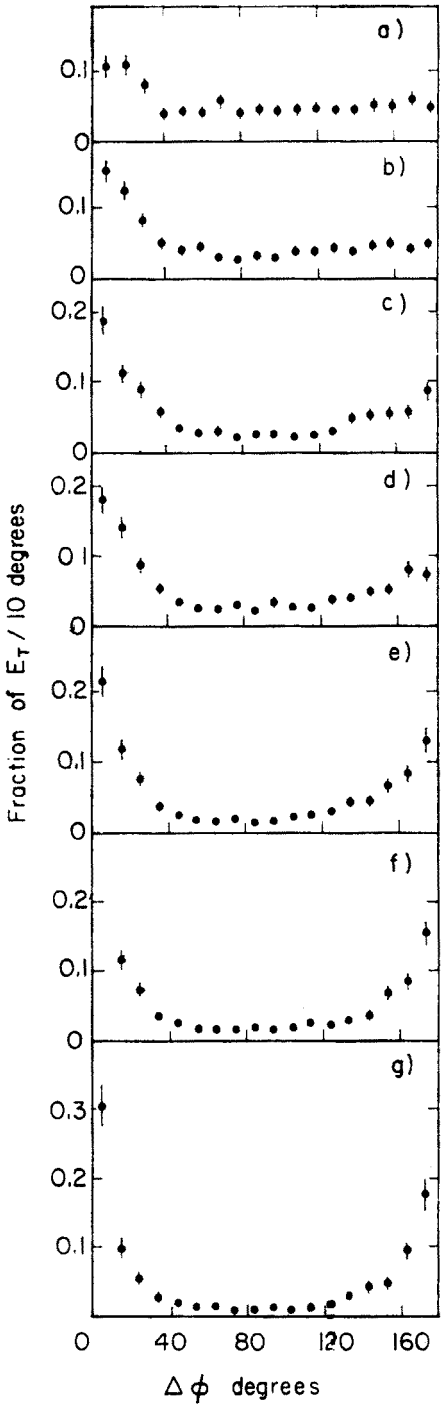

Fig. 29. Fraction of transverse energy carried by charged particles per 10° $\Delta\varphi$ bin. $\Delta\varphi$ is measured with respect to the $\vec{E}'$ axis (see text) in the roof calorimeter, and the plots represent bins of E_T in the calorimeter: a) 1.5–3 GeV, b) 6–7.5 GeV, c) 7.5–8.5 GeV, d) 8.5–10 GeV, e) 10–11 GeV, f) 11–12 GeV and g) 12–14 GeV. Data from [90]

Carlo program ISAJET [91]. In the model, the basic parton parton scattering is described by lowest order QCD, and the scattered partons may emit hard gluons. The fragmentation of the scattered partons (including the spectators) is treated in the Feynman-Field parametrization. For the purpose of this analysis, the program was modified to include a primordial k_T of 0.88 GeV/c (FWHM) of the incoming partons. ISAJET also provides a model for minimum bias events which contains leading baryons, short range rapidity correlations (through resonances) and approximate KNO scaling of the hadron multiplicity distribution. It has been tuned to reproduce the observed ISR and SPS collider multiplicities.

At low E_T, the ISAJET model for minimum bias events described the T distribution well, as shown by the line in Fig. 27a. At higher E_T, the 4-jet model described the peak at high T well, as evidenced by the shaded areas in Fig. 27, but it failed to account for the full distribution. A sum of two contributions, a minimum bias-like, and a hard scattering part, gave a good description of the data, however. (Full lines in Fig. 27.)

Such a two component model has little theoretical justification, but may be used as a convenient parametrization, in part suggested by the data, to extract the cross section for jet production. The result of this will be discussed in the next section. At the same time it is clear that a better understanding of the full shape of the T distributions would be very

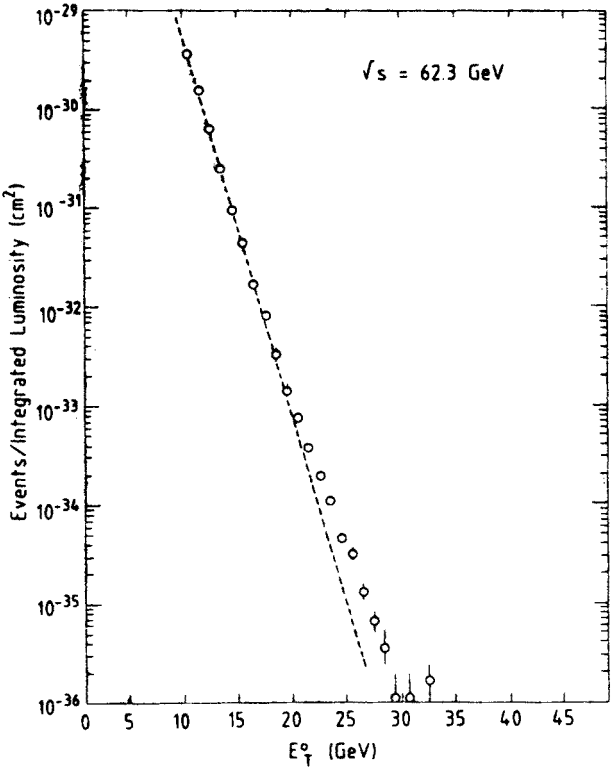

Fig. 30. Spectrum of detected neutral transverse energy, E_T^0, in pp collisions at $\sqrt{s} = 63$ GeV. For the (φ, y) coverage, see text. The spectrum is uncorrected for resolution, etc. [92]

welcome. At present it does not seem unlikely that the parton shower model is capable of this.

Results on the shape of events with large E_T in calorimeters covering $\Delta\varphi = 2\pi$ have come from two ISR experiments.

The COR collaboration uses arrays of lead glass blocks and shower counters to select events with a large E_T^0 mostly carried by γ's or neutral particles with electromagnetic decay (π^0, η, ...) [92]. The (φ, y) coverage is somewhat uneven, the four shower counter modules each covering (50°, ± 1.1) and the two lead glass arrays each covering (57°, ± 0.6).

The spectrum of detected E_T^0 (uncorrected for resolution, etc.) is shown in Fig. 30. It is close to an exponential, with a slope of $-0.89\ \mathrm{GeV}^{-1}$, at low E_T^0, but deviates from this shape for $E_T^0 > 20$ GeV. The charged transverse energy, E_T^C, was measured by the central drift chambers. E_T^C/E_T^0 decreases from about 0.5 to 0.25 over the E_T^0 range, illustrating the trigger bias on the charged/neutral ratio imposed by triggering on neutral energy alone.

In order to study the shape of the events, the COR collaboration uses a variable S, which is similar to sphericity. One finds the hemisphere (I) with the large $\sum \vec{p}$, and let this vector sum determine an axis (i.e. the thrust axis). $\sum \vec{p}$ in the other hemisphere (II) determines a second axis. S is then calculated as

$$S = 3 \sum_{\mathrm{I}} q_{\mathrm{T}i}^2 / 2 \sum_{\mathrm{I}} p_i^2 + 3 \sum_{\mathrm{II}} q_{\mathrm{T}i}^2 / 2 \sum_{\mathrm{II}} p_i^2, \tag{9}$$

where the $\vec{q}_{\mathrm{T}i}$ are the transverse momenta with respect to the two axes, respectively. For the limited y-range used, S is rather similar to the circularity discussed in Appendix A.

The distribution of S changes from a broad distribution centered at $S \approx 0.5$, to a narrow distribution peaked at 0 as E_T^0 increases from 10 to $\sim$ 25 GeV. Fig. 31 shows the distribution of S in two intervals of E_T^0, and $\langle S \rangle$ as a function E_T^0, showing a rather smooth decrease over the range covered. This again is clear evidence for the emergence of jets at high transverse energy.

In the fully installed AFS calorimeter, the total transverse energy, E_T, can be measured within a rapidity coverage varying from $|y| < 0.6$ to $|y| < 1.2$, with an average of $|y| < 0.9$. Uncorrected E_T spectra are shown in Fig. 32 for pp collisions at three ISR energies [93]. At $\sqrt{s} = 63$ GeV, the spectrum now extends to $E_T = 45$ GeV.

The $\sqrt{s}$ dependence of the spectrum is small at low values of E_T, $E_T \lesssim 12$ GeV, consistent with the expectation from approximate Feynman scaling. In this region, the dominant source of transverse energy comes from fluctuations in the multiplicity and p_T of the particles [94], and the events show a rather isotropic particle distribution, consistent with the NA5 findings at lower $\sqrt{s}$.

At higher E_T there is a strong $\sqrt{s}$ dependence — thus at $E_T > 20$ GeV, the cross section increases by about two orders of magnitude when going from $\sqrt{s} = 30$ GeV to $\sqrt{s} = 63$ GeV.

As E_T gets large, a clear change of event structure is seen. Fig. 33 shows the distribution of circularity C, which is the two dimensional analog of sphericity, defined from the transverse momentum vectors (see Appendix A for a definition). C is simply related to the

planarity P, by $C = 1 - P$. For $E_T > 25$–30 GeV a peak near $C = 0$ develops, characteristic of the emergence of high p_T jets.

A plot of $\langle C \rangle$ vs E_T, Fig. 34a, shows that this transition to jet dominance seems to be relatively independent of $\sqrt{s}$ (and thus the clear jet signal is not seen at $\sqrt{s} = 30$ GeV, because the collision energy is not sufficiently large to reach the transition E_T), and furthermore there is an indication that it is rather sharp in E_T.

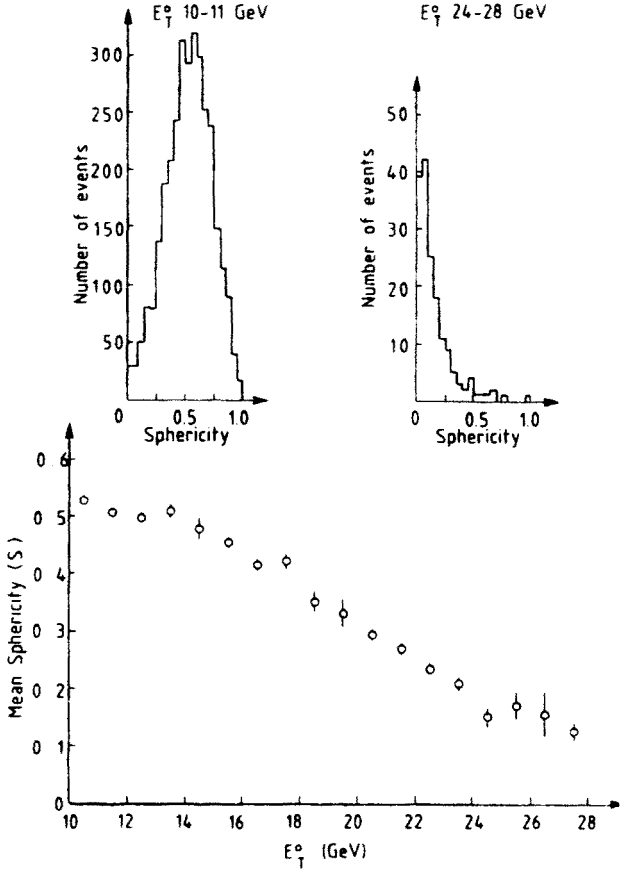

Fig. 31. Distribution of "sphericity", S (see text), in two intervals of E_T^0, from pp collisions at $\sqrt{s} = 63$ GeV. Also shown is $\langle S \rangle$ as a function of E_T^0 [92]

Fig. 34 also shows a number of other observables, characterizing the events, as functions of E_T. They are: b) the fraction of events with $C < 0.2$, c) the fraction of events with more than 60% of E_T in two non-overlapping clusters ("jets") of $\Delta\varphi = 60°$ and $\Delta y = 1$, and d) estimate of the total multiplicity (charged + neutral). The latter is obtained by dividing the total E_T with the average E_T of a charged track for each bin of total E_T, thus assuming this to be the same for charged and neutral particles. The multiplicity rises strongly with E_T up to 25 GeV, then seems to saturate, so that increasing E_T results in higher p_T particles.

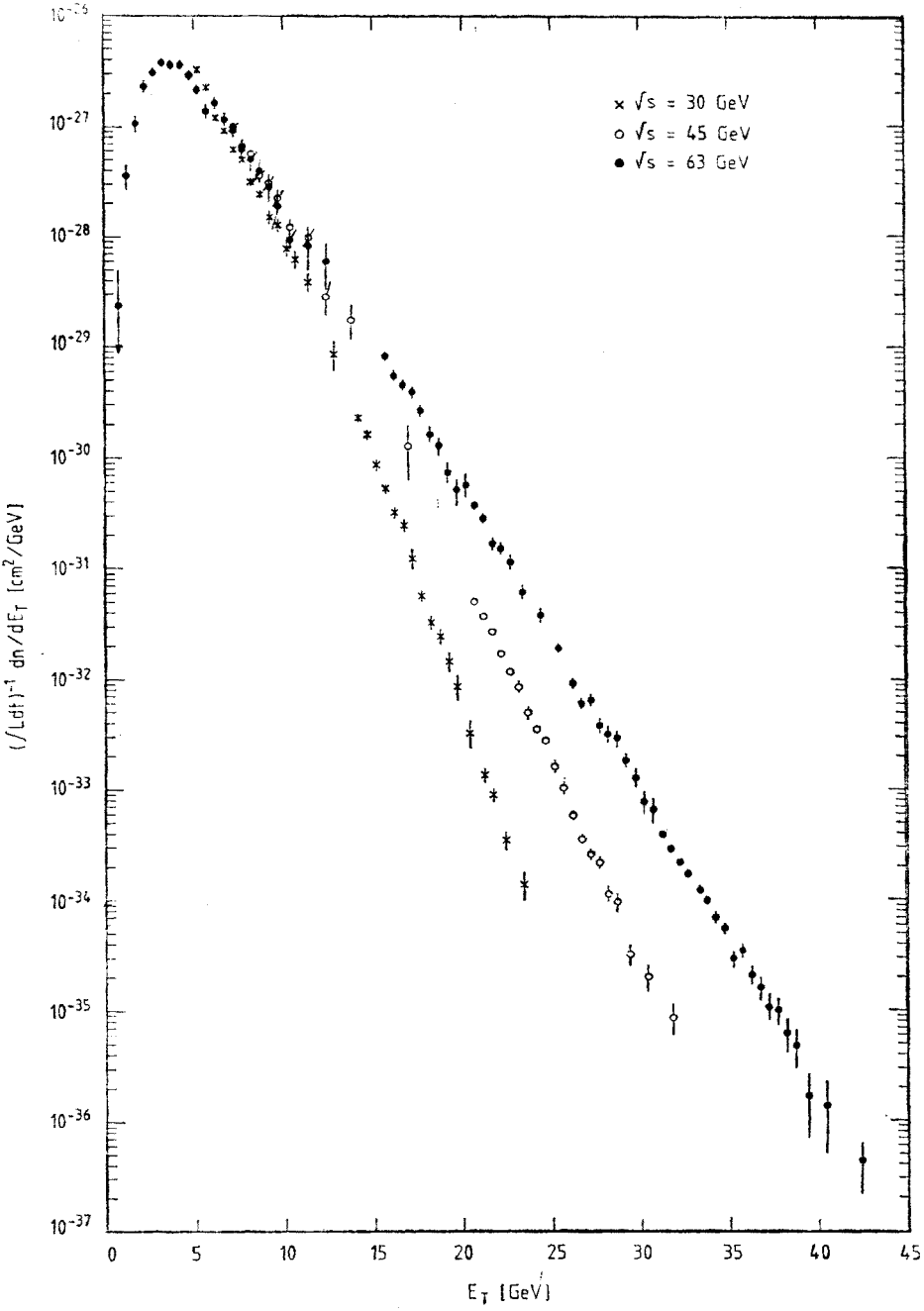

Fig. 32. Uncorrected E_T spectra in pp collisions at $\sqrt{s}$ = 30, 45 and 63 GeV; error bars are statistical. The y coverage varies with φ from $|y| < 0.6$ to $|y| < 1.2$, with an average of $|y| < 0.9$ [93]

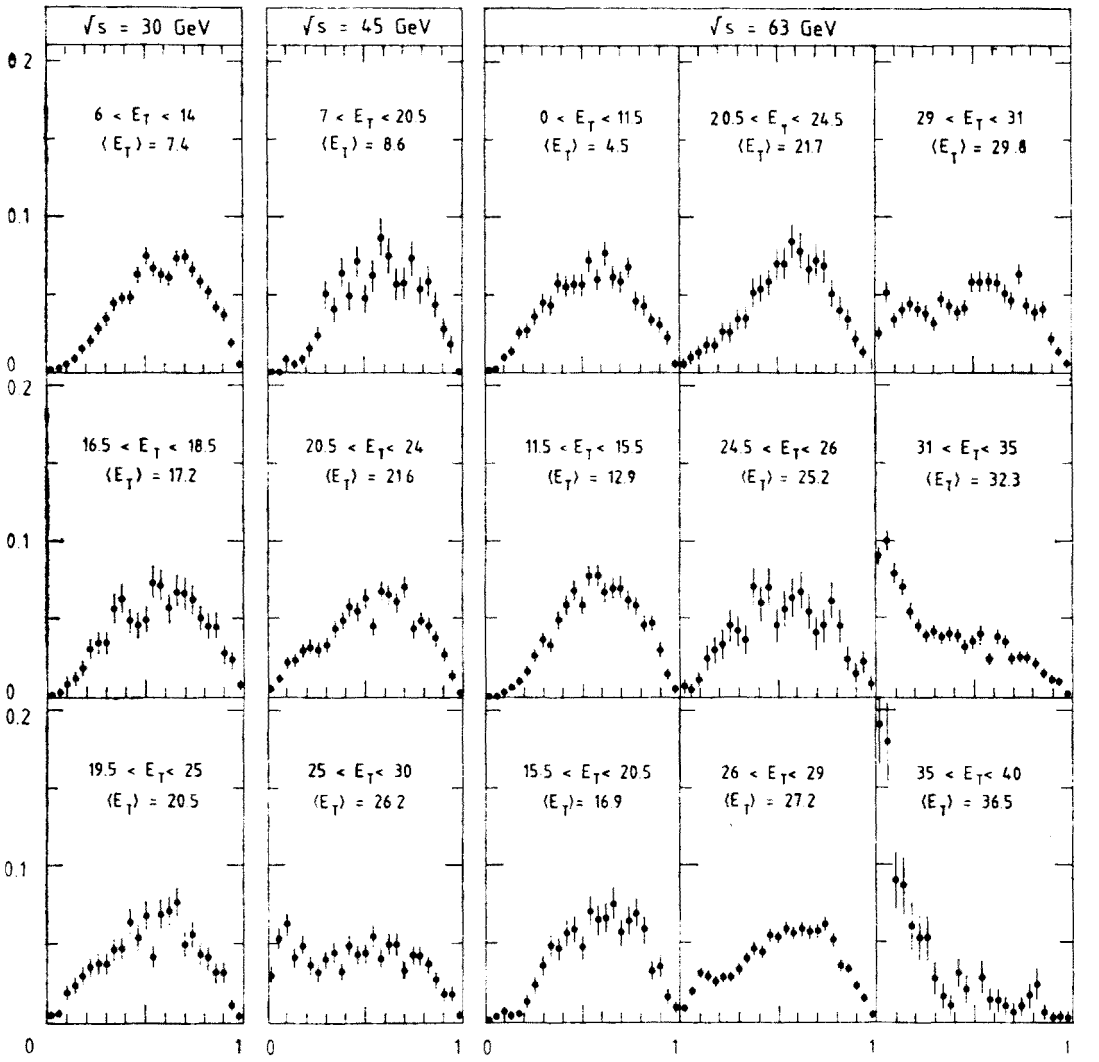

Fig. 33. Circularity distributions in bins of E_T in pp collisions at three values of $\sqrt{s}$ [93]

A comparison of these results with predictions of the QCD shower model (see Section 3.3) shows rather good agreement [95], but a detailed comparison must take into account the full corrections to the data for effects of acceptance and resolution.

A discussion of the transition from the unstructured events dominated by multiplicity fluctuations to the events dominated by jet production at large E_T can be found in [96]. It is based on the Lund model for high p_T collisions, and a rather primitive model for the effects of multiplicity and p_T fluctuations in low p_T events. The authors conclude that the transverse energy at which jet production starts to dominate is rather independent of $\sqrt{s}$, and roughly a linear function of the $(\Delta\varphi, \Delta y)$ intervals included. This is in qualitative agreement with the findings here.

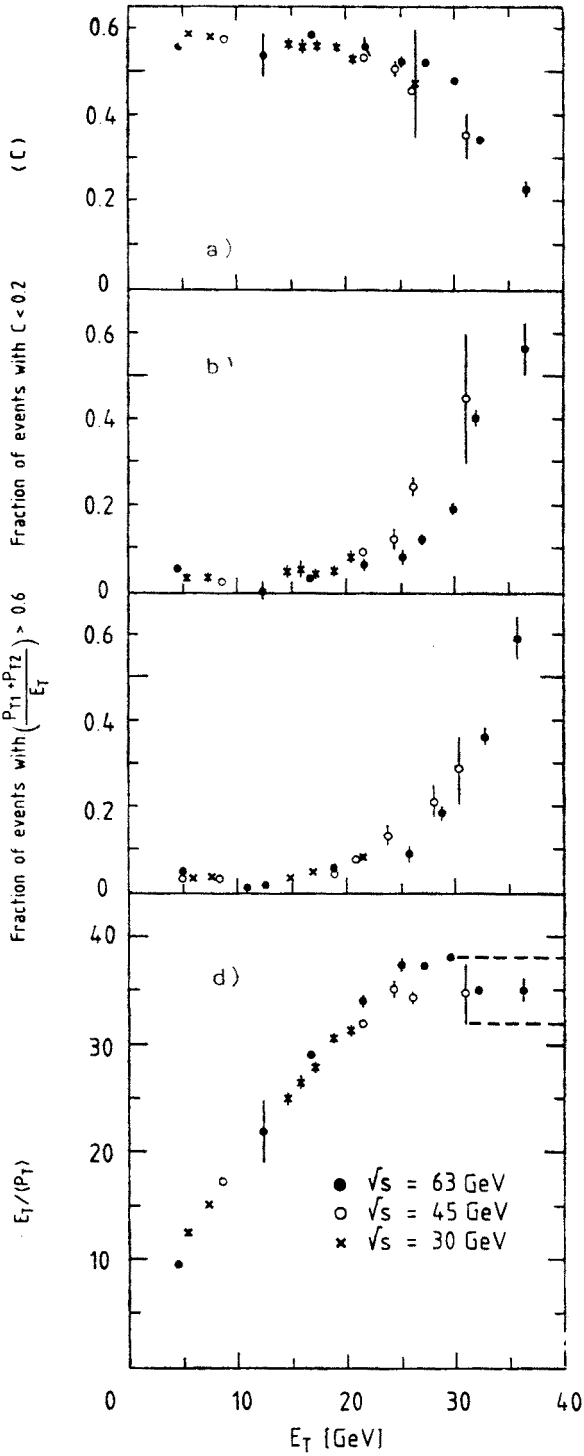

Fig. 34. a) Average circularity vs E_T; b) Fraction of events with $C < 0.2$ vs. E_T; c) Fraction of events with more than 60% of their E_T in two non-overlapping regions of $\Delta\varphi = 60\%$ and $\Delta y = 1$, vs E_T; d) Estimated multiplicity, $E_T/\langle p_T$ (single charged particle)$\rangle$, vs E_T. Data from the AFS [93]

At the SPS collider, the clarity of the jet signal seen at large E_T (see Fig. 25) makes it possible to make similar studies on the basis of rather simple cluster algorithms.

The UA1 calorimeter, shown schematically in Fig. 35, has a cell granularity roughly given by $(\Delta\eta, \Delta\varphi) = (0.3, 15°)$ for the hadron calorimeter, and $(\Delta\eta, \Delta\varphi) = (0.08\text{–}0.16, 180°)$ for the e.m. calorimeter, but φ_{em} can be further resolved to $\Delta\varphi_{em} \simeq 17°/\sqrt{E}$ (E in GeV).

In the UA1 cluster algorithm [97], an energy vector is associated with each calorimeter cell. Cells with $E_T > 2.5$ GeV are grouped if their distance in (η, φ) space,

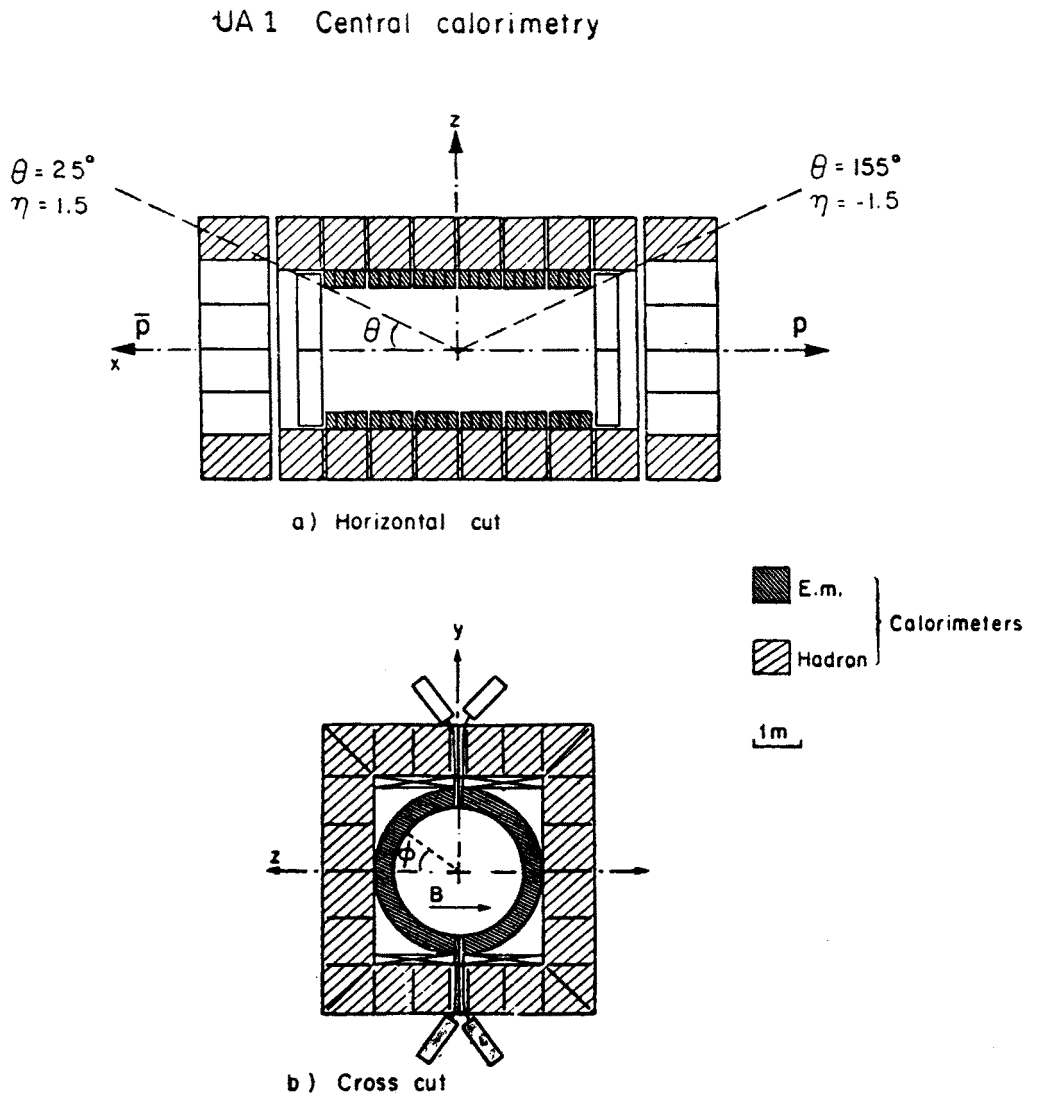

Fig. 35. The UA1 central calorimeters [97]: a) horizontal cut, b) cross cut. Hatched areas represent the calorimeter cells used for the jet analysis

$d = \sqrt{\Delta\eta^2 + \Delta\varphi^2}$ (φ in radians), is smaller than 1. Vectors with $E_T < 2.5$ GeV are then associated with the closest cluster, if they make an angle relative to the cluster axis smaller than 45°, and a transverse energy relative to the cluster axis less than 1 GeV.

The UA2 calorimeter, shown in Fig. 36, has a basic cell size $(\Delta\theta, \Delta\varphi) = (10°, 15°)$. In the UA2 cluster algorithm [98], cells with $E_T > 0.4$ GeV are first joined if they have a common side, and clusters are then split if they have two or more local maxima separated by a valley deeper than 5 GeV.

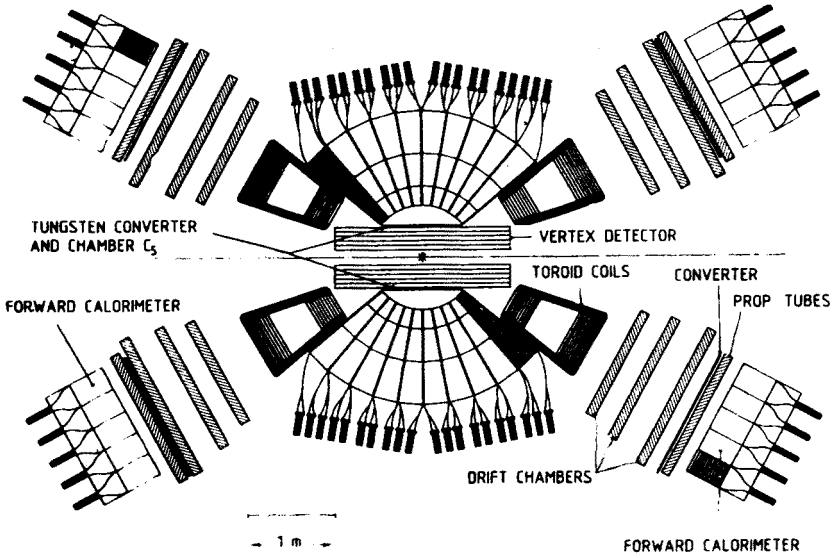

Fig. 36. Schematic drawing of the UA2 set-up [98], in a longitudinal cut. The detector is rotationally symmetric around the beam axis, except for a wedge of $\Delta\varphi = 60°$, used for a single particle spectrometer

To illustrate quantitatively the dominance of the two-jet configuration at high transverse energy, UA2 plots the fractions of the total $\sum E_T$ taken by the highest E_T cluster ($h_1 = E_T^1/E_T$) and by the two highest E_T clusters ($h_2 = (E_T^1 + E_T^2)/\sum E_T$) as functions of $\sum E_T$ (Fig. 37). An event containing only two jets of equal transverse energies would have $h_1 = 0.5$ and $h_2 = 1.0$. At high $\sum E_T$ a large fraction of $\sum E_T$ is shared by two clusters only.

Not surprisingly, the azimuthal angle between the two highest transverse energy clusters peaks sharply at 180°.

The transition from "unstructured" events to events dominated by two high p_T jets occurs at $\sum E_T = 50$–80 GeV at this $\sqrt{s}$. This is only a factor ~ 2 higher than at the ISR, although the collision energy is increased by almost an order of magnitude. This again illustrates the relatively slow change of the transition, which is governed by the balance between the slow increase in particle yield and $\langle p_T \rangle$ for the minimum bias type of events, and the strong increase in jet yield at fixed p_T.

For the UA1 data, a similar conclusion is reached. For both data samples, direct inspection of events with large E_T confirms the dominance of the two-jet configuration

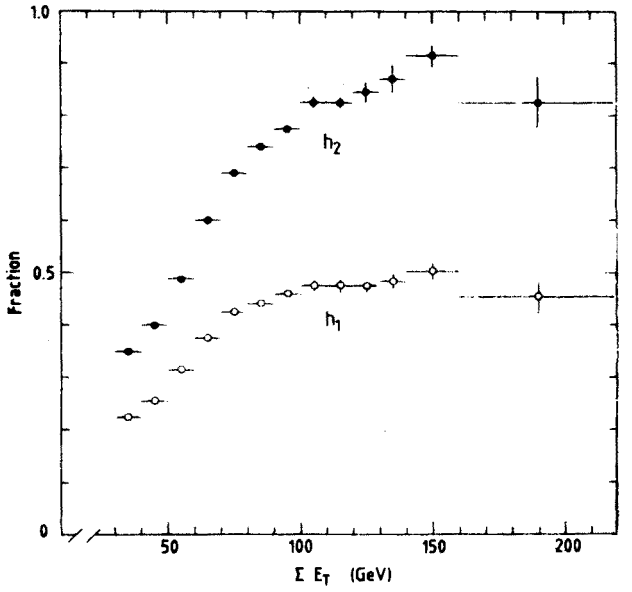

Fig. 37. Fractions of total ΣE_T taken by the highest E_T cluster ($h_1 = E_T^1/\Sigma E_T$), and by the sum of the two highest E_T clusters ($h_2 = (E_T^1 + E_T^2)/\Sigma E_T$), as functions of ΣE_T. Data from $\bar{p}p$ collisions at $\sqrt{s} = 540$ GeV [98]

(+ two forward jets), but also indicates that the events are occasionally more complicated. There are strong indications for the presence of radiative jets (hard gluon bremsstrahlung), as will be discussed in the next section, giving rise to a three-jet event topology. Also four-jet events have been seen, which are possible candidates for double hard parton collisions [99].

5.2. Jet properties[6]

After the demonstration of the dominance of clear jet structures in highly inelastic pp and $\bar{p}p$ events, a first round of results on jet properties have recently become available.

Fig. 38, from the UA2 experiment [98b], shows the azimuthal distribution, $\varrho(\Delta\varphi) = dn/d\Delta\varphi$, of charged tracks in events which have two clusters with $E_T > 15$ GeV and a separation $\Delta\varphi_{12} > 150°$. $\Delta\varphi$ is measured from the direction of the largest energy cluster in the event. The tracks are registered in the vertex detector, which covers polar angles down to $\theta = 20°$.

The narrow enhancements at $\Delta\varphi = 0$ and π correspond to the two jets. Around $\Delta\varphi = \pi/2$ the distribution is rather flat, at a level, ϱ_0, which is ~ 2 times as large as $dn/d\varphi$ in minimum bias events. If one assumes that particles not associated with the jets are distributed uniformly in $\Delta\varphi$[7] at a level $\lambda\varrho_0$ ($0 \leqslant \lambda \leqslant 1$), the mean multiplicity of charged particles in jets, $\langle n_{ch}^{jet}\rangle$, can be obtained simply from integrating $\varrho(\Delta\varphi) - \lambda\varrho_0$. For $\lambda = 1$,

[6] This section is based on material that has become available after the School.

[7] Within the framework of the parton shower model (see Section 3.3) this assumption is questionable.

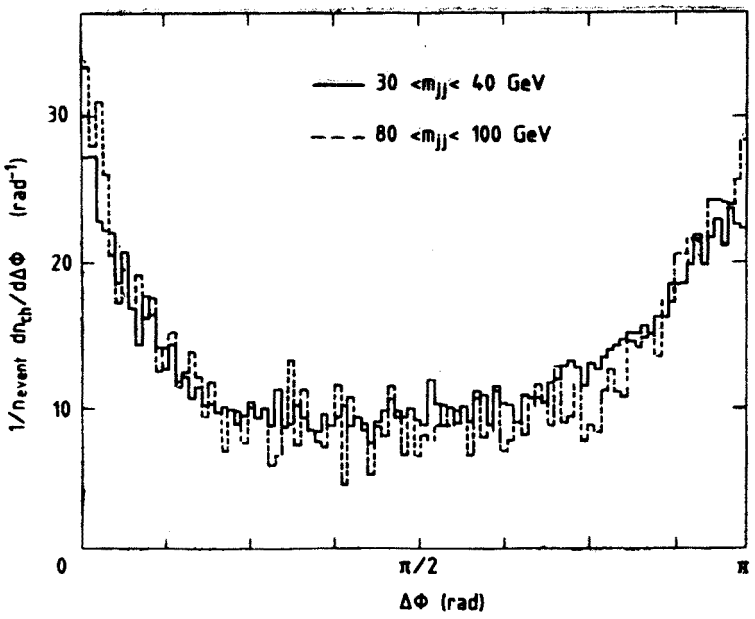

Fig. 38. Azimuthal separation between the largest energy cluster and charged tracks with $20° < \theta < 160°$ in $\bar{p}p$ collisions at $\sqrt{s} = 540$ GeV [98]. The events have two clusters with $E_T > 15$ GeV and a separation $\Delta\varphi_{12} > 150°$

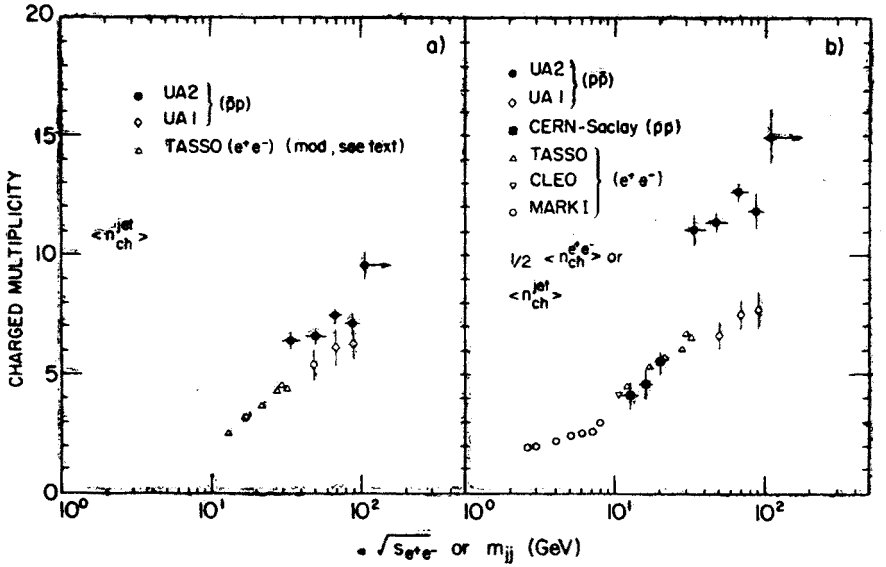

Fig. 39. Mean charged multiplicities in jets, $\langle n_{ch}^{jet} \rangle$, as a function of the invariant two jet mass, m_{jj} ($\bar{p}p$ data) or $\sqrt{s_{e^+e^-}}$ (e^+e^- jets): a) lower bound on $\langle n_{ch}^{jet} \rangle$, b) corrected value of $\langle n_{ch}^{jet} \rangle$ for $\bar{p}p$ data. Data from [97, 98, 100, 29]

one obtains a lower bound for $\langle n_{ch} \rangle$, which would apply if the jets had no associated particles at 90° to the jet axis (this is e.g. not true for jets in e^+e^- annihilation). The results are shown in Fig. 39a as a function of the two-jet mass, m_{jj}, together with results from e^+e^- jets at lower $\sqrt{s}$, which are analysed in the same way [100].

The UA1 group prefers to study the pseudorapidity profile of the jet, as shown in Fig. 40 for jets with $E_T > 35$ GeV. At small $\Delta\eta$ there is a strong peak arround the reconstructed jet direction, whereas the $\Delta\eta$ distribution is rather flat for $|\Delta\eta| > 1$. The level is about twice the "plateau height" in minimum bias events (40% higher if only "pure two-jet events" are used). If one assumes a flat $\Delta\eta$ distribution at the level observed for $1 < |\Delta\eta| < 2$, one arrives at the estimates of $\langle n_{ch}^{jet} \rangle$ shown in Fig. 39a [101]. They are roughly consistent with the UA2 results, and both sets of points are close to a logarithmic extrapolation from the e^+e^- results.

Since these estimates are obviously lower bounds, both groups try to correct the results, using models to estimate the loss of jet particles.

In the case of UA1, both the high p_T jets, and the "spectator" jets are parametrized

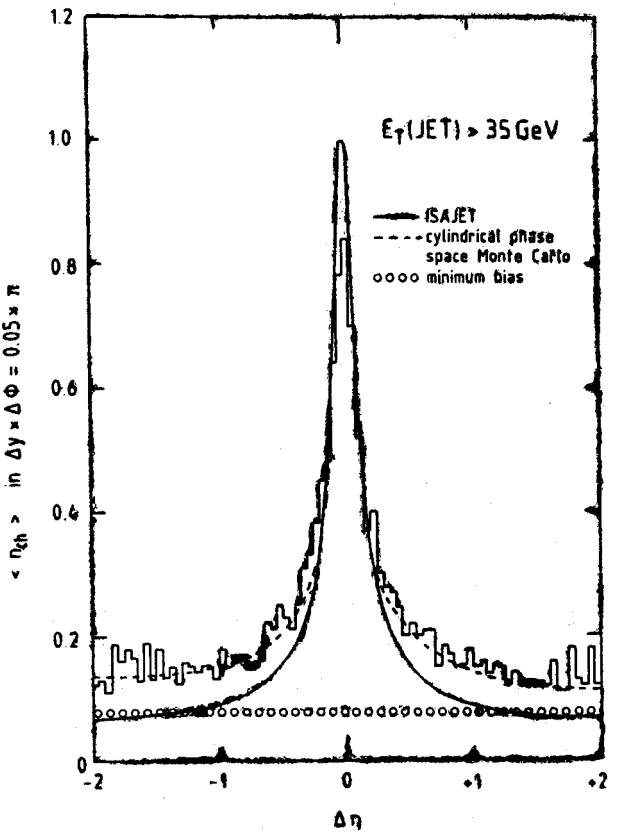

Fig. 40. Charged multiplicity in jets with $E_T > 35$ GeV as a function of pseudorapidity difference, $\Delta\eta$, from the jet axis. Also shown are calculations using the ISAJET model [91], and a cylindrical phase space model. Data from $\bar{p}p$ collisions at $\sqrt{s} = 540$ GeV [97b]

according to cylindrical phase space, and the number of jet particles missed in the region $|\Delta\eta| > 1$ is evaluated in the model.

In the case of UA2, a more sophisticated approach based on the parton shower model in the formulation of B. Webber [58] is used to estimate λ, and thereby $\langle n_{ch}^{jet} \rangle$.

The results are shown in Fig. 39b, together with results at lower $\sqrt{s}$ from jets in e^+e^- and pp collisions. The results from UA1 and UA2 are seen to disagree by almost a factor two. The origin of this disagreement must primarily be in the different model assumptions made.

From the UA2 results, one concludes that jets at low x_T, which are expected to be mainly gluon jets, have a higher multiplicity than quark jets at a similar p_T, as extrapolated from e^+e^- collisions. At higher x_T, the collider results seem to get closer to an extrapolation of the e^+e^- results. These findings are in agreement with recent calculations of gluon fragmentation [58d].

The difficulty in (impossibility of) assigning large angle jet fragments "correctly" is of less importance when one considers energy flow, and the jet may be more precisely defined in terms of the energy distribution around the jet axis [97, 98]. The transverse energy density in the residual event is found to be substantially higher in jet events than in minimum bias events (roughly a factor two if events with just two high p_T jets are considered [98]).

The fragmentation function of jets is studied by UA1 for charged particles in terms of the variable $z = p_L/E_{jet}$ [102]. p_L is the momentum component of the charged particle along the jet axis, and E_{jet} is the jet energy, obtained by summing vectorially the energy deposits in the calorimeter belonging to the jet according to the cluster analysis. Only jets with $E_{jet} > 30$ GeV are studied.

The distribution $D(z) = 1/N_{jets}(dN_{ch}/dz)$ is shown in Fig. 41. Only particles inside a cone with half opening angle 35° are used. The loss of low z particles with large emission angles (less than 5% for $z > 0.07$, but substantial at lower z), and the background from particles uncorrelated with the jet has been obtained using the cylindrical phase space model described above. Furthermore, $D(z)$ has been corrected for smearing due to the limited momentum resolution. Smearing due to the measurement of E_{jet} ($\sim 15\%$) has, however, not been corrected for.

The distribution is compared to the similar distribution of $x_L = p_L/p_{beam}$ obtained by the TASSO collaboration [100, 103] for jets in 34 GeV e^+e^- collisions, where the jet axis is found by minimizing the sphericity. There is good agreement, and because the scaling violations in e^+e^- jets are known to be small at large z, one concludes that the fragmentation functions for jets initialized by quarks and gluons are very similar as functions of z. This is not in disagreement with the conclusion reached above for the charged particle multiplicities, as the distributions may still disagree at low z, where a large fraction of the multiplicity is located.

A direct comparison between gluon dominated jets at the collider and light quark dominated jets, as observed at the ISR (or in deep inelastic lepton scattering), would be interesting, and could potentially clarify the situation, although the low z region is even more difficult to treat at the lower collision energy.

As a first step in this direction, we may look at the fragmentation function obtained by the AFS collaboration at the ISR from events with $E_T > 33$ GeV at $\sqrt{s} = 63$ GeV [104]. These events are dominated by two jets, as shown in the previous section, and the clean two jet part of the sample is selected for further investigation with a (rather loose) cut on circularity, $C < 0.4$.

In this case one has chosen to study the x_p distribution, where $x_p = 2p/\sqrt{\hat{s}}$. This requires, on an event to event basis, a determination of which particles to include in the

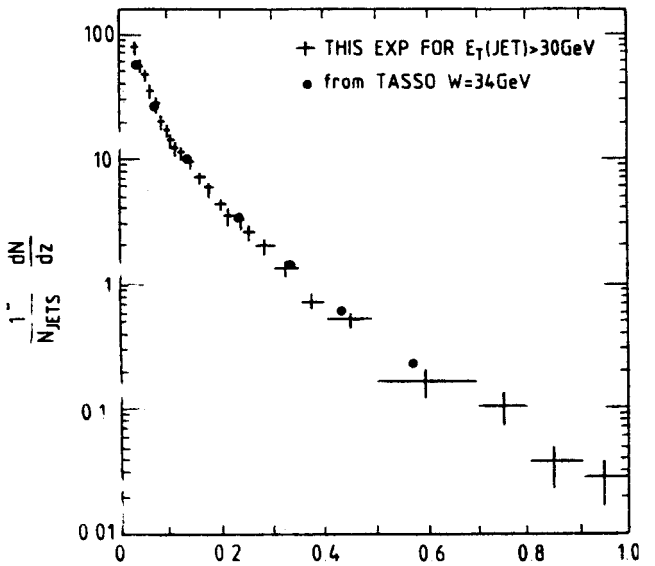

Fig. 41. Charged particle fragmentation function as a function of $z = p_L/E_{jet}$, for $E_{jet} > 30$ GeV. Data from $\bar{p}p$ collisions at $\sqrt{s} = 540$ GeV [102] are compared with data from e^+e^- annihilations at $\sqrt{s} = 34$ GeV [100, 103]

jets, both in order to calculate $\hat{s}$, and to decide which particles to include in the fragmentation function. In order to reduce ambiguities inherent in this choice, events were selected with two jets centrally in the calorimeter, and the two jet mass, W, was calculated from clusters in the calorimeter with $E_T > 1$ GeV/c. A Monte Carlo simulation was used to establish the relation between W and $\sqrt{\hat{s}}$, and a corrected two jet mass, W', was calculated. From both the Lund model [52] and the ISAJET model [91], one finds that $\sqrt{\hat{s}}$ is about 20% higher than W at the values of p_T^{jet} studied ($\langle p_T^{jet} \rangle = 13$ GeV/c).

The resulting x_p distribution is shown in Fig. 42, together with a representation of data from e^+e^- collisions at a CMS energy of 30 GeV [105], close to $\langle W' \rangle$, which is 32 GeV for the sample used. In the region $x_p > 0.05$, where the comparison is meaningful, there is an excellent agreement between the two sets of data.

To study the width of the jets, one must reconstruct the jet axis. In the AFS analysis referred to, this is done by means of a cluster analysis [106], which basically operates by

iteratively joining the pair of momentum vectors in the event with the smallest relative transverse momentum ($= |\vec{p}_1 \times \vec{p}_2|/|\vec{p}_\perp + \vec{p}_2|$), until this exceeds a given value, q_T^{cut}. In this way a number of clusters, dependent on the value of q_T^{cut}, is found. For the high E_T events q_T^{cut} was chosen so that nearly always two clusters were found. The jet axis is then given by the sum of the momentum vectors in each cluster. From the Lund model [52], the resulting jet axis is on the average 4° from the direction of the scattered parton.

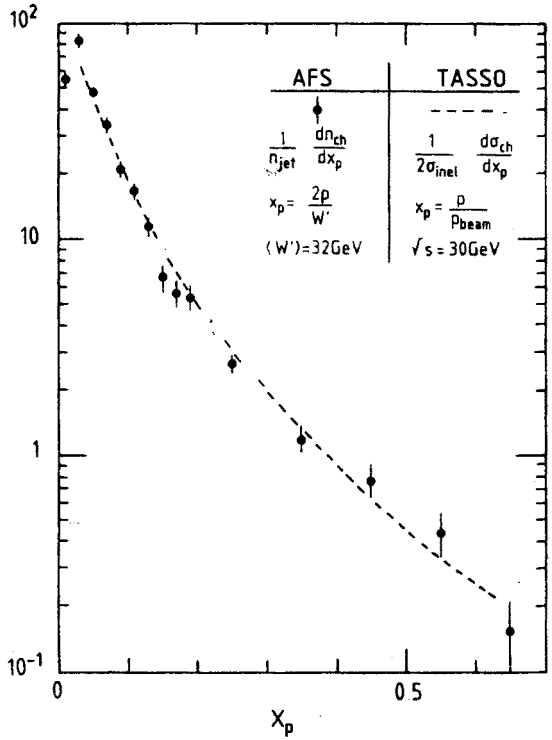

Fig. 42. Distribution of $x_p = 2p/W'$ in jets from pp collisions with $E_T > 33$ GeV at $\sqrt{s} = 63$ GeV [104], compared with e^+e^- data [105]. W' is the total two jet mass, obtained from the total mass of particles with $p_T > 1$ GeV/c in the detector (see text), applying a correction obtained from ISAJET [91]

Fig. 43 shows the resulting values of the average transverse momentum with respect to the jet axis, $\langle q_T \rangle$, as a function of $z = 2q_L/W'$. The figure also shows predictions of the Lund model with two different values of a parameter $\langle Q_T \rangle$, which determines the average transverse spread of the quark-antiquark (or diquark-antidiquark) pairs in the fragmentation. The data are consistent with the rather high value of 0.65 GeV/c.

This value is, however, in good agreement with e^+e^- data at $\sqrt{s} \approx W'$ if all events are analysed as two-jet events. The large effective $\langle Q_T \rangle$ may therefore represent the expected jet broadening due to hard gluon emission. A more detailed analysis is needed to establish this.

The values found are consistent with the results of a similar analysis by the UA1 collaboration [102], whereas the UA2 collaboration [98b] finds a somewhat lower value of

$\langle q_T \rangle$ (0.42 ± 0.04 GeV/c for $z > 0.1$). It is, however, based on particles with small values of q_T ($q_T^2 < 0.5$ GeV$^2/c^2$) alone, and must therefore be rather insensitive to effects of gluon radiation.

In conclusion jets found in events with large transverse energy at the ISR and SPS collider show a fragmentation structure quite consistent with jets found in e^+e^- annihilations at PETRA. Jets at low x_T in $\bar{p}p$ annihilations at the collider may show differences

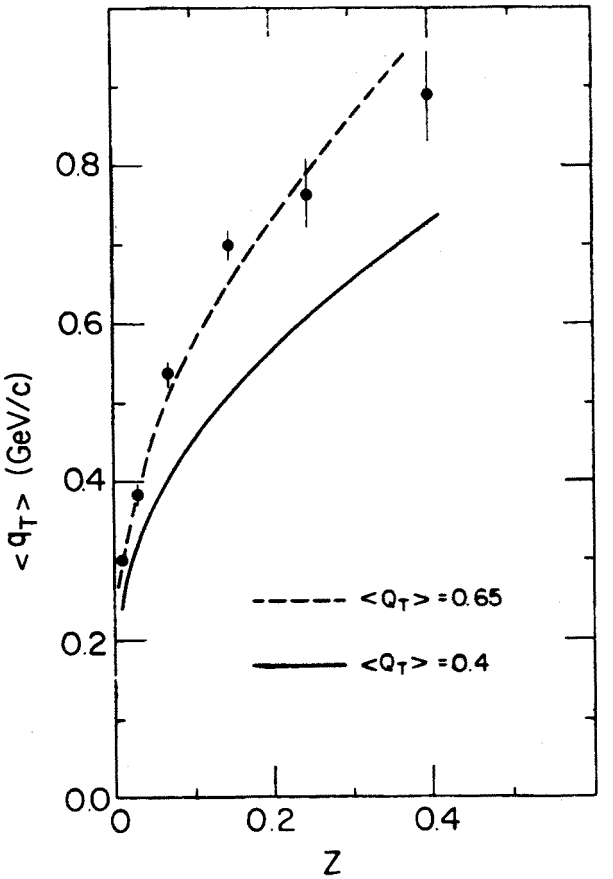

Fig. 43. Mean transverse momentum, $\langle q_T \rangle$, in jets from pp collisions with $E_T > 33$ GeV at $\sqrt{s} = 63$ GeV [104] as a function of z, when all events are analysed as two jet events. The data are compared with predictions from the Lund model [52], assuming an internal transverse momentum of the $q\bar{q}$ pairs in the jet fragmentation of $\langle Q_T \rangle = 0.40$ GeV/c and 0.65 GeV/c

at low z, as indicated by the first results on charged particle multiplicities in the jets. This would then mean that gluon jets at the collider give rise to more hadrons than quark jets. The transverse structure of the jets gives hints of the expected jet broadening effects due to gluon radiation, but firm conclusions on this must await further analysis.

5.3. The jet cross section

The inclusive cross section for jet production is a meaningful quantity only to the extent that jets are well defined objects. As we have seen, this is more easily fulfilled the higher the energy, and is difficult below ISR energies. In the framework of the parton model this cross section has a simple interpretation as the inclusive cross section for parton production, summed over all parton types. In the more sophisticated parton shower models, such a direct interpretation is not possible, but the jet cross section may still be regarded as an observable which is related rather closely to the fundamental hard scattering. In this context, the emphasis tends to shift, however, to more directly obtainable event characterizations, such as the cross section for emission of a certain (tranverse) energy into a certain solid angle, Ω, as a function of E_T and Ω.

In the analysis of event shape as a function of E_T by the AFS collaboration, the inclusive jet cross section was obtained from the two component fit discussed in Section 5.1. The hard scattering part is indicated in Fig. 27 by the shaded areas, and is in the range of 20–80% of the events in a given E_T bin (E_T is here the transverse energy into a calorimeter wall of ~ 1.7 sr). Corrections for geometrical jet acceptance, contributions from particles uncorrelated with the jet, energy scale and the effects of energy resolution were obtained from Monte Carlo calculations using the ISAJET model [91].

For e.g. a 10 GeV constituent directed into the centre of the calorimeter an average of 8.4 GeV was detected. This could be broken down as 7.4 GeV from the fragments of the parton, 0.9 GeV from the beam jets and 0.1 GeV from the recoil parton.

A similar analysis was performed on data obtained at $\sqrt{s} = 45$ GeV [107], and the results are shown together in Fig. 44. The data are compared to predictions from the ISAJET model, using in the model the fit to the proton structure functions by Baier et al. [108]. The agreement is very good.

Using the fit to the structure functions by Owens and Reya [54], which has a considerably softer gluon distribution, also gives a reasonable fit [90]. In the first case, quark-quark collisions are the dominant contribution to the jet cross section in the p_T range studied (6–14 GeV/c), in the second case quark-gluon collisions dominate.

Since data are obtained at two energies, one can make a fit to the scaling form (1). Parametrizing $f(x_T)$ as $A(1-x_T)^m$, one finds:

$$A = (1.6 \pm 1.0) \cdot 10^{-26}\ \text{cm}^2\ \text{GeV}^{N-2}, \quad m = 10.6 \pm 1.0 \quad \text{and} \quad N = 5.3 \pm 0.2.$$

Only the statistical errors are included in the fit. The value of N is considerably lower than that found for inclusive pion production, whereas the values of m are quite similar in the two cases [14]. N is not far from the value (6) found for single γ production (see Section 4.6). This suggests that part of the scaling violation (i.e. the deviation from the simple $N = 4$ rule) is associated with the jet fragmentation, whilst $f(x_T)$ describes the convolution of the proton structure functions.

The jet cross section found at $\sqrt{s} = 63$ GeV is about a factor 1000 larger than the inclusive cross section for π^0's at the same energy [15]. This is a direct confirmation of the trigger bias effect, which is an important prediction of jet fragmentation models (see Section 3.4).

At the SPS collider, the cross section for jet production has been measured by the UA1 [97] and UA2 [98] collaborations. The UA1 experiment used a localized transverse energy trigger, requiring $E_T > 15$ GeV in an aperture of roughly $\Delta\eta = 0.75$, $\Delta\varphi = \pi$, whereas the UA2 experiment has based the measurement on their total E_T trigger. In both cases the cross section determinations are based on the cluster algorithms for isolating the

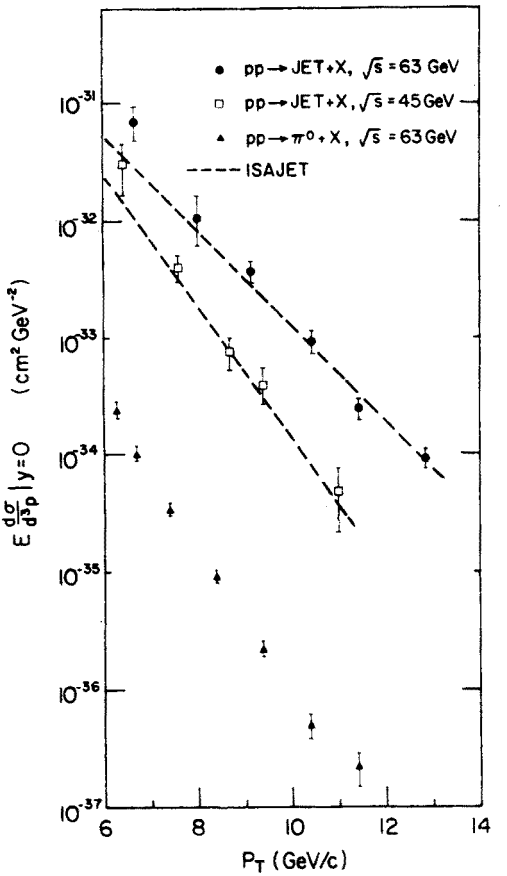

Fig. 44. The inclusive cross section for jet production at $y = 0$ in pp collisions at $\sqrt{s} = 45$ GeV and 63 GeV measured by the AFS [107]. Also shown are the predictions of the ISAJET model [91], using the fit to the proton structure functions of [108], and data for the inclusive π^0 spectrum at $\sqrt{s} = 63$ GeV [15]

jets described in Section 5.1. The jet acceptances are found by Monte Carlo simulations of the detectors and effects of the analysis cuts.

The results are shown together in Fig. 45. They agree in normalization within a factor ~ 2, which is consistent with the quoted systematic errors.

Due to the cleanness of the jet signal, the acceptance does not depend strongly on the fragmentation model assumed. The major contribution to the systematic uncertainty comes from the overall uncertainty in the energy scales, which are quoted as 7.5% for UA1 and

6% for UA2. The total systematic uncertainties in the jet cross sections are estimated to be a factor 1.65 (UA1) and 40% (UA2).

The results are at a level compatible with QCD calculations. In particular the cross section is a factor $\sim$ 1000 higher than at the ISR at fixed p_T[8], as predicted by early calculations [109]. The experimental confirmation of this large ratio is a major success for perturbative QCD. It is mainly due to the rapid increase in parton density encountered,

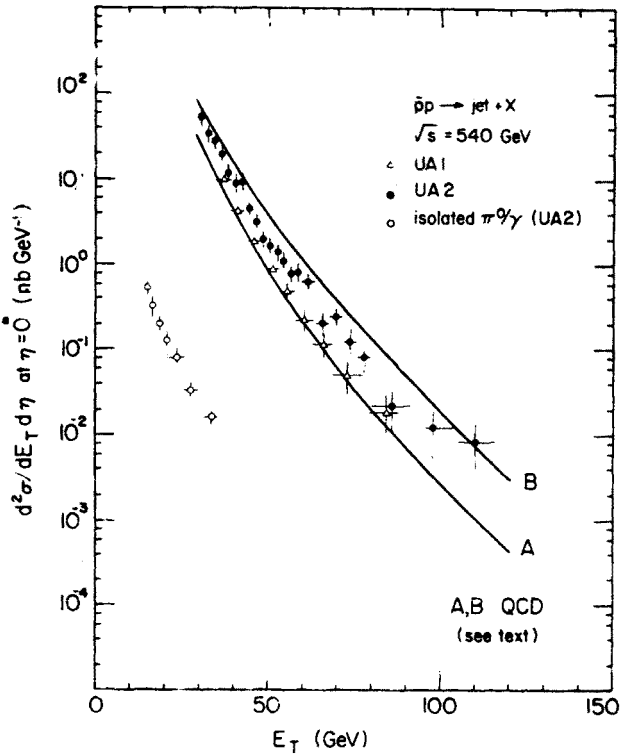

Fig. 45. The inclusive cross section for jet production in $\bar{p}p$ collisions at $\sqrt{s}$ = 540 GeV [97, 98]. Also shown are recent QCD calculations [110] based on the parametrizations of the proton structure functions by Owens and Reya [54] (A) and Baier et al. [108] (B). The open circles indicate the cross section for isolated, electromagnetic clusters in the UA2 experiment [98]

when going to smaller x_T. The lines on the figure are from a recent calculation [110], using the two different parametrizations of the proton structure functions mentioned above.

The UA2 collaboration has also measured the cross section for isolated electromagnetic showers, consistent with the conversion of at most two photons in their 1.5 radiation length Tungsten converter. These are expected to represent 1/3–1/2 of the combined inclusive cross section for γ and π^0's. The comparison with the jet cross section confirms the single/jet ratio of $\sim 10^{-3}$ discussed above.

[8] The 1981 data from UA2 go down to E_T = 15 GeV, but need a rescaling of the energy by a factor 1.33 to agree with later data [98].

The combined data of the AFS at $\sqrt{s} = 63$ GeV and the UA2 at $\sqrt{s} = 540$ GeV can be fitted to the scaling form of Eq. (1). With $f(x_T) = A_1(1-x_T)^m$, one finds $A_1 = 1.5 \cdot 10^4$ μb GeV^{N-2}, $m = 13.3 \pm 0.6$ and $N = 4.8 \pm 0.1$. A slightly better fit is obtained with $f(x_T) = A_2 e^{-bx_T}$, giving $A_2 = 2.5 \cdot 10^4$ μb GeV^{N-2}, $b = 18.2 \pm 0.8$ and $N = 4.7 \pm 0.1$. The cross sections scaled with $p_T^{4.7}$, are shown in Fig. 46 as functions of x_T, together with the result of the exponential fit.

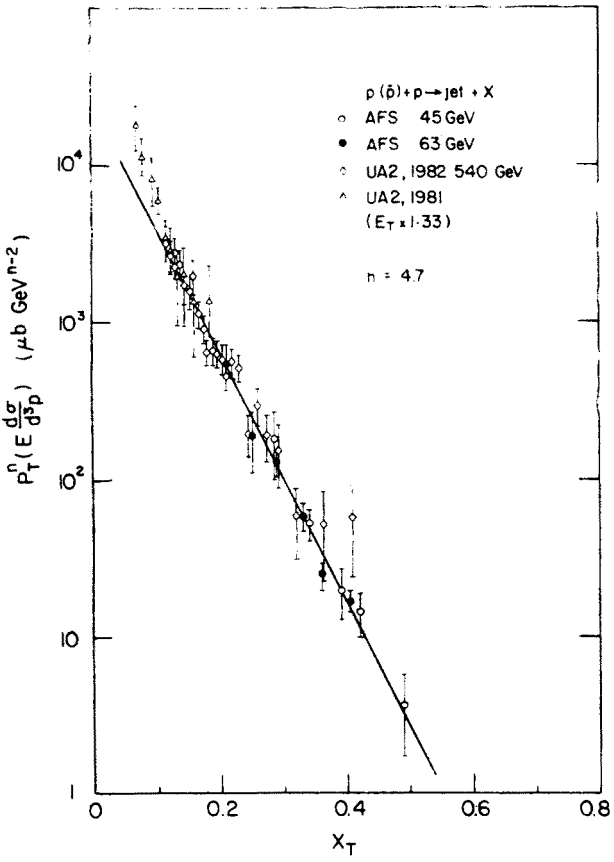

Fig. 46. The inclusive cross sections for jet production in pp and $\bar{p}p$ collisions, scaled with $p_T^{4.7}$, as functions of x_T. The line is the result of an exponential fit (see text). Data from the AFS [107] and UA2 [98]. Only the ISR data at 63 GeV and the UA2 data from 1982 were used in the fit

The UA2 measurements, based on their 1981 data, are also plotted, but were not used in the fit.[8] They extend to very low x_T, and indicate a rise above the exponential (and even more above the $(1-x_T)^m$ form) for $x_T < 0.1$.

In the range x_T covered by the two experiments there is thus good evidence that the data follow the scaling form (1), with a power N close to 5.

The measurement at the ISR of both the inclusive jet cross section and the inclusive direct γ cross section (Section 4.6), makes it possible to form the ratio γ/jet [83]. This is

shown in Fig. 47 as a function of p_T. Within the rather large errors, the ratio is constant with p_T, at a level about $4 \cdot 10^{-4}$.

This ratio is in principle a good test of theory, as it is calculable in perturbative QCD with relatively little phenomenological input.

Naively one may wonder why it is not just $\alpha/\alpha_s \simeq 4.10^{-2}$. Consider, however, as an example the subprocesses $qg \to qg$ and $qg \to \gamma q$, where the latter is expected to be the dominant source of direct γ's.

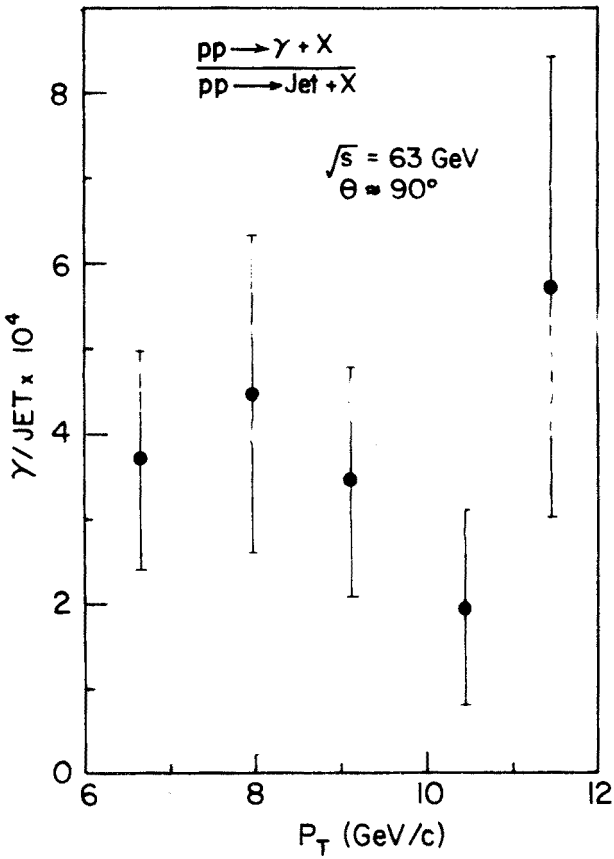

Fig. 47. The ratio between the inclusive cross sections for direct γ's and jets near $\theta = 90°$ in pp collisions at $\sqrt{s} = 63$ GeV [83]. Data from ABC [81] and the AFS [90]

The cross sections are [40]:

$$\frac{d\sigma}{dt}(qg \to qg) = \frac{\pi\alpha_s^2}{s^2}\left[-\frac{4}{9}\frac{s^2+u^2}{su} + \frac{s^2+u^2}{t^2}\right], \tag{10}$$

$$\frac{d\sigma}{dt}(qg \to \gamma q) = \frac{\pi\alpha\alpha_s e_q^2}{s^2}\left[-\frac{s^2+u^2}{3su}\right], \tag{11}$$

where e_q is the quark charge and s, t, u are the Mandelstam variables in the subprocess. At $\theta = 90°$, this gives:

$$\frac{pp \to \gamma + X}{pp \to g + X} = \frac{1}{2\,2} \cdot \frac{\alpha}{\alpha_s(p_T^2)} \tag{12}$$

independent of structure functions etc. As both the quark and the gluon give rise to jets, and as qq and gg scattering contributes about as much as qg scattering in the p_T range considered, we may expect

$$\gamma/\text{jet} \simeq \frac{1}{8\,8} \frac{\alpha}{\alpha_s(p_T^2)} \simeq 4 \cdot 10^{-4} \tag{13}$$

taking $\alpha_s = 0.2$. This is in good agreement with the observed value.[9]

Studies of correlations between jets are in progress, and a first set of results are available in recent papers by the UA1 and UA2 collaborations [97, 98, 111, 112]. They include observations of a rather large transverse momentum of the two-jet system ($\langle p_T^{jj} \rangle = 5 \pm 2$ GeV/c, UA2), studies of the angular distribution of the two jets from which one attempts to measure the angular distributions in parton parton scattering, and evidence from the study of p_{out}(UA1), or angular correlations between three clusters (UA2) on the presence of radiative jets. The UA1 collaboration has extracted an effective structure function from the data, and finds that it is in good agreement with extrapolations from quark and gluon distributions obtained in deep inelastic scattering experiments. For details the reader is referred to the original papers.

6. *Conclusions*

Following Altarelli [113], we may broadly classify the predictions of QCD in three groups: 1) topological signatures in the event structures, 2) estimates of rates and cross sections at the order of magnitude level and 3) precise, quantitative predictions.

In the first class we may place the expectations of two high p_T jets + two low p_T jets in events triggered by a single high p_T hadron, or a large total transverse energy, a structure for which there is now very good evidence. Also some evidence has been seen for the occasional occurrence of a third (radiative) jet. A specific point is that single γ's at high p_T should not be part of a hadronic jet. This seems to be fulfilled.

Early calorimeter experiments at SPS and Fermilab energies, which did not see the characteristic four jet pattern, have triggered important theoretical developments, which lead to the realization of the importance of a correct treatment of the effects of gluon bremsstrahlung. Thus for high E_T events, the dominance of the four jet structure is expected, and indeed seen, only at ISR energies and above.

In general event structures are expected to depend on the specific requirements made at the trigger level (single particle, symmetric pair, jet trigger, E_T trigger, etc.). Compari-

[9] I thank D. M. Scott for a discussion on these points.

sons of data obtained with different trigger requirements may be a powerful tool to test models.

The second class of predictions concern some large ratios that had to come out right, or QCD would be in deep trouble. They are the jet/π ratio, predicted to be 10^2–10^3 (depending on x_T), the γ/jet ratio ($4 \cdot 10^{-4}$), and related to these the γ/π ratio predicted to be $O(0.1$–$1)$ at large p_T. One may add the prediction that going from the ISR to the SPS collider at a p_T accessible to both (a factor 10 in $\sqrt{s}$), the jet yield should increase by a factor $\sim 10^3$.

The fact that these order of magnitude predictions all come out right implies that the basic analysis in terms of hard scattering of quarks and gluons is correct.

As far as predictions from the third class — quantitative results aimed at a detailed numerical confrontation with data — are concerned, one may say that models now reproduce and predict data fairly well, as evidenced e.g. by the fact that most of the results from the SPS collider, impressive as they are, could be predicted rather well. But the models still need substantial phenomenological input, and are basically classical, in that they rely on incoherent probability distributions in the description of the wave functions.

Thus at this level, if a specific model disagrees with data in quantitative details, it probably does not mean that QCD is wrong, but that our undertanding of QCD must be modified.

With the new experimental developments in the field, opened up by the $p\bar{p}$ collider, and by new instrumentation at the ISR, it is quite possible that high p_T physics will soon start to contribute to the testing of QCD at the quantitative level. Let us hope that the untimely closure of the ISR will not hamper the progress in the field too much.

It is a pleasure to thank the organizers, and in particular A. Białas and K. Zalewski for their hospitality and the warm atmosphere at the School.

APPENDIX A

Shape variables in the transverse plane

In high p_T collisions, the CMS system of the partons in a hard subprocess is in general not the same as the CMS system of the colliding hadrons. Furthermore, the subprocess occurs in the complicated environment of a hadronic interaction, and a clear separation of the subprocess from the rest of the event is in principle not well defined (although at high E_T at the SPS collider the separation can be fairly good).

Therefore the shapes of high p_T events are often most easily studied in the transverse plane. We collect here a few definitions of the more commonly used shape variables used in this kind of analysis. For a more complete survey of shape variables used in e^+e^- and high p_T collisions see e.g. [114].

Circularity, C, is the two dimensional analog of sphericity. If a and b are the major and minor eigenvalues of the transverse momentum tensor,

$$T^{\alpha\beta} = \sum_{i=1}^{n} \vec{p}_{Ti}^{\,\alpha} \cdot \vec{p}_{Ti}^{\,\beta}.$$

C is defined as

$$C = \frac{2b}{a+b} \tag{A1}$$

and the circularity axis is the major axis of $T^{\alpha\beta}$. This is easily calculated by making a linear fit through (0, 0) to the end points of the p_T vectors, and utilizing

$$C = 2 \cdot \mathrm{Min} \sum_i q_{Ti}^2 / \sum_i p_{Ti}^2, \tag{A2}$$

where q_{Ti} are the transverse momenta (in the plane) with respect to the axis. For a linear distribution (2 back-to-back narrow jets) $C \to 0$, and for an isotropic distribution of many particles $C \to 1$. The greatest merit of C is that it can be calculated easily analytically.

Planarity, used e.g. by NA5 [46], P is simply related to circularity:

$$P = 1 - C = \frac{a-b}{a+b}. \tag{A3}$$

Thrust, T, is easily restricted to two dimensions, and is defined as:

$$T = 2 \max \sum_{q_L > 0} |\vec{q}_L| / \sum |\vec{p}|, \tag{A4}$$

where $\vec{q}_L$ are the projections of the p_T vectors on the thrust axis. In practice, one finds the half plane π with maximum $\sum_\pi \vec{p}_T$, and gets

$$T = \sum_\pi \vec{p}_T / \sum_\pi |p_T|. \tag{A5}$$

In this formulation, one sees that for relativistic particles, $T = \beta$ of the particles in π. For a linear distribution (pencil-like jet) $T \to 1$ and for an isotropic distribution of many particles $T \to 2/\pi$. Because T is linear in the momenta, it is relatively insensitive to the emission of low momentum gluons, resonance decays, etc., and also to instrumental problems such as splitting or merging of energy clusters in a calorimeter.

As an aside we remark that the relation $T \simeq \beta$ above implies that a cluster analysis based on invariant mass as a measure of distance between particles, is equivalent to a thrust analysis in the case where two clusters are found. Such a cluster analysis may be an interesting generalization of the thrust analysis in cases with more than two jets (e.g. 3-jet events in e^+e^- collisions), having the special advantage of being Lorenz invariant.

Fox-Wolfram moments [115] are rotationally invariant moments characterizing event shapes. In the two-dimensional case, one may use

$$C_m = \sum_{ik} \frac{E_{Ti} E_{Tk}}{s} \cos m(\varphi_i - \varphi_k), \qquad m = 0, 1, 2, \ldots \tag{A6}$$

One finds $C_0 = (\sum E_T)^2/s = x_T^2$ and $C_1 = 0$ if there is transverse momentum balance among the detected particles. For an isotropic event with high multiplicity $C_m/C_0 \to 0$

for all $m > 0$; for 2-jet events $C_m/C_0 \to 1$ for m even, 0 for m odd; for 3-jet events C_3/C_0 is large, etc. The set of C's gives a description of the event shape which is independent of any determination of jet axes. It is, however, difficult to visualize the shape of an event from the set of C's, and this constitutes a minor difficulty, which may be the reason they have not yet been used to any large extent.

REFERENCES

[1] H. G. Fischer, Rapporteurs talk, EPS Conf. on High Energy Physics, Lisbon 1981.
[2] G. Wolf, Rapporteurs talk, 21st Int. Conf. on High Energy Physics, Paris 1982.
[3] M. Jacob, Rapporteurs talk, EPS Conf. on High Energy Physics, Geneva 1979.
[4] P. Darriulat, *Ann. Rev. Nucl. Part. Sci.* **30**, 159 (1980).
[5] N. A. McCubbin, *Rep. Progr. Phys.* **44**, 1027 (1981).
[6] H. Bøggild, CERN-EP/82-187, inv. talk at [7].
[7] Europhysics Study Conference *Jet Structure from Quark and Lepton Interactions*, Erice, Sept. 1982.
[8] J. D. Bjorken, *Phys. Rev.* **179**, 1547 (1969).
[9] R. D. Feynman, *Photon Hadron Interactions*, Benjamin, New York 1972.
[10] S. Berman, J. D. Bjorken, J. Kogut, *Phys. Rev.* **D4**, 3388 (1971).
[11] B. Alper et al., *Phys. Lett.* **44B**, 521, 527 (1973).
[12] M. Banner et al., *Phys. Lett.* **44B**, 537 (1973).
[13] F. W. Büsser et al., *Phys. Lett.* **46B**, 471 (1973).
[14] B. Alper et al., *Nucl. Phys.* **B100**, 237 (1975).
[15] C. Kourkoumelis et al., *Z. Phys.* **C5**, 95 (1980).
[16] A. L. S. Angelis et al., *Phys. Lett.* **79B**, 505 (1978).
[17] A. Breakstone et al., *Production of Charged Pions at High Transverse Momentum in pp Collisions at* $\sqrt{s}$ *= 44 and 63 GeV*, Contr. to the Int. Europhysics Conf. on High Energy Physics, Brighton 1983.
[18] R. Odorico et al., Contr. to XXI Conf. on High Energy Physics, Paris 1982.
[19] R. Blankenbecker, S. J. Brodsky, J. F. Gunion, *Phys. Lett.* **39B**, 649 (1972); *Phys. Rev.* **D6**, 2652 (1972); *Phys. Lett.* **42B**, 461 (1973); *Phys. Rev.* **D8**, 287 (1973).
[20] S. J. Brodsky, G. Farrar, *Phys. Rev. Lett.* **31**, 1153 (1973); *Phys. Rev.* **D11**, 1309 (1975).
[21] V. Matveev, R. Muradyan, A. Tavkhelidze, *Nuovo Cimento Lett* **7**, 719 (1973).
[22] R. Blankenbecker, S. J. Brodsky, J. F. Gunion, *Phys. Rev.* **D18**, 900 (1978).
[23] H. J. Frisch et al., *Phys. Rev. Lett.* **44**, 511 (1980).
[24] P. Darriulat et al., *Nucl. Phys.* **B107**, 429 (1976); *Nucl. Phys.* **B110**, 365 (1976).
[25] M. G. Albrow et al., *Nucl. Phys.* **B135**, 461 (1978); *Nucl. Phys.* **B145**, 305 (1978); *Nucl. Phys* **B160**, 1 (1979).
[26] M Della Negra et al., *Nucl. Phys.* **B104**, 365 (1976); *Nucl. Phys.* **B127**, 1 (1977).
[27] C. Finocchiaro et al., *Phys. Lett.* **50B**, 396 (1974); Kephart et al., *Phys. Rev.* **D14**, 2909 (1976).
[28] *Phys. Scr.* **19**, 69 ff (1979).
[29] A. G. Clark et al., *Nucl. Phys.* **B160**, 397 (1979).
[30] A. L. S. Angelis et al., *Phys. Scr.* **19**, 116 (1979).
[31] D. Drijard et al., *Nucl. Phys.* **B166**, 223 (1980).
[32] J. D. Bjorken, *Acta Phys. Pol.* **B5**, 145 (1974).
[33] M. Jacob, P. Landshoff, *Nucl. Phys.* **B113**, 395 (1976).
[34] C. Bromberg et al., *Phys. Rev. Lett.* **38**, 1447 (1977); *Nucl. Phys.* **B134**, 189 (1978); *Phys. Rev. Lett.* **43**, 565 (1979); *Nucl. Phys.* **B171**, 1 (1980).
[35] R. Feynman, R. D. Field, G. Fox, *Nucl. Phys.* **B128**, 1 (1977).
[36] R. D. Field, R. Feynman, *Phys. Rev.* **D15**, 2590 (1977).
[37] R. D. Field, R. Feynman, *Nucl. Phys.* **B136**, 1 (1978).

[38] R. Baier et al., *Nucl. Phys.* **B118**, 139 (1977).
[39] R. Cutler, D. Sivers, *Phys. Rev* **D16**, 679 (1977).
[40] B. Combridge, J. Kripfganz, J. Ranft, *Phys. Lett.* **70B**, 234 (1978).
[41] R. D. Field, *Phys. Rev. Lett.* **40**, 997 (1978); R. P. Feynman, R. D. Field, G. Fox, *Phys. Rev.* **D18**, 3320 (1978); R. D. Field, in [28].
[42] S. Brodsky, in [28]; E L Beiger, T. Gottschalk, D. Sivers, *Phys. Rev.* **D23**, 99 (1981).
[43] C. O. Escobar, *Nucl. Phys.* **B98**, 173 (1975); *Phys. Rev.* **D15**, 355 (1977); G. Farrar, S. Frautschi, *Phys Rev. Lett.* **36**, 1017 (1976); G. Farrar, *Phys. Lett.* **67B**, 337 (1977); H. Fritzch, P. Minkowski, *Phys. Lett.* **69B**, 316 (1977); F. Halzen, D. Scott, *Phys. Rev. Lett.* **40**, 1117 (1978); R. Rückl, S. J. Brodsky, J. F. Gunior, *Phys. Rev.* **D18**, 2469 (1979); R. D. Field, in [28]; A. P. Contogouris, S. Papadopoulos, M. Hongoh, *Phys. Rev.* **D19**, 2607 (1979).
[44] M. Diakonou et al., *Phys. Lett.* **87B**, 292 (1979); *Phys. Lett.* **91B**, 296 (1980); E. Amaldi et al., *Phys Lett.* **84B**, 360 (1979); R. M. Baltrusaitis et al., *Phys. Lett.* **88B**, 372 (1979); A. L. S. Angelis et al., *Phys. Lett.* **94B**, 106 (1980).
[45] W. Ochs, L. Stodolsky, *Phys. Lett.* **69B**, 225 (1977); W. Ochs, in [28].
[46] C. De Marzo et al., *Phys. Lett.* **112B**, 173 (1982); *Nucl. Phys.* **B211**, 375 (1983).
[47] P. Bagina et al., CERN-EP/83-94, subm. to *Z. Phys. C.*
[48] S. Sumorok (UA1), Talk at the European Conference on High Energy Physics, Brighton 1983.
[49] M. G. Albrow, Mini-rapporteur's talk at the European Conference on High Energy Physics, Brighton 1983.
[50] N. G. Antoniou et al., *Phys. Lett* **128B**, 257 (1983).
[51] B. Andersson, G. Gustafson, C. Peterson, *Z. Phys.* **C1**, 105 (1979); B. Andersson, G. Gustafson, *Z. Phys.* **C3**, 223 (1980); B. Andersson, G. Gustafson, T. Sjöstrand, *Z. Phys.* **C6**, 235 (1980); B. Andersson et al., *Phys. Rep.* **97**, 31 (1983).
[52] H. U. Bengtsson, The Lund Monte Carlo for High-p_T Physics, LU TP 82-15.
[53] G. Altarelli, G. Martinelli, *Phys. Lett.* **76B**, 89 (1978).
[54] J. F. Owens, E. Reya, *Phys. Rev.* **D17**, 3003 (1978).
[55] G. Gustafson, *Z. Phys.* **C15**, 155 (1982).
[56] G. C. Fox, R L Kelly, LBL 13985 (CALT-68-890) preprint; R. D. Field, G. C. Fox, R. L. Kelly, *Phys. Lett.* **119B**, 439 (1983); R. D. Field, *Jet Formation in QCD*, invited talk at XIII Int. Symp. on Multiparticle Dynamics, Volendam, The Netherlands, 1982; R. D. Field, G. C. Fox, University of Florida preprint TP-82-30 (CALT-68-965)
[57] R Odorico, *Phys. Lett.* **118B**, 151 (1982); *Nucl. Phys.* **B199**, 189 (1982).
[58] G Marchesini, B. R. Webber, CERN preprint TH 3525; B. Webber, Talk given at XVIII Renc. de Moriond, March 1983, CERN TH 3569; B. Webber, G. Marchesini, talks at this school; B. R. Webber, CERN TH 3713.
[59] N. Paver, D. Treleani, ISAS-preprint 52/82/EP; P. V. Landshoff, in [28].
[60] A. L. S. Angelis et al., *Nucl. Phys.* **B209**, 284 (1982).
[61] T. Åkesson et al., CERN-EP/82-104; R. Møller, Inv. talk at XIII Int. Symp. on Multiparticle Dynamics, Volendam 1982.
[62] A. L. S. Angelis et al., CERN-EP/83-46, subm. to *Phys. Lett. B.*
[63] T. Åkesson et al., *Phys. Lett.* **121B**, 439 (1983).
[64] A. L. S. Angelis et al., *Comparison between $\bar{p}p$ and pp Interactions at the ISR for High p_T and E_T^0 Spectra*, subm. to the Int. Europhys. Conf. on High Energy Physics, Brighton 1983.
[65] M. K. Chase, W. J. Stirling, *Nucl. Phys.* **B133**, 157 (1978).
[66] R. Horgan, M. Jacob, ISR Discussion Meeting Report, Series 2, No 1 (1980).
[67] CMOR Collaboration, A. L. S. Angelis et al., Ref. [64].
[68] R. Baier et al., *Z. Phys.* **C2**, 265 (1979); J. F. Gunion, B. Petersson, *Phys. Rev.* **D22**, 629 (1980); R. Baier, private communication.
[69] D. Drijard et al., *Nucl. Phys.* **B208**, 1 (1982).

[70] T. Åkesson et al., *Particle Ratios at High Transverse Momentum in pp Collisions at $\sqrt{s}$ = 63 GeV and Correlations between High p_T Identified Charged Particles and Associated Identified Charged Particles*, contr. to the Int. Europhys. Conf. on High Energy Physics, Brighton 1983.
[71] A. Breakstone et al., *High p_T Baryons Emitted at 10°, 20° and 45° in pp Collisions at $\sqrt{s}$ = 63 GeV; Relative Production of Charged Kaons and Pions at High Transverse Momentum in pp Collisions at the ISR*, contr. to the Int. Europhys. Conf. on High Energy Physics, Brighton 1983.
[72] D. Antreasyan et al., *Phys. Rev. Lett.* **38**, 112 (1977); *Phys. Rev.* **D19**, 764 (1979).
[73] D. Drijard et al., *Phys. Lett.* **121B**, 433 (1983).
[74] R. J. Fisk et al., *Phys. Rev. Lett.* **40**, 985 (1978).
[75] C. Bromberg et al., *Phys. Rev. Lett.* **43**, 561 (1979).
[76] T. Sjöstrand, *Comput. Phys. Commun.* **27**, 243 (1982).
[77] R. Brandelik et al., *Phys. Lett.* **100B**, 357 (1981).
[78] Ch. Berger et al., DESY 82-058.
[79] T. Åkesson et al., CERN — EP/83-75, to be published in *Nucl. Phys.* B.
[80] W. Geist, CERN/EP 82-184; D. Drijard et al., CERN/EP 82-212, contr. to [7].
[81] E. Anassontzis et al., *Z. Phys.* **C13**, 277 (1982).
[82] S. Contogouris et al., *Phys. Lett.* **104B**, 143 (1981).
[83] V. Burkert, Talk at XVIII Rencontre de Moriond, La Plagne 1983.
[84] M. McLaughlin et al., *Phys. Rev. Lett.* **51**, 971 (1983).
[85] T. Åkesson et al., *Phys. Lett.* **123B**, 367 (1983).
[86] T. Åkesson et al., *Phys. Lett.* **118B**, 178 (1982).
[87] F. Halzen, M. Dechanstreiter, D. M. Scott, *Phys. Rev.* **D22**, 1617 (1980); R. Baier, J. Engels, B. Petersson, *Z. Phys.* **C6**, 309 (1980).
[88] O. Benary et al., *Z. Phys.* **C16**, 211 (1983).
[89] J.-P. Repellin, UA2 Collaboration, Proc. of 21st Int. Conf. on High Energy Physics, Paris 1982, p. 571.
[90] T. Åkesson et al., *Phys. Lett.* **118B**, 185, 193 (1982).
[91] F. Paige, S. D. Protopopescu, ISAJET, *A Monte Carlo Event Generator for pp and $\bar{p}p$ Interactions*, BNL 31987 (1982) & BNL 29777.
[92] A. L. S. Angelis et al., CERN-EP/83-46 and Contr. to Int. Europhysics Conf. on High Energy Physics, Brighton 1983.
[93] T. Åkesson et al., *Phys. Lett.* **128B**, 354 (1983).
[94] T. Åkesson et al., CERN-EP/82-104 (unpublished); R. Møller, in XIII Int. Symp. on Multiparticle Dynamics, Volendam 1982, Ed. by W. Kittel et al.
[95] R. D. Field, private communication.
[96] T. Åkesson, H. U. Bengtsson, *Phys. Lett.* **120B**, 233 (1983).
[97] G. Arnison et al., *Phys. Lett.* **123B**, 115 (1983); CERN-EP/83-118, subm. to *Phys. Lett.* B.
[98] M. Banner et al., *Phys. Lett.* **118B**, 203 (1982); P. Bagnaia et al., *Z. Phys.* **C20**, 117 (1983).
[99] M. Jacob, *Collider Physics — Present and Prospects*, SLAC Topical Conf. 1983, CERN Th. 3693.
[100] R. Brandelik et al., *Phys. Lett.* **86B**, 243 (1979); *Phys. Lett.* **89B**, 418 (1980) and private communication to the UA2 collaboration; G. Wolf, DESY 81-086.
[101] H. Kowalski, mini-rapporteur talk, Brighton HEP Conf. 1983, DESY 83-099.
[102] G. Arnison et al., CERN-EP/83-119, subm. to *Phys. Lett.* B.
[103] TASSO Collaboration, private communication to the UA1 Collaboration.
[104] T. Åkesson et al., *Properties of Jets in High-E_T Events Produced in pp Collisions at $\sqrt{s}$ = 63 GeV*, paper subm. to Brighton HEP'83 Conf.
[105] R. Brandelik et al., *Phys. Lett.* **100B**, 357 (1981).
[106] T. Sjöstrand, preprint LU TP 82-7.
[107] T. Åkesson et al., *Phys. Lett.* **123B**, 133 (1983).
[108] A. Baier et al., *Z. Phys.* **C2**, 265 (1979).
[109] R. Horgan, M. Jacob, *Nucl. Phys.* **B179**, 441 (1981).

[110] B. Humpert, quoted in [98b].
[111] G. Sauvage, J. Schacher, Invited talks at the Brighton HEP'83 Conf., CERN EP/83-135.
[112] K. Sumorok, C. Rubbia, Invited talks at the Brighton HEP'83 Conf.
[113] G Altarelli, Third Topical Workshop on $p\bar{p}$ Collider Physics, Rome 1983, CERN 83-04, p. 372.
[114] G. Fox, Lectures at the 1981 SLAC Summer School, CALT-68-863.
[115] G. Fox, S. Wolfram, *Nucl. Phys.* **B149**, 413 (1979).

Note added in proof: $R^{+/-}$ on the away side has been measured previously also by the CCOR collaboration, with a similar result. See A.L.S. Angelis et al., *Phys. Lett.* **98B**, 115 (1981).